Octupolar Ordering in the $b > 0$ Bilinear-Biquadratic Heisenberg Pyrochlore

by

Cyrus Cerkauskas

A thesis
presented to the University of Waterloo
in fulfillment of the
thesis requirement for the degree of
Master of Science
in
Physics

Waterloo, Ontario, Canada, 2019

Author's Declaration

I hereby declare that I am the sole author of this thesis. This is a true copy of the thesis, including any required final revisions, as accepted by my examiners.

I understand that my thesis may be made electronically available to the public.

Abstract

We investigate the bilinear-biquadratic Heisenberg model on the pyrochlore lattice. While negative biquadratic couplings result in a first-order transition into a nematic ordered state with spins aligned mutually collinearly, it is found that positive biquadratic interactions lead to spins orienting in mutually perpendicular directions, described as octupolar or tetrahedral ordering. This transition is probed using classical Monte Carlo and it is found that the system undergoes a first-order transition into a octupolar ordered state with no long-range order. Unfortunately, we find that single spin-flip Monte Carlo simulations freeze completely at the transition with exceptionally slow dynamics and an extreme lack of ergodicity. The application of parallel tempering does not improve simulation results, which, due to the poor ergodicity of the simulation, cannot be reweighted using histogram techniques. We also present and discuss a potential loop algorithm which may allow simulations to overcome local energy barriers and regain ergodicity.

Upon warming Monte Carlo simulations initialized in potential octupolar long-range ordered states, we observe the dynamics of weathervane modes; zero energy rotational excitations in the lattice. Taking the form of 2D membranes in the lattice, these weathervane modes may rotate at no energy cost, allowing for the successful use of the single spin-flip Monte Carlo algorithm. We find that these weathervane modes exist at rotational angles of 0 and π corresponding to alternating layers of spins, in agreement with previous work. Depending on the long-range ordered state that the simulation is initialized in, weathervane modes may be stabilized by the periodic boundary conditions or, if free to rotate at will, may enter a weathervane manifold state where fast dynamics permit the simulation to rapidly sample various weathervane ordered states.

Acknowledgements

I would like to thank my supervisor, Michel Gingras, for his role as a mentor over the course of these last several years. His guidance and motivation helped me grow and mature as a researcher over the course of this project. His enthusiasm and drive helped immensely.

I would like to thank Roger Melko for his guidance and help with Monte Carlo and bringing things to a close.

I would like to thank Jeffrey Rau for his time and patience and our many interactions and whose conversations were of immeasurable value. I would like to thank Yuan Wan who helped to introduce me to this project and motivate my understanding. I greatly appreaciate your advice and helpful comments throughout this project.

Thanks must be given to the numerous people I have worked alongside over the past several years; Jianying Sheng, Wen Jin, Kristian Chung, and Darren Pereira who helped keep me motivated.

Finally, I would like to thank my family for supporting me through this endeavour.

Table of Contents

List of Figures

Chapter 1

Introduction

Though often taken for granted, the importance of magnetism in our daily lives cannot be understated. The discovery of the compass allowed the explorers of old to explore the world and chart unknown lands. The development of the electric motor and generator which utilizes magnets to induce current led to the widepread adoption of electricity throughout the world bringing what was before a scientific curiosity into the household. Storage of information on magnetic tape and hard drives led to the rise and proliferation of the internet in the late 20th century. Magnetism is an intrinsic part of today's technology with uses ranging from ordinary consumer headphones and speakers to magnetic resonance imaging (MRI) in hospitals to plasma confinement in reseach labs developing fusion technology. Areas of magnetism such as high temperature superconductivity are not yet understood, yet hold much potential for real world applications.

An understanding of magnetism, like many phenenoma in physics, is bolstered by the observation and modeling of the basic fundamental principles that underpin magnetic properties. Simple theoretical *toy models* such as the nearest-neighbour Ising model have greatly bolstered our understanding of magnetic behaviour and have been successfully utilized as a starting point in describing many real world materials despite appearing on the surface as hopelessly naive. For instance, the two-dimensional Ising model, in which magnetic spins on a 2D surface may only align upwards or downwards, beautifully illustrates a phase transition and is useful as a proxy for much more complex systems due to the universal criticality in many body systems at the phase transition. Thus complex many body effects and interactions in real world materials can be reduced and investigated as much simpler theoretical models allowing for the setting of a starting point in the laboratory. For this reason, there is much interest and work being done to model these

simple toy models using both analytic techniques and computational techniques such as Monte Carlo simulation and use them as a proxy for complex magnetic materials.

1.1 Magnetic Frustration

Magnetic *frustration* occurs when it is impossible to simultaneously satisfy all competing lattice interactions for all terms in the Hamiltonian. The ground state of these systems possesses a tremendous degeneracy – multiple configurations exist that possess that same (lowest) energy with no states (or set of states) being energetically preferred over the others. This frustration occurs in two forms; random frustration and geometric frustration. Random frustration can occur when a system has multiple competing interactions at the same energy level with rivaling spatial correlations or if the system has some degree of randomness (i.e. the Edwards Anderson model [1] in which the lattice bonds are randomly assigned to be ferromagnetic or antiferromagnetic). Here, however, we are interested in geometric frustration whereby the lattice prohibits the placement of spins that would simultaneuosly allow all lattice interactions to be satisfied. Consider a simple nearest-neighbour Hamiltonian:

$$H = J \sum_{<i,j>} S_i \cdot S_j \ , \tag{1.1}$$

with $J < 0$ the system is ferromagnetic and spins seek to align parallel to their neighbours while for $J > 0$ the system is antiferromagnetic and the spins seek an antiparallel alignment. This poses no issue on a square lattice where spins can be placed in such orientations, however, on a triangular lattice, the third spin on the antiferromagnetic triangular plaquette cannot be placed without violating a pairwise interaction with one of the other two spins (Figure 1.1). Placing the third spin in an up or down configuration has no effect on the total energy of the plaquette – there are multiple degenerate arrangements of spins on the plaquette which possess the same energy and which are not preferentially preferred over one another. Expanding this single plaquette to the entire lattice reveals a hugely degenerate macroscopic ground state dependent on system size and posessing a residual entropy [2]. Naturally, one wants to know the physics of this ground state and by which additional interactions or perturbations it is possible to break this degeneracy and induce some form of long-range magnetic order.

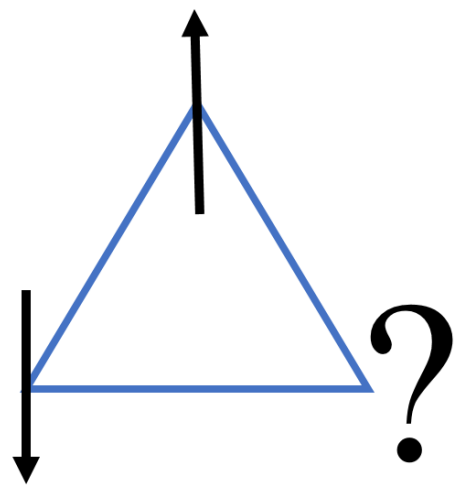

Figure 1.1: The third spin cannot be placed such that it simultaneously satisfies an antiferromangetic interaction with both of its neighbours.

As shown previously, geometrical frustration is not driven by mutually competing terms in the Hamiltonian but rather by lattice geometry. Lattices of note possessing the requisite geometry include the triangular lattice, the kagome lattice (a 2D network of triangles and hexagons), and the pyrochlore lattice (a network of corner sharing tetrahedra). Here we investigate the pyrochlore lattice which has been extensively studied in the literature and which is present in many real materials such as the cubic pyrochlore oxides [3].

1.2 Frustration on the Pyrochlore Lattice

The pyrochlore lattice is composed of a network of corner-sharing tetrahedrons with chemical formula $A_2B_2O_7$ where A and B are metal atoms. The structure of the lattice is the cubic face-centered space group $Fd\bar{3}m$. Frustration on the lattice can be seen through the extension of frustration on the triangular lattice – there is no spin configuration that will simultaneously satisfy all 6 antiferromagnetic interactions between the four spins of a given tetrahedron.

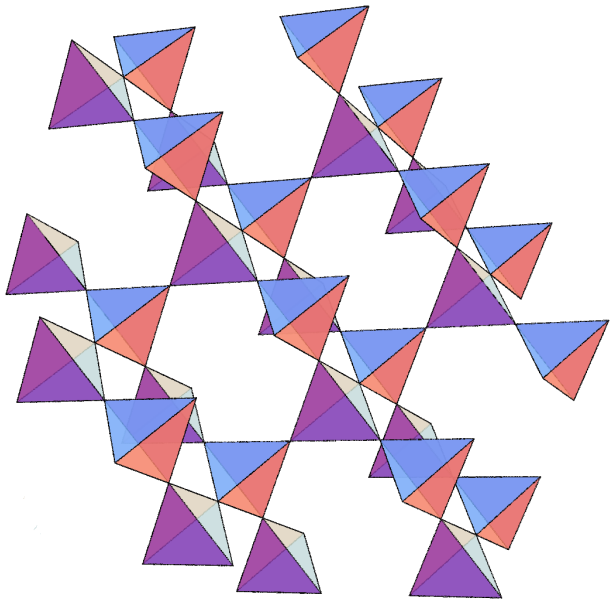

Figure 1.2: The pyrochlore lattice, a series of corner-sharing tetrahedra. Two types of tetrahedra, a and b, are present, distinguished by orientation (shown in purple/beige and blue/orange). As the a and b tetrahedra are corner sharing, the pyrochlore lattice may be described as a singular arrangement of either a or b tetrahedra.

In the 1950s, it was predicted by Anderson [4] that no long-range-order would exist for the antiferromagnetic Ising pyrochlore at any temperature and thus a Néel-like ground state could not be stabalized. Decades later, Villain [5] made the same proposal for the classical pyrochlore Heisenberg antiferromagnet, deeming the system an example of a *cooperative paramagnet* or classical spin liquid, and showing that the system would not possess a long range ordered state. Numerical Monte Carlo simulations of Heisenberg systems by Reimers [6] and Moessner and Chalker [7] later confirmed that, indeed, no long-range-order develops for the antiferromagnetic Heisenberg pyrochlore and that the system remains disordered for all finite temperatures.

Looking deeper at the antiferromagnetic nearest-neighbour Heisenberg pyrochlore and its ground state manifold, we observe that the ground state consists of tetrahedra with no net moment i.e. the fours spins on each tetrahedra sum to 0 ($S_1 + S_2 + S_3 + S_4 = 0$). The

tetrahedra are interlocked with one another and share corner spins (each spin belongs to two tetrahedra) however, there are no other restrictions on the orientations of the spins. Thus the system possesses a huge macroscopic ground state degeneracy and there is no long-range order. Thermal fluctuations or 'order-by-disorder' could break this degeneracy and select a ground state however this has not been observed in the pyrochlore lattice [7]. However, the low temperature disordered state of the nearest-neighbour Heisenberg pyrochlore has been found to be quite unstable and magnetic ordering is observed in the presence of additional interactions such as dipole interactions [8], further neighbour interactions [9] [10], lattice distortion [11] [12] or bond disorder [13] [14].

1.3 The Biquadratic Interaction

The low temperature states of real materials are often quite subtle and complex. The typical order parameter for the nearest-neighbour Ising and Heisenberg model, the magnetization m, may be insufficient to describe states which possess $\langle \vec{S} \rangle = 0$ but that still break spin rotational symmetery. These states are termed "spin nematic" states and are described by multipolar order parameters of which the simplest such example is the quadrupolar or nematic ordering first described by Blume and Hsieh [15]. This quadrupolar ordered state possesses a nematic axis or *director* with spins aligned parallel or antiparallel to this axis. These spins do not possess the positional ordering that would be observed in an antiferromagnetically ordered state with alternating "up" and "down" spins – the spins are, disregarding their tendency to order parallel or antiparallel to the nematic axis, otherwise ordered randomly. In terms of fluctuations the spins in the ordered phase display anisotropic fluctuations [16], they rotate at significantly lower energy cost perpendicular rather than parallel to the director.

Quadrupolar ordering about a nematic axis can be quite easily induced by the addition of a biquadratic term to the nearest neighbour Hamiltonian (Equation 1.2) with b $<$ 0. For convenience this Hamiltonian is often parameterized into the form shown in Equation 1.3. Some theoretical work has been done on the bilinear-biquadratic model favouring the much more approachable and potentially more experimentally realizable [17] $b < 0$ collinear ordered or nematic states. Work by Shannon and Penc [18] with $b < 0$ showed that in the absence of an applied magnetic field, the bilinear-biquadratic model undergoes a first order transition into a quadrupolar nematic state (i.e. no long-range order) at T $\sim b$. This phase, with two spins oriented 'up' and two spins oriented 'down' with respect to the O(3) nematic axis possesses zero magnetization; the quadrupolar tensor order parameter[1]

[1]We will describe this tensor order parameter in more detail later.

is required to observe the transition into the ordered phase. While Shannon and Penc did not observe long-range order with $b < 0$, they found that the application of a magnetic field or a ferromagnetic third nearest neighbour interaction produced a variety of unconventional states such as a vector multipole phase (canting of a nematic phase) or the stabilization of long-range order.

$$H = J \sum_{<i,j>} S_i \cdot S_j + b(S_i \cdot S_j)^2 \ , \tag{1.2}$$

$$H = J \sum_{<i,j>} \cos\theta_b S_i \cdot S_j + \sin\theta_b (S_i \cdot S_j)^2 \ . \tag{1.3}$$

Firm evidence for the existence of spin nematic ordering in real materials is lacking, but a number of materials are under investigation such as NpO_2 [19][20] which has been suggested to display triple $\vec{q}$ [2] octupolar and induced quadrupolar order and CeB_2 in which antiferroquadrupolar ordering is believed to be present and in which the presence of a magnetic field induces antiferro-aligned octupoles [21][22][23][24]. The pyrochlore $Tb_2Ti_2O_7$ is also believed to potentially possess a hidden long range ordered state consisting of parallel and antiparallel aligned electric quadrupole moments [25][26][27].

While a biquadratic value of $b < 0$ will favour collinear spins, minimizing the angles between spins while still maintaining $\sum_i S_i = 0$, the minimum energy configuration with $b > 0$ will have mutually perpendicularly aligned spins[3]. This describes tetrahedral or octupolar ordering (Figure 1.3) in which spins on each tetrahedron point away from the center of the tetrahedron[4]. Therefore we note that the Hamiltonian as shown in Equation 1.2 serves as an easily approachable toy model to describe both quadrupolar and octupolar ordering by simply flipping the sign of b. While more complex descriptions of multipolar ordering can be constructed, the essential physics of phenomena giving rise to this ordering, such as spin-lattice coupling [28][29] is sufficiently and more easily described by our Hamiltonian of choice. Favouring collinear or coplanar configurations, the biquadratic interaction mimics thermal and quantum fluctuations [30]. We thus utilize the bilinear-biquadratic Hamiltonian (Equation 1.3) as a toy model capable of describing both quadrupolar and octupolar ordering.

[2]Characterized by the existence of multiple ordering q vectors.

[3]Geometrically this is not possible in a 3D environment. The statement of "mutually perpendicular" is thus taken to mean that the angles between spins are maximized i.e. $\sim 109.5°$.

[4]These spins possess O(3) symmtery and so can globally rotate. The convention of spins pointing toward or away from the center of the tetrahedron is used for clarity only with angles of $\sim 109.5°$ between spins.

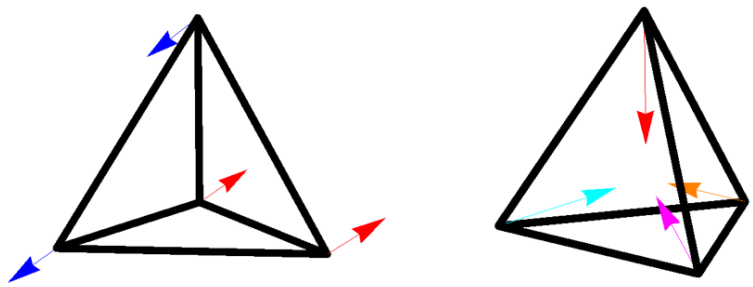

Figure 1.3: The ground state arrangement of spins on a single tetrahedron for mutually parallel or collinear ($b < 0$) (left) and mutually perpendicular or *octupolar/tetrahedral* ($b > 0$) (right) spins.

Figure 1.3 shows mutually parallel (left) and mutually perpendicular (right) spins on a single tetrahedron. In this figure, the collinear spins have been coloured red and blue to indicate up and down orientations. The perpendicular spins are distinct and so have been assigned four different colours. If multiple tetrahedra are present, the only way in which spins in a given tetrahedron can point in mutually perpendicular directions is if each tetrahedron contains one and only one spin of each colour (this restriction is known as the *colour ice rule*). We term this state a *colour ice state* [31] and note that a large number of distinct colour ice states will exist if the colour ice rule is imposed on the lattice.

Wan and Gingras [31] have investigated octupolar ordering of the $b > 0$ bilinear-biquadratic pyrochlore and have confirmed that the ground state of the system should possess octupolar ordering. However, much of the focus of their work was on the interesting low temperature of an octupolar ordered state. They found that for $b > 0$ octupolar ordered spins, there exist zero energy rotational modes [31] similar to that of the classical kagome Heisenberg antiferromagnet [32][33][34][35][36][37]. These so called *weathervane modes* consist of spin rotations on segments of the lattice that are isolated from the rest of the lattice by a boundary of spins aligned ferromagnetically with respect to one another (i.e. the weathervane pole) shown in Figure 1.4 on the kagome lattice. As these pole spins all possess the same orientation and isolate the chunk of the lattice from the rest of the lattice, they may rotate with respect to the boundary spins by an angle ϕ as a zero energy excitation. Wan and Gingras also conducted an investigation of order-by-disorder

on several potential long-range dipolar ordered states and found that weathervane angles of 0 and 180° possess the same minimum zero point energy and maximum degeneracy. These order-by-disorder calculations imply that weathervane modes will exist in only two configurations distinguished by a 180° rotation.

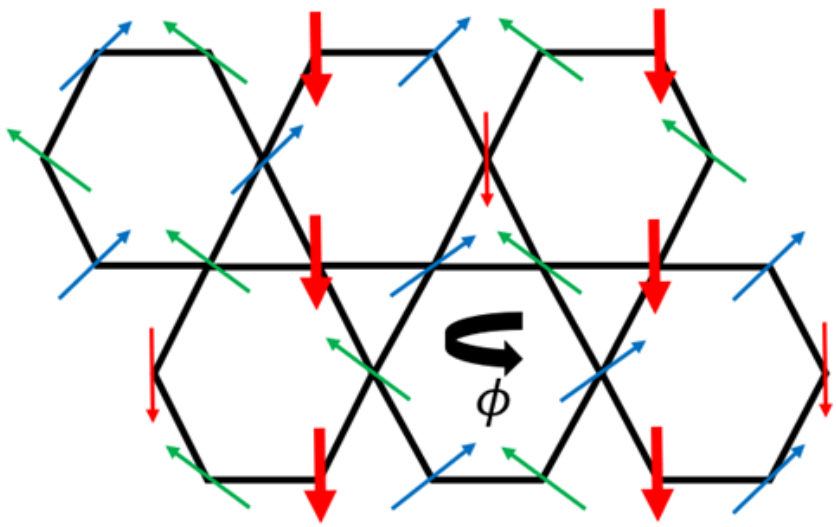

Figure 1.4: A weathervane mode on the kagome lattice. Thick red spins (pointing downward) are used to delineate the boundary of the weathervane membrane i.e. they are the "pole" spins. Weathervane membrane spins may rotate by any angle ϕ with respect to the boundary spins at no energy cost as weathervane rotations do not change the angles between any spins. In this figure, a weathervane rotation with $\phi = \frac{\pi}{2}$ would result in the blue and green spins in the membrane pointing into and out of the page respectively. The angles between spins of any colour would remain the same – this rotation is accomplished at no additional energy cost. Note that weathervane boundaries delineated by green and blue spins can all be seen in the figure.

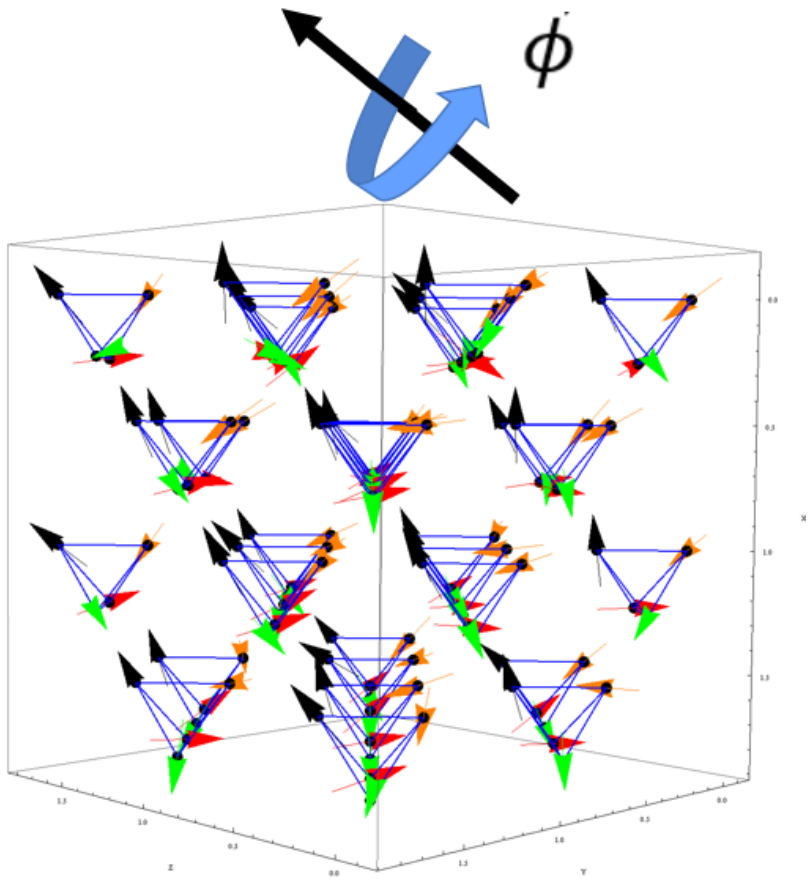

Figure 1.5: Weathervane modes on the pyrochlore lattice at some temperature T in a dipolar ordered state. The pyrochlore lattice consists of alternating stacked triangular and kagome layers. If the spins in the triangular layers are all the same colour (here black) the spins in the kagome planes can all be rotated by angle ϕ with respect to the black weathervane pole spins at no energy cost. As each kagome plane is separated by black triangular spins, the kagome planes may independently rotate by any angle without incurring energy penalties.

This is interesting as we would naively expect weathervane modes, separated by boundary spins, to rotate independently of one another with no prefered weathervane angles. In this thesis we will perform Monte Carlo simulations of these weathervane modes in an attempt to observe the low temperature physics of an octupolar ordered phase.

1.4 Outline

This work will investigate the predicted octupolar ordering on the Heisenberg pyrochlore lattice with positive biquadratic interactions and attempt to describe the nature of the expected paramagnetic to octupolar transition that is believed to occur as argued by Wan and Gingras [31]. The nature of the ground state and potential long-range order will be addressed. This endeavour is broken into a number of parts. In Chapter 2, the methods and numerical techniques we use will be outlined both in their theoretical context and application to other similar problems. General properties of multipolar transitions will be introduced in Chapter 3 where the quadrupolar nematic phase as previously described in the literature [18] will be briefly reviewed and reproduced, outlining the general properties of multipolar transition, before the sign of the biquadratic interaction is flipped to generate octupolar ordering. Chapter 4 will present our attempts to probe the octupolar state and outline the properties of the paramagnetic to octupolar transition, potential low temperature ordered phases, and confirm the presence of weathervane modes. Finally, Chapter 5 will conclude this work and suggest potential future avenues of research.

Chapter 2

Methods

2.1 The Classical Metropolis Monte Carlo Simulation

The Monte Carlo Method, initially developed by Nicholas Metropolis [38] and later generalized into what is now known as the Metropolis-Hastings algorithm is a very powerful tool in the field of stochastic processes (i.e. a course of non-deterministic and random events which cannot be directly inferred but do possess statistics). Widely used in the field of condensed matter physics, Monte Carlo simulations allow for the efficient sampling of states from a distribution of states in which direct sampling is difficult, reducing computationally untractable many-body problems to significantly more manageable levels. Systems containing large numbers of particles with exponentially many energy levels can thus be effectively reduced to a probability distribution whose statistics can be obtained with a high degree of accuracy.

The Monte Carlo algorithm and its variants are only one of many tools used to probe many-body systems. In the following section, the Monte Carlo algorithm and associated methods as well as other algorithms used in this thesis to probe the biquadratic interaction will be briefly reviewed. A more detailed description of the Monte Carlo method can be found in many reference materials such as Newman and Barkema [39] and Landau and Binder [40]. As will be shown in this chapter, specific care must be used in selecting an algorithm that will efficiently and accurately characterize the physics under consideration.

2.1.1 Single Spin-Flip Monte Carlo

In statistical mechanics, the thermal average of classical observable O is defined (Equation 2.1) where $Z = \sum_\mu e^{-E_\mu/k_\mathrm{B}T}$ is the partition function, μ represents all possible states of the system, E_μ is the energy of each respective state, T is the temperature and k_B is the Boltzman constant. Naturally, for systems with any significant number of particles, the number of states becomes rapidly unmanageable. The solution therefore is to sample the distribution of states and obtain a very good estimate of the observable O from that sample. This is what our Monte Carlo simulation allows us to achieve.

$$\langle O \rangle = \frac{1}{Z} \sum_\mu O_\mu e^{-E_\mu/k_B T} \ . \tag{2.1}$$

Consider a system starting in state μ and possibly ending up in a particular state v. Let us define the $R(\mu \to v)$ to be the transition rate at which the system moves from state μ to state v. Then the probability that the system will be in state v some time dt later can be written as $P(\mu \to v) = R(\mu \to v)dt$. This is then generalized to the many other states v that the system could take. Thus after some amount of time the system could conceiveably be in any one of these many states. But which ones? Defining the probability that the system will be in state μ at time t as $a_\mu(t)$, the **master equation** [39] for the evolution of the system from one state to another can be written as given by Equation 2.2, where a_μ and a_v are a set of weights that represent the probability that the system exists in state μ or v at a given time t.

$$\frac{\mathrm{d}a_\mu}{\mathrm{d}t} = \sum_v \left[a_v(t) R(v \to \mu) - a_\mu(t) R(\mu \to v) \right] \ . \tag{2.2}$$

The first term on the right hand side of Equation 2.2 represents the rate at which the system enters state μ from state v while the second term represents the rate at which the system in state μ enters other states v. Eventually the system will reach an equilibrium, that is $\frac{\mathrm{d}a_\mu}{\mathrm{d}t} = 0$. We can note that this is a Markov process – the system does not possess 'memory'; the future state of the system is independant of its past states and only depends on the system's current state. This lack of *memory* is critical[1] to sampling the entire phase space of the system and obtaining an accurate statistical description of the system.

The key component of the Monte Carlo scheme lies in the generation of the set of random sample states from the full set of states from the Boltzmann distribution. Monte

[1] Especially so for the positive biquadratic interaction investigated here.

Carlo schemes almost exclusively rely on Markov processes to generate new states. Markov processes are mechanisms which, when given one state μ, will generate some other state v in some random fashion with some transition probability $P(\mu \to v)$ satisfying two conditions; 1) that the transition probabilities are not time-dependant and 2) that the transition probabilities are not influenced by past states of the system. Thus the probability that the system will move from state μ to state v should not evolve in time.

Using our Monte Carlo scheme, a Markov chain of states is generated by starting with some initial state and feeding that state into our Markov process over and over again to generate a set of states with weights given by the Boltzmann distribution. For the Monte Carlo scheme to work, two conditions must be met: **ergodicity** and **detailed balance**. For a Monte Carlo scheme to be ergodic, it must be possible for the scheme, starting in any one particular state, to reach any other particular state in some finite amount of time. There must be at least one 'path' between states that can occur with nonzero probability; no state can be isolated from other states. Detailed balance implies that for any two states μ and v, the probability of transition from state μ to state v (which we here redefine as $P(\mu \to v)$) is the same as the probability of transition from state v to state μ ($P(\mu \to v)$). Thus the probability of the simulation being in state μ, p_μ multiplied by the probability that the simulation enters state v is equal to the probability of the simulation being in state v (p_v) and entering state μ (Equation 2.3). Given that we want the equilibrium distribution to obey the Boltzmann distribution, the condition of detailed balance must satisfy Equation 2.4

$$p_\mu P(\mu \to v) = p_v P(v \to \mu) \ , \tag{2.3}$$

$$\frac{P(\mu \to v)}{P(v \to \mu} = \frac{p_v}{p_\mu} = e^{-(E_v - E_\mu)/T} \ , \tag{2.4}$$

If our Monte Carlo scheme satisfies the constraints of ergodicity and detailed balance, the equilibrium set of states that it produces will be weighted according to the Boltzmann distribution. Even following the constraints above, there is some flexibility in how the transition probabilities are chosen. In general and in this work, the Metropolis scheme (Equation 2.5) is chosen to describe transition probabilities.

$$P(\mu \to v) = \begin{cases} e^{-(E_v - E_\mu)/T}, & \text{if } E_v - E_\mu > 0 \ , \\ 1, & \text{otherwise} \ . \end{cases} \tag{2.5}$$

If states are generated and rejected according to the criteria given in Equation 2.5, then our Monte Carlo algorithm should accurately sample the probability distribution of the system. Here the most simple and general method for selecting new states is presented; the *single spin-flip* algorithm. In this algorithm, a single spin is chosen at random from the lattice and a new random orientation selected for it. For Ising spins this procedure is quite simple; with only two orientations possible (spin *up* or spin *down*) we simply elect to flip the spin from one orientation to another. Heisenberg spins however, may point in any direction on the unit sphere and so "*flipping*" a Heisenberg spin is a slightly more elaborate but still simple procedure. In short, however, new random orientation on the unit sphere is chosen[2]. The magnitude of this new vector is then doubled and the two vectors (the newly chosen vector and the vector giving the spin's current location) added together and renormalized[3] such that $|S| = 1$. Thus the third vector, representing the new potential orientation of the spin, is calculated as a movement away from its initial orientation.

The spin is *flipped* to its new position with probabilities given by the change in energy between its original and proposed orientations and flipped according to the Metropolis criteria (Equation 2.5). A Monte Carlo simulation utilizing the single spin-flip algorithm for the classical nearest-neighbour Heisenberg model (Equation 2.6) (where $\langle i, j \rangle$ denotes the sum over nearest-neighbour pairs) proceeds as follows:

$$H = J \sum_{<i,j>} S_i \cdot S_j \tag{2.6}$$

1. Spins in the lattice are set to the initial starting orientations. The spins on the lattice may be initialized in many different starting configurations (random, aligned, etc).

2. A random 'trial' spin with initial orientation S_i is selected to be 'flipped' and its new potential orientation, S_f, generated.

3. The energy difference $\Delta E = E_f - E_i$ between the new and old states is computed.

4. If $\Delta E \leq 0$, the spin is 'flipped' and the move accepted. If $\Delta E > 0$, then the Boltzmann weighted acceptance probability is calculated $e^{-\beta \Delta E}$. A random number

[2]Specific care must be taken to ensure this distribution is truly random. Picking spherical coordinates (θ, ϕ) at random will result in a distribution with points "bunched" near the poles. A random distribution on the unit sphere can be obtained by choosing the random variables; $a = \cos\phi \in [-1, 1]$ and $\theta \in [0, 2\pi)$. Cartesian coordinates can then be generated as $x = \sqrt{1 - a^2}\cos\theta$, $y = \sqrt{1 - a^2}\sin\theta$ and $z = a$.

[3]We double the magnitude of the new vector so that the addition of the new vector with the vector giving the current position of the spin will result in a complete 180° flip of the original vector if the new vector was randomly chosen antiparallel to the current spin.

$0 < r < 1$ is generated; if $r \leq e^{-\beta\Delta E}$ then the flip is accepted, if $r > e^{-\beta\Delta E}$ then the spin is left untouched. The probability of acceptance is thus given by the Metropolis criteria $\mathrm{P}_{\mathrm{accept}} = \min(1, e^{-\beta\Delta E})$.

5. These steps are performed a suitably large number of times for the system to reach equilibrium. The elementary timescale of the simulation is given in Monte Carlo (MC) steps where 1 step represents N attempted spin-flips where N is the number of spins in the lattice. The number of Monte Carlo steps required to reach equilibrium (Figure 2.1) varies greatly depending on the underlying physics at play in the system. For a simple nearest-neighbour Heisenberg antiferromagnet on a cubic lattice, equilibrium may be reached in a few thousand MC steps. Other systems may require millions or more equilibrium Monte Carlo steps to reach equilibrium, particularly glassy systems. After the system has reached equilibrium, the sampling stage begins and observables such as the energy and magnetization are periodically measured. The number of samples required for good statistics varies greatly from system to system. The time series values of the observable are then averaged and their arithmetic mean recorded.

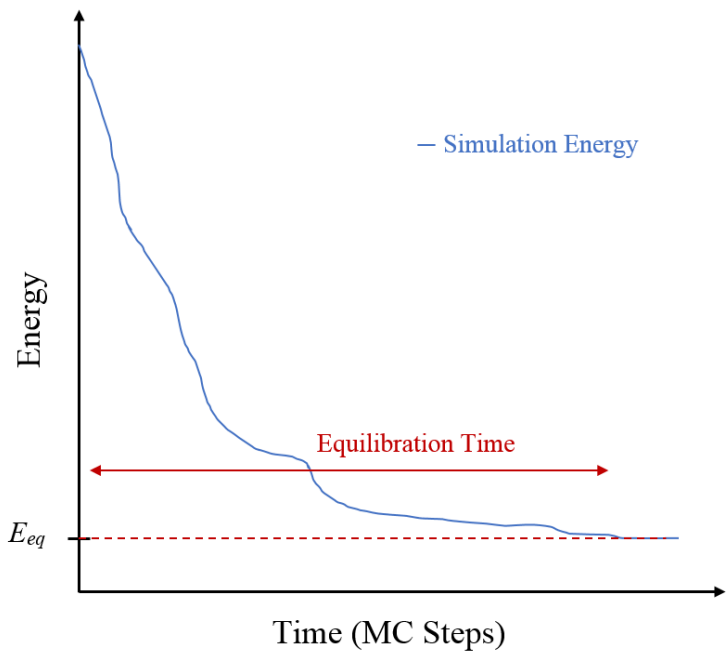

Figure 2.1: The energy of a Monte Carlo simulation started in a disorded state. After a period of time, the *equilibration* time, the simulation will have reached equilibrium energy E_{eq} and measurements of thermodynamic quantities can begin.

The single spin-flip algorithm is a good starting point for many numerical simulations. It suffers, however, from a number of problems including but not limited to slow dynamics, large autocorrelation times, and freezing at low temperature. As the single spin-flip algorithm proceeds through a series of small local moves,[4] it can experience extreme difficulty transitioning between distinct states with similar energies but whose traversal using single spin local moves would require the simulation to enter high energy intermediate states – that is, transitions between states separated by an energy barrier.

For instance, in the 2D ferromagnetic nearest-neighbour Ising model, we would expect the system to order in either an all-up or all-down spin configuration with equal probability as the two states have equal energy. However, the transition between the all-up and all-down state becomes increasingly unlikely as the temperature is decreased and the probability to flip a spin with four neighbours with the same orientation becomes exponentially low ($P = e^{\frac{-4J}{k_B T}}$). The quenching of the transition between the two states occurs because

[4] The transition from one distinct state to another must be completed through a series of individual single spin-flips.

while a configuration of all-up spins or all-down spins is a ground state a configuration of one down spin with all other spins up is not. The system cannot transition between the all-up and all-down states without moving through a number of intermediate states, none of which are ground states, but which the system must traverse if it is to move from one ground state to the other. As the temperature drops, the simulation is less likely to enter the intermediate states bridging the all-up or all-down states to such an extent that the simulation may effectively no longer transition between the states, despite the all-up or all-down states having the same energy. This is a loss of ergodicity as the simulation is unable to alternate between the all-up and all-down states – the system cannot access potential states.

A number of techniques have been proposed to address these issues involving adaptations to the single spin-flip algorithm (simulated annealing, parallel tempering [41][42], over-relaxation [43][44], etc.). Other techniques involve grouping spins into specific "clusters" or "loops" [42][45] which may be "flipped" at once at minimal or no energy cost. Some of these techniques such as parallel tempering may be applied almost universally while loop and cluster algorithms generally require tailoring to the problem under consideration. We discuss these techniques below.

2.1.2 Simulated Annealing and Parallel Tempering

As we will discuss later, the energy landscape (energies of the system corresponding to various spin configurations) which our Monte Carlo simulation samples is frequently nonuniform, possessing many local energy extrema or *metastable states*[5] that our Monte Carlo simulation may enter and fail to leave. Other states with lower energies may then fail to be sampled. To aid the Monte Carlo algorithm and prevent it from remaining in local metastable states we may elect to start our simulation at a higher temperature where the simulation can easily sample the entire energy landscape without being trapped in local minima and gradually cool the system. As the simulation is slowly cooled, it is far less likely to enter and remain in a local metastable state. This process, known as *simulated annealing*, is a term that takes its name from the field of metallurgy. In that field, to anneal is to gradually cool a metal or compound such that defects are minimized and the metallic structure is uniform.

Simulated annealing has been employed to great success in a variety of optimization problems [46][47][48]. Here, we employ simulated annealing in all our Monte Carlo simu-

[5]Metastable states correspond to local energy minima, i.e. a region that the Monte Carlo simulation may enter and have difficulty leaving.

lations to minimize the glassy behaviour displayed by the biquadratic model with postive biquadratic couplings. Simulated annealing is relatively easy to implement in any Monte Carlo routine: one simply starts the simulation at some high temperature before equilibrating and generating statistical data. The temperature of the simulation is then lowered and this process repeated.

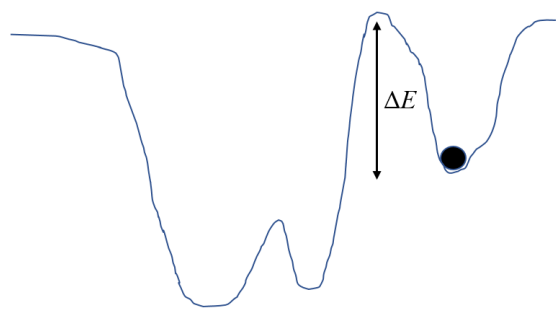

Figure 2.2: Energy landscape showing a simulation denoted by the black circle in a local energy minimum by a barrier of height ΔE. At low temperatures, the simulation may fail to leave this metastable state entirely.

Another method for dealing with a system with many local extrema involves running a number of simulations at a series of temperatures and periodically swapping spin configurations between simulations at neighbouring temperatures. Known as *parallel tempering* [41][42], it allows states generated by high temperature simulations above potential energy barriers to be "carried down" to low temperature simulations thus aiding in the exploration and movement in and out of metastable states.

Parallel tempering requires a signficant increase in computational resources due to the number of simultaneous parallel simulations involved (as the name implies). However, it can dramatically reduce autocorrelations and produce better statistics than simulations without parallel tempering which may encounter ergodicity issues [39]. The basic principles of parallel tempering are as follows. A number of simulations, M, of the same physical system are performed at different temperatures $T_0 < T_1 < T_2 < ... < T_M$ with the simulation run at T_0 corresponding to the system whose statistics we would like to acquire. All M independent simulations are run as normal Monte Carlo simulations with equilibration and sampling stages as described previously. However, periodically, every so many Monte Carlo steps during the sampling stage, the energies of the simulations are computed. The energy difference between a simulation and its neighbours (i.e. simulations up or down one

temperature "step") are then calculated. The states of the simulations (i.e the orientation of their spins) are then "swapped" between adjacent simulations with a probability (2.7) depending on the difference in energy between the states such that the state of each simulation satisfies the Boltzman distribution. The states of higher temperature simulations, which are capable of overcoming any energy barriers present, are thus capable of 'being transmitted' down to the lower energy simulations.

$$P(\mu \to v) = \begin{cases} e^{-(\beta_{\text{low}} - \beta_{\text{high}})\Delta E}, & \text{if } \Delta E > 0, \\ 1, & \text{otherwise.} \end{cases} \tag{2.7}$$

The parallel tempering algorithm, which is both ergodic and satisfies detailed balance [39], has been used extensively in the literature [49], [50], [51], [52] and has been shown to be of particular use in highly frustrated systems such as spin glasses [53], [54]. Intuitively is it clear why the parallel tempering algorithm is so powerful for these systems. As an example, consider a simulation with parallel tempering involving two temperatures of a glassy system that undergoes ordering at some temperature T_c. In this case we might have a simulation with a temperature T_{low} below the transition and a simulation at T_{high} above the transition. The low temperature simulation might be stuck in a metastable glassy state while the high temperature simulation above the transition is rather unconstrained. If the high temperature simulation should happen to fall into a lower energy minima, then swapping the spin configurations between the two simulations will allow the low temperature simulation to explore a new energy minima, aiding in the search for the lowest energy state. Note that as the parallel tempering algorithm only depends on the energy of the system, it can be used in conjunction with other Monte Carlo algorithms beyond single spin-flips.

2.1.3 Histogram Methods

When performing a Monte Carlo simulation, thermodynamic quantities such as the internal energy, specific heat, magnetization, etc. are obtained at the chosen discrete temperature points. If we were only to utilise data from these specific points, calculations such as the finite size scaling of the specific heat curve would be difficult unless we obtained enough temperature points to accurately capture the peak in the specific heat to high precision (with a curve consisting of only a few points it may not be possible to pick out the maximum value of the specific heat). Both the single [55] and multiple [56] histogram methods allow us to interpolate the values of statistical quantities between our temperature points. The single histogram method developed by Ferrenberg and Swendsen [55] takes a histogram of

the simulation measurements obtained at one temperature T and *reweights* them, allowing for a very good approximation of quantities at temperatures close to T.

In a classical system, the expected value of a thermodynamic quantity of interest O at temperature T (or inverse temperature β) is given in Equation 2.8 which calculates such a quantity as an average over all states μ of the system with each state weighted by its Boltzmann probability. However, such a calculation is only possible for small systems; for larger systems we must instead select a sample of states. Consider a Monte Carlo simulation at temperature T_1. Here we sample M states at random from a specified probability distribution[6] p_μ; the average value of therdynomatic quantity O will be given by Equation 2.9 which describes the selection of a subset of M states at random with total energies E_{μ_i} from a specified probability distribution p_{μ_i}. Therefore, Equation 2.9 gives the predicted value of O at a temperature β_1 as calculated by our Monte Carlo simulation. For clarity, we note that the index i is used to denote the subset of states that have been selected from the system by our Monte Carlo simulation i.e. our sampled states.

$$\langle O \rangle = \frac{\sum_\mu O_\mu e^{-\beta E_{\mu_i}}}{\sum_\mu e^{-\beta E_\mu}} \ , \tag{2.8}$$

$$\langle O \rangle = \frac{\sum_{i=1}^{M} O_{\mu_i} p_{\mu_i}^{-1} e^{-\beta_1 E_{\mu_i}}}{\sum_{j=1}^{M} p_{\mu_j}^{-1} e^{-\beta_1 E_{\mu_j}}} \ . \tag{2.9}$$

In the Monte Carlo schemes discussed previously, the weights in which we selected individual sample states was given by the Boltzmann distribution (the "probability distribution" of the previous paragraph). However, having already obtained a sample of states weighted by the Boltzmann distribution at one particular temperature, we may choose to instead reweight our entire set of samples by the Boltzmann distribution of another nearby temperature $\frac{1}{k_B T_2} = \beta_2$ as given by Equation 2.10. Here Z_2 is the partition function at temperature T_2.

$$p_{\mu_i} = \frac{1}{Z_2} e^{-\beta_2 E_{\mu_i}} \ . \tag{2.10}$$

Substituting Equation 2.9 into Equation 2.10, we obtain Equation 2.11, a quite simple formula for the reweighting of measurements of quantity O taken at T_1 to a nearby temperature T_2. In other words, once we have obtained a series of samples of quantity O at a

[6] Given by the Boltzmann distribution at the temperature of interest.

given temperature T_1, we may use Equation 2.11 to obtain an estimate of quantity O at nearby temperatures T_2.

$$\langle O \rangle_{T_2} = \frac{\langle \sum_{i=1}^{N} O_{\mu_i} e^{-(\beta_2-\beta_1)E_{\mu_i}} \rangle_{T_1}}{\langle \sum_{j=1}^{N} e^{-(\beta_2-\beta_1)E_{\mu_j}} \rangle_{T_1}} \ , \tag{2.11}$$

Single histogram reweighting allows for the generation of thermodynamic data at numerous temperatures from a single simulation point. Thus it allows for the resolution of features that are difficult to accurately sample such as sharp peaks and/or allows us to run simulations at far fewer temperatures (thus taking far less time and resources) and interpolate the results for temperatures between our simulation points. One notable historical drawback of the single histogram method is that the entire time series of measurements must be stored[7], however the rise of faster and more powerful computers with more memory has made this issue irrelevant. We further note that saving a time series of data allows for further post-simulation analysis and so can be useful.

Single histogram reweighting "returns" good results near the initial chosen temperature. However, as one moves to temperatures corresponding to the tails of the histograms, one is unable to accurately reweight as the tails do not provide adequate statistics. We thus turn to a technique known as the *multiple* histogram method developed by Ferrenberg and Swendsen in 1979 [56] in which overlapping simulation data from multiple temperatures are *stitched* together to allow for the extrapolation of simulation results across a far broader temperature regime.

An in-depth explanation of multiple histogram reweighting can be found in many texts such as Newman and Barkema [39]; here we simply provide a brief overview. In short the Monte Carlo simulation is run at several temperatures $T_1 < T_2 < T_3 ... < T_M$ spaced such that the energy histograms of each simulation overlap with one another[8]. The simulations are then reweighted and stitched together to create a distribution encapsulating the entire temperature set from T_1 to T_M that can be reweighted to obtain the statistics for any arbitrary temperature between T_1 to T_M. Despite appearing quite complex, the actual implementation is quite straightforward. Naturally, in the reweighting procedure we must numerically compute a numerical estimate of the partition function Z_k of the simulation at each of our j starting temperatures [39]. This is given by Equation 2.12

[7] Originally due to computational constraints, the simulation data was first binned and the corresponding histogram reweighted hence the name.

[8] If the simulations do not overlap then attempts to reweight at a temperature corresponding to a tail will be inaccurate due to the poor statistics that the tails possess.

$$Z_k = \sum_{i,m} \frac{1}{\sum_j n_j Z_j^{-1} e^{(\beta_k - \beta_j)E_{i,m}}} \ , \tag{2.12}$$

in which we sum over all m samples taken during the ith simulation and over the n_j samples in simulation j. Equation 2.12 is a little confusing, we have in fact a set of j Equation 2.12s which must be solved self consistently. For a particular Z_k the sum in the denominator represents a sum over the j values of Z (i.e. temperatures T_1 to T_M) – these values of Z are iteratively solved for until convergence. A good gauge of this convergence is given in Equation 2.13 [39]; where x represents the iteration number and Z_k^x is the value of the partition function at that temperature k on iteration x. We say that convergence has been achieved when Δ^2, a measure of much the values of Z_k change between successive iterations, is less than some cutoff.

$$\Delta^2 = \sum_k \left[\frac{Z_k^x - Z_k^{x-1}}{Z_k^x}\right]^2 \ . \tag{2.13}$$

A numerical estimate of the partition function at a given inverse temperature β can then be calculated as given in Equation 2.14 once we have obtained a good estimate of the Z_j for the initial j temperatures.

$$Z(\beta) = \sum_{i,m} \frac{1}{\sum_j n_j Z_j^{-1} e^{(\beta - \beta_j)E_{i,m}}} \ . \tag{2.14}$$

The values of thermodynamic quantities such as the energy can then be calculated using Equation 2.15.

$$\langle E(\beta) \rangle = \frac{1}{Z(\beta)} \sum_{i,m} \frac{E_{i,m}}{\sum_j n_j Z_j^{-1} e^{(\beta - \beta_j)E_{i,m}}} \ . \tag{2.15}$$

2.1.4 Nonlocal or Cluster Moves

As discussed in the previous sections, single spin updates tend to result in great difficulties in moving the simulation from one low energy state to another if the states are separated by energy barriers that cannot be relatively easily traversed by a series of local moves without entering high energy intermediate states. One might also just desire a more efficient algorithm with reduced autocorrelations for the simulation of large systems near a phase

transitions. For this reason, a number of non-local *cluster* moves have been proposed such as the Swendsen-Wang [42] and Wolff [45] algorithms which flip groups of spins with 0 energy cost. With regards to frustrated pyrochlore systems we will focus on the *ice loop move* as used by Melko and Gingras [57] to study dipolar spin ice, a method previously used for other ice models [39].

Dipolar spin ice at low temperatures enters the so called *two-in/two-out* spin configuration where, on each tetrahedron, two of the four spins point inwards along their local axes toward the center of the tetrahedron, while the other two spins point outwards away from the center. This is a highly degenerate state with high energy barriers – to exit one two-in-two-out state and enter another one must create intermediate higher energy *three-in-one-out* and *one-in-three-out* states at a significant energy cost. In their investigation of Ising dipolar spin ice, Melko and Gingras [57] utilized a loop move to show the existence of a first order transition into a long-range ordered state; previous work having used solely single spin-flips [58] showed a disordered low temperature state. Unlike the single spin algorithm which must traverse high energy intermediate states, the loop algorithm flips groups of spins at once moving the simulation quickly and efficiently through the *two-in/two-out* spin ice manifold. This clearly demonstrates the strength of multiple spin-flip algorithms – the removal of single spin-flip energy barriers allows the simulation to sample configuration space more effectively and find potential long-range ordered states at temperatures when $T \ll J$. Thus, for frustrated systems, loop or cluster algorithms may be of particular use.

The loop algorithm presented by Melko and Gingras [57] proceeds quite simply; spins on the lattice are assigned a colour, black if they point inward towards the center of the tetrahedron and white if they point outward. A loop consisting of at least 6 spins of alternating colours is constructed as long as each tetrahedron that the loop traverses is composed only of *two-in/two-out* tetrahedra[9]. The spins on the loop are then "flipped" by reversing them (inward pointing spins now point outwards and vice versa) with the resulting state still obeying the two-in/two-out ice rule. Due to the presence of additional dipolar interactions, the energy to "flip" a loop may not be exactly zero. If this is the case, the loop is "flipped" according to the Metropolis critereon. At nonzero temperatures, the loop algorithm must be combined with single spin-flip moves as loops do not enter or affect defect tetrahedra thus breaking ergodicity.

This loop algorithm has been extended to the biquadratic Heisenberg pyrochlore with $b < 0$ biquadratic interactions by Shinaoka *et al.* [59] [60]. There are several notable difficulties involved in the generalization to Heisenberg spins. First, recall that while the nematic phase expected for negative biquadratic coupling does break symmetry, Heisenberg

[9] To maintain detailed balance.

systems will still possess a global O(3) symmetry. Simply put, while spins will order with respect to the nematic axis, the nematic axis is not fixed and will freely rotate as the simulation proceeds. Thus the vector describing the nematic axis – the director – must be determined each time a measurement is made. Furthermore, by possessing O(3) symmetry, every spin in the lattice is distinct – all 'black' and all 'white'[10] spins are expected to possess slightly different orientations and thus the energy of a loop will increase with loop size and temperature. Nevertheless, an *extended loop algorithm* was shown to significantly reduce autocorrelations as compared to single spin-flips, especially at low temperatures [59].

The extended loop algorithm proceeds [60] in more or less the same manner as the original loop algorithm used by Melko and Gingras [57]. The nematic axis (or director) is calculated by randomly selecting a number of tetrahedra in the lattice m and iteratively computing a projection axis by means of Equation 2.16 (in which the sum runs over the spins i in each of the m tetrahedrons, sgn is the sign function, and $\vec{a}_n$ is an estimate for the director) for those tetrahedron. Shinaoka *et al.*[59][60] proposes three different ways in which one can modify the colours in a loop; i) flip the parallel components of the spin with regards to the director (*flip-parallel*), ii) flip the xyz components of the spin (*flip-xyz*), or iii) rotate spins in the loop from one position in the loop to another (*rotate*)[11]. In general, these three methods represent a significant improvement over single spin-flips, although this improvement depends on temperature and biquadratic strength.

$$\vec{a}_{n+1} \propto \sum_{i \in \{T_m\}} \mathrm{sgn}(S_i \cdot \vec{a}_n) S_i \ . \tag{2.16}$$

While a negative biquadratic interaction leads to a collinear ground state, a positive biquadratic interaction leads to ordering in which spins on a tetrahedron orient in four mutually distinct directions (angles of $\sim 109.5°$ between spins) each of which we assign a colour. The pyrochlore lattice with a postive biquadratic interaction will thus possess four "colours" of spins as opposed to two. With no ordering axis or director present, modifications to the loop algorithms introduced in this section are necessary. Later in this thesis we will report an investigation of the modification of this alternating two colour loop into an environment where spins can posses not two but four colours.

[10] Colour is assigned with regards to a spin's parallel or antiparallel orientation with respect to the nematic ordering director.

[11] The spins in the loop are sequentially labeled one through k. The spin with label 1 is moved into the position in the lattice occupied by the spin labeled 2. The spin labeled 2 is moved into the position in the lattice occupied by the spin labeled 3. Etc.

2.1.5 Measurements and Errors in Monte Carlo Simulations

Evidence for phase transitions is given by changes in thermodynamic quantities tracked by the Monte Carlo simulation. For instance, a discontinuity in the energy as the system approaches the critical temperature T_c is evidence for a first-order phase transition. The order parameter should likewise display a clear jump at the transition temperature. Quantities such as the energy, magnetization, heat capacity, etc., generated in a Monte Carlo simulation possess some associated error as a Monte Carlo simulation only samples the distribution of states and so will contain sampling error. In this thesis we calculate errors using the Jacknife method [39]. Here, the average value of some quantity such as the energy is calculated from the set of N measurements. The N energy measurements are then divided into M blocks. For each block labelled i the $M_{\mathrm{i}}^{\mathrm{th}}$ block is removed from the data set and the average value of the energy computed over the other $M-1$ data blocks giving an energy E_i. The error in the energy is given by Equation 2.17, where E is the average energy of all N measurements.

$$\delta E = \sqrt{\sum_{i=1}^{M} (E_i - E)^2} \ . \tag{2.17}$$

It is important to note that the computed errors are by no means guaranteed to be accurate. A simulation that does not accurately sample the configuration space of the system due to poor ergodicity will give erroneous results with errors that are not meaningful. Ultimately generated results and their associated errors depend on the simulation itself – a misbehaving simulation (with for instance extreme ergodicity issues) will not return accurate results of, perhaps, any nature.

Finally, we remark on the more subtle details of our Monte Carlo simulations. It is convenient for computational purposes to structure the pyrochlore lattice as a set of 4 interlocking FCC lattices centered at the following coordinates; (0, 0, 0), (0, 0.5, 0.5), (0.5, 0, 0.5) and (0.5, 0.5, 0). These four FCC sublattices form the conventional 16 spin pyrochlore unit cell which has a length of 1 along the x, y, and z directions – the lattice then consists of $16L^3$ spins. We use periodic boundary conditions for all calculations in this work.

All Monte Carlo simulations in this thesis make use of simulated annealing. In general, sampling of thermydynamic quantities occurs every so many steps (in this work chosen as 4 or 8) steps to reduce correlations between samples. Simulation data is often saved as a time series – though cumbersome and space consuming, this allows for post-processing of data (e.g. in the histogram reweighting method).

2.2 Correlations and Structure Factors

It is often useful to investigate correlations between spins in the lattice. For this reason we compute quantities such as the spin structure factor given below

$$S(\vec{q}) = \sum_{i,j;\alpha,\beta} \left[e^{i(\vec{r_{i\alpha}} - \vec{r_{j\beta}})\cdot\vec{q}} \right] \langle S_{i\alpha} \cdot S_{j\beta} \rangle \ , \tag{2.18}$$

$$\vec{q} = \frac{2\pi}{L}(n_x\vec{x} + n_y\vec{y} + n_z\vec{z}) \ . \tag{2.19}$$

Here the indices i and j run over the conventional cubic cells in the lattice while α and β run over the 16 sublattice spins. The displacement vector from one spin to another is given by $(\vec{r_{i\alpha}} - \vec{r_{j\beta}})$ and $\langle S_{i\alpha} \cdot S_{j\beta} \rangle$ is the scalar product between the Heisenberg spins, averaged over the number of samples taken during the Monte Carlo simulation.

We can simplify Equation 2.18 by taking the real part of the exponential ($e^{ix} = \cos x + i \sin x$) and rewrite it as

$$S(\vec{q}) = \sum_{i,j,\alpha,\beta} \left[\cos\left((\vec{r_{i\alpha}} - \vec{r_{j\beta}}) \cdot \vec{q} \right) \right] \langle S_{i\alpha} \cdot S_{j\beta} \rangle \ . \tag{2.20}$$

2.3 Summary

An exposition of the Monte Carlo methods employed in this work has been presented. Basic single-spin Metropolis Monte Carlo as well as a number of refinements such as parallel tempering and simulated annealing have been discussed. The non-local loop moves previously employed for the pyrochlore lattice for similar models such as dipolar spin ice and the $b < 0$ bilinear-biquadratic Heisenberg pyrochlore have been reviewed and their particular effectiveness in equilibration brought to light. More nuanced details of our Monte Carlo simulations have been presented to give context to Chapter 4 which highlights the difficulties of equilibration into the octupolar phase. Various post-processing methods such as histogram reweighting that can improve the quality of simulation results have also been discussed.

In the following chapters, we will employ these methods first on the bilinear-biquadratic model with negative biquadratic interactions as presented in the literature [18] before flipping the sign of the interaction and investigating the octupolar phase expected in the bilinear biquadratic model with $b > 0$.

Chapter 3

The $b < 0$ Bilinear-Biquadratic Heisenberg Pyrochlore

In this section, we briefly investigate the $b < 0$ bilinear-biquadratic Heisenberg model (Equation 3.1).

$$H = J \sum_{<ij>} s_i \cdot s_j + b \sum_{<ij>} (s_i \cdot s_j)^2 \ , \tag{3.1}$$

As shown in previous work [18], a weak first-order phase transition is observed at $T \sim b$ from the paramagnetic state into a nematic state. The work by Shannon, Penc, and Motome [18] shows a sharp peak in the heat capacity that scales with the size of the system and a clear jump in the order parameter[1]. Another group [60] has investigated the bilinear-biquadratic ($b < 0$) and proposed a non-local loop move. As both quadrupolar and octupolar ordering can be described by the same Hamiltonian (apart from the sign on b), it is hoped that the bilinear biquadratic model with $b < 0$ will provide a fertile testing ground for our later investigation with $b > 0$.

3.1 Order Parameters for the Biquadratic Model

In our investigation of the bilinear-biquadratic model, a variety of order parameters will be used to characterize the states that our simulation enters into. To describe ordering

[1] To observe ordering into a nematic phase, the quadrupolar tensor order parameter (Q) is used. This order parameter is described later in the chapter.

into a nematically ordered phase, the quadrupolar order parameter is used as defined by Shannon , Penc and Motome [18]. The quadrupolar order parameter is defined using a rank-2 tensor (Equation 3.2) and is composed of 5 independent components (labeled α and shown in Equation 3.3). The components of the spins, S_x, S_y, S_z, are defined globally across the entire lattice.

$$Q^{\alpha} \equiv \frac{1}{N} \sum_{i=1}^{N} Q_i^{\alpha} \ . \tag{3.2}$$

$$\begin{aligned} Q_i^{3z^2-r^2} &\equiv \frac{1}{\sqrt{3}} \left[2(S_i^z)^2 - (S_i^x)^2 - (S_i^y)^2 \right] \ , \\ Q_i^{x^2-y^2} &\equiv (S_i^x)^2 - (S_i^y)^2 \ , \\ Q_i^{xy} &\equiv 2S_i^x S_i^y \ , \\ Q_i^{xz} &\equiv 2S_i^x S_i^z \ , \\ Q_i^{yz} &\equiv 2S_i^y S_i^z \ . \end{aligned} \tag{3.3}$$

Spins in the system described by Equation 3.1 with $b < 0$ will order along a common nematic axis which is invariant under O(3) rotations. This can be detected using the order parameter given in Equation 3.4 where each of the five components is first calculated across all spins in the lattice e.g. $Q^{3z^2-r^2} = \frac{1}{N} \sum_{i=1}^{N} Q_i^{3z^2-r^2}$.

$$Q \equiv \sqrt{(Q^{3z^2-r^2})^2_+ (Q^{x^2-y^2})^2 + (Q^{xy})^2 + (Q^{xz})^2 + (Q^{yz})^2} \ . \tag{3.4}$$

For simplicity, references to the quadrupolar order parameter generally refer to this **magnitude** Q (and likewise for the octupolar order parameter which we shall describe shortly). In a perfectly nematic ordered state with all spins collinear, the quadrupolar order parameter takes on its maximal value of $\frac{4}{3}$. In a completely disordered state this tensor order parameter takes on a value of 0 [2].

The octupolar phase, predicted by Wan and Gingras [31] to exist in the $b > 0$ bilinear-biquadratic Heisenberg pyrochlore model, is best described by an octupolar order parameter, a rank-3 traceless tensor order parameter [18] and whose value is 0 in a disordered state

[2] In the disordered state, the orientations of spins are random and uncorrelated i.e. $\langle S_i \rangle = 0$ and $\langle S_x \rangle^2 = \langle S_y \rangle^2 = \langle S_z \rangle^2$. Each of the 5 components of the quadrupolar order parameter as shown in Equation 3.3 then reduces to 0.

and $\frac{2}{3}\sqrt{2} \sim 0.942809$ in an perfectly ordered octupolar or tetrahedral state. This global tensor order parameter is defined in Equation 3.5 with its 7 independent components given in Equation 3.6.

$$T^{\alpha} \equiv \frac{1}{N}\sum_{i=1}^{N} T_i^{\alpha} \ . \tag{3.5}$$

$$\begin{aligned}
T_i^{x^3-3xy^2} &\equiv (S_i^x)^3 - 3(S_i^x)(S_i^y)^2 \ , \\
T_i^{y^3-3yx^2} &\equiv (S_i^y)^3 - 3(S_i^y)(S_i^x)^2 \ , \\
T_i^{z(x^2-y^2)} &\equiv \sqrt{6}[(S_i^x)^2 - (S_i^y)^2](S_i^z) \ , \\
T_i^{xyz} &\equiv 2\sqrt{6}S_i^x S_i^y S_i^z \ , \\
T_i^{x(r^2-5z^2)} &\equiv \sqrt{\frac{3}{5}}S_i^x[(S_i^x)^2 + (S_i^y)^2 - 4(S_i^z)^2] \ , \\
T_i^{y(r^2-5z^2)} &\equiv \sqrt{\frac{3}{5}}S_i^y[(S_i^x)^2 + (S_i^y)^2 - 4(S_i^z)^2] \ , \\
T_i^{z(3r^2-5z^2)} &\equiv \sqrt{\frac{2}{5}}S_i^z[3(S_i^x)^2 + 3(S_i^y)^2 - 2(S_i^z)^2] \ .
\end{aligned} \tag{3.6}$$

To address the O(3) symmetry present in the model we compute and use the magnitude of the octupolar tensor order parameter to detect the presence of octupolar ordering in the same manner as for quadrupolar ordering; each of the seven components is computed across all N spins before the total magnitude is computed.

$$\begin{aligned}
T^2_{\text{Zhit}} \equiv (T^{x^3-3xy^2})^2 + (T^{y^3-3yx^2})^2 + (T^{z(x^2-y^2)})^2 + (T^{xyz})^2 + \\
(T^{x(r^2-5z^2)})^2 + (T^{y(r^2-5z^2)})^2 + (T^{z(3r^2-5z^2)})^2 \ .
\end{aligned} \tag{3.7}$$

There exist numerous equivalent descriptions of the octupolar order parameter. Another way of writing the octupolar order parameter is given by Zhitomirsky [61] (Equation 3.8) in which the sum over i, j runs over all spin in the lattice.

$$T^2 = \frac{1}{N^2}\sum_{i,j}\left[\langle (S_i \cdot S_j)^3\rangle - \frac{3}{5}\langle (S_i \cdot S_j)\rangle\right] \ , \tag{3.8}$$

which ranges from 0 in a disordered state to $\frac{3}{15\sqrt{3}}+\frac{1}{10} \sim 0.21547$ in a fully tetrahedral state[3]. Though seemingly complex, the tensor octupolar parameter given used by Shannon, Penc, and Motome [18] has been decomposed in such a way that it avoids pairwise interactions thus making it far less time consuming to calculate[4]. A final subtlety must be noted, looking at Equation 3.8, one notices that the value of the octupolar order parameter will actually be maximized not when spins are organized in a tetrahedral arrangement but when spins are *ferromagnetically* aligned with the scalar product $S_i \cdot S_j = 1$. The octupolar order parameter as defined in Equation 3.8 will have a value of $\frac{2}{5}$ in a ferromagnetically-ordered state. This is likewise true for the octupolar tensor order parameter which possesses a maximal value of $\frac{2}{5}\sqrt{10}$ in a ferromagnetic state.

Quadrupolar and octupolar order can often coexist [18][61][62] and one must assign the correct order parameter to the system at hand. Consider a tetrahedron with the spins on each of its corners in a perfectly tetrahedral state. If the spins are subjected to a uniaxial interaction along the z-axis (i.e. placed in a magnetic field), they will then start to possess a rod-like symmetry as they begin to align with respect to the magnetic field. "Stretched" along the z axis, the tetrahedron placed in the field will be distinguished from its previous state by a nonzero quadrupolar order parameter. Thus we can see that if both order parameters are present, determining which order parameter is the primary order parameter can by a subtle process.

3.2 Reproduction of Previous Literature Results

Although it is not the direct focus of this work, the $b < 0$ bilinear biquadratic Heisenberg pyrochlore provides a well-characterized testing ground for our Monte Carlo simulations. We therefore briefly reproduce the results of Shannon, Penc and Motome[18] before flipping the sign of the biquadratic interaction in Chapter 4. As expected, the system undergoes a first-order transition at $T \sim b$, entering a nematic 2-up/2-down as shown in Figure 3.1[5] state with no long-range order [18] (Figure 3.1). The specific heat and quadrupole tensor order parameter obtained from our Monte Carlo simulations are shown in Figure 3.2

[3]In a tetrahedral state, spins are arranged into four mutually tetrahedral groups. A comparison *between* groups of spins reveals that $\frac{3}{4}$ of spins are are oriented such that $S_i \cdot S_j = -\frac{1}{\sqrt{3}}$ (i.e. spins within one group compared to spins in the other three groups). The remaining $\frac{1}{4}$ spins (spins all in the same group) are aligned parallel to one another with $S_i \cdot S_j = 1$. Substituting these two values into Equation 3.8 returns a value of $\frac{3}{15\sqrt{3}} + \frac{1}{10} \sim 0.21547$.

[4]Scales as $O(N)$ rather than $O(N^2)$.

[5]The nematic axis is *unfixed* and possesses O(3) symmetry and so the *up* and *down* spin states have no *a priori* global orientation.

along with the curve obtained using the Ferrenberg Swendsen multihistogram reweighting technique (open red circles).

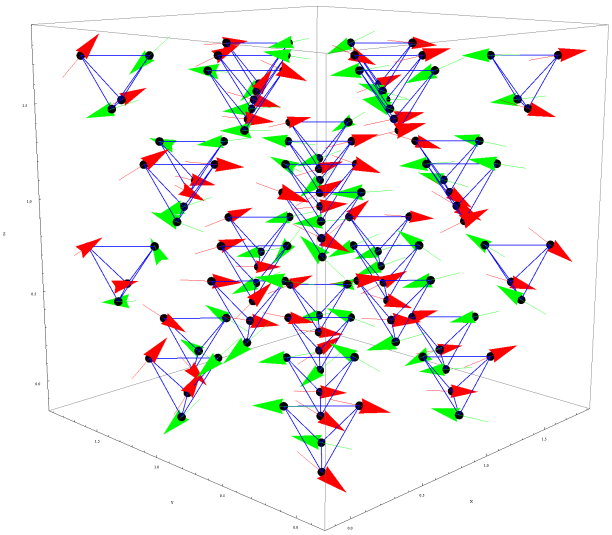

(a)

Figure 3.1: The nematic phase for $b < 0$ for a $2 \times 2 \times 2$ chunk of the lattice. Spins are arranged in a 2-up/2-down nematic phase with 'up' and 'down' spins coloured green and red respectively.

The results obtained from histogram reweighting is quite sensitive to the quality of the Monte Carlo simulation data. Figure 3.3 shows the time series of the energy and quadrupolar order at the peak of the specific heat in Figure 3.2a. We note that ergodicity does not appear to be an issue and that the Monte Carlo simulation does not freeze or get "stuck" – Chapter 4 shows that this is not true with $b > 0$. Furthermore, as the size of the system is relatively small and the transition does not appear to be strongly first order, a bimodal energy distribution is not observed. We note that though histograms of the energy at the transition are *wider* than those away from the transition, they do not possess separate peaks and so histogram reweighting returns accurate results as evidenced in Figure 3.3 where the calculated reweighted results agree with the simulation results away from the temperature points used in the reweighting.

For larger simulation sizes, a bimodal structure was observed to develop in the energy histograms as expected for large systems undergoing a first-order transtion. Finally, we note that our simulation results agree with those of Shannon, Penc, and Motome [18].

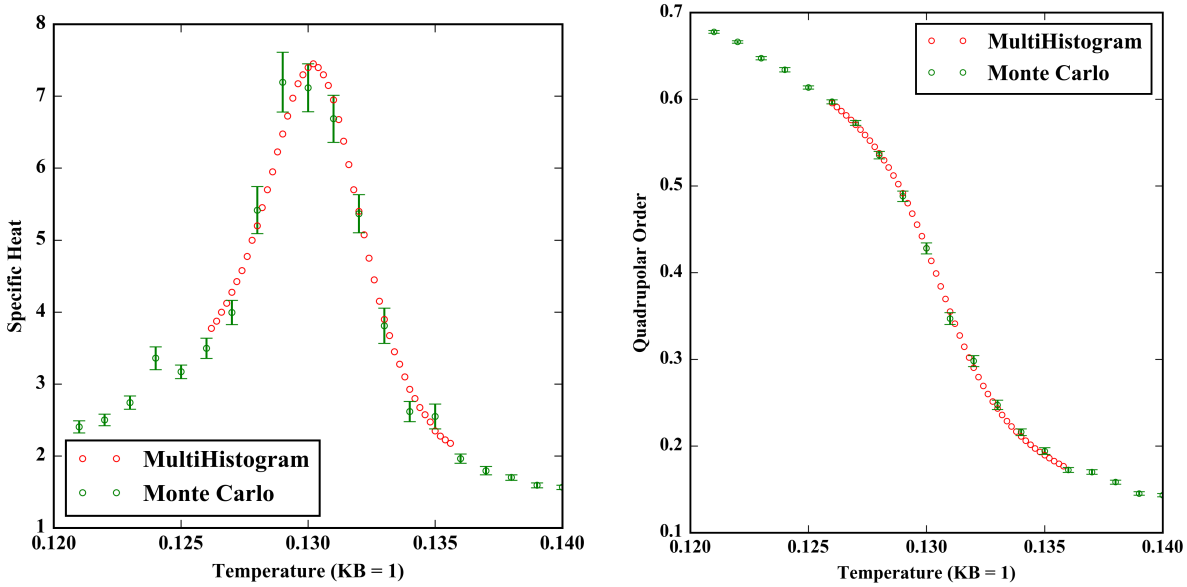

(a) Specific Heat

(b) Quadrupole Order

Figure 3.2: The specific heat and quadrupolar order parameter for θ_b = -0.09966, $L = 4$ from Monte Carlo simulation and reweighting. A θ_b value of -0.09966 corresponds to a ratio of $b/J \sim$ -0.1 ($\tan\theta_b$). For reweighting, three temperatures ($T = 0.126$, 0.130, and 0.136) were used. 250,000 Monte Carlo steps were computed for each data point.

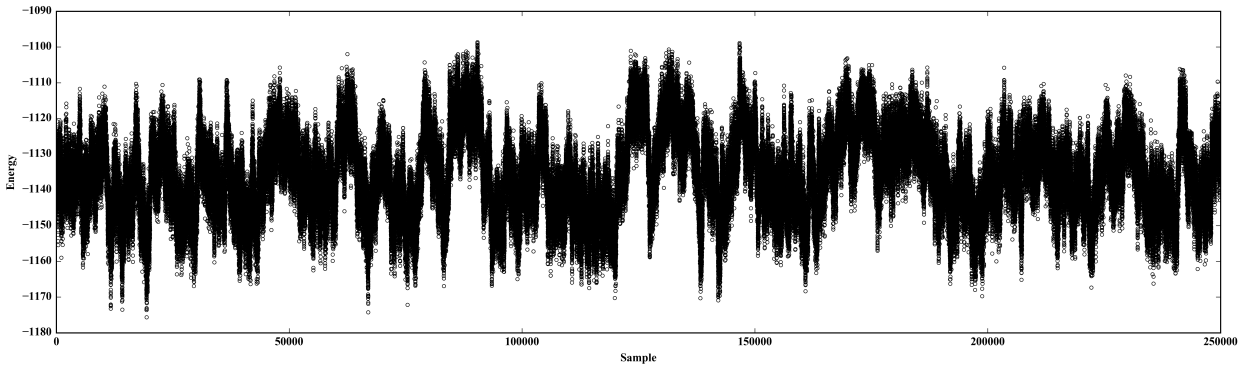

(a) Energy

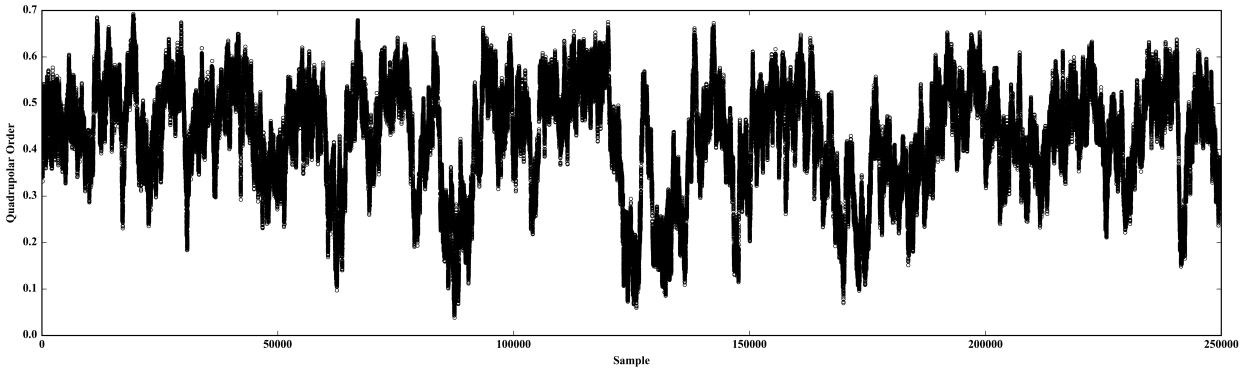

(b) Quadrupole

Figure 3.3: Time series of a) the energy and b) the quadrupolar order parameter at a temperature of $T = 0.13$ (θ_b = -0.09966, $L = 4$) corresonding to the peak of the specific heat shown in Figure 3.2a. Each sample represents a measurement after one Monte Carlo sweep of the lattice.

The spin-spin $S(q)$ and quadrupolar $Q(q)$ structure factors

$$Q(\vec{q}) = \sum_{i,j,\alpha,\beta} \left[e^{i(\vec{r_{i\alpha}} - \vec{r_{j\beta}})\cdot\vec{q}} \right] \langle Q_{i\alpha} \cdot Q_{j\beta} \rangle \ , \tag{3.9}$$

are calculated above and below the transition temperature and are shown in Figure 3.4. Above the $T \sim 0.13$ transition, we note the characteristic "pinch-points" of the antiferromagnetic Heisenberg ($b = 0$) model [30][63][65]. As we slowly cool below the transition temperature, this pinch-point scattering is slowly "quenched" (much more significantly so at lower temperatures). Likewise, above the transition, we note the onset of quadrupolar ordering with $\vec{q} = 0$ in the quadrupolar structure factor which condenses into sharp peaks in the ordered phase. Bragg peaks at [1,1,1] and its associated points are seen representing scattering off the FCC lattice sublattices (with four FCC sublattices we note that the intensity of these peaks is precisely $\frac{1}{4}$ that of the $\vec{q} = 0$ peaks).

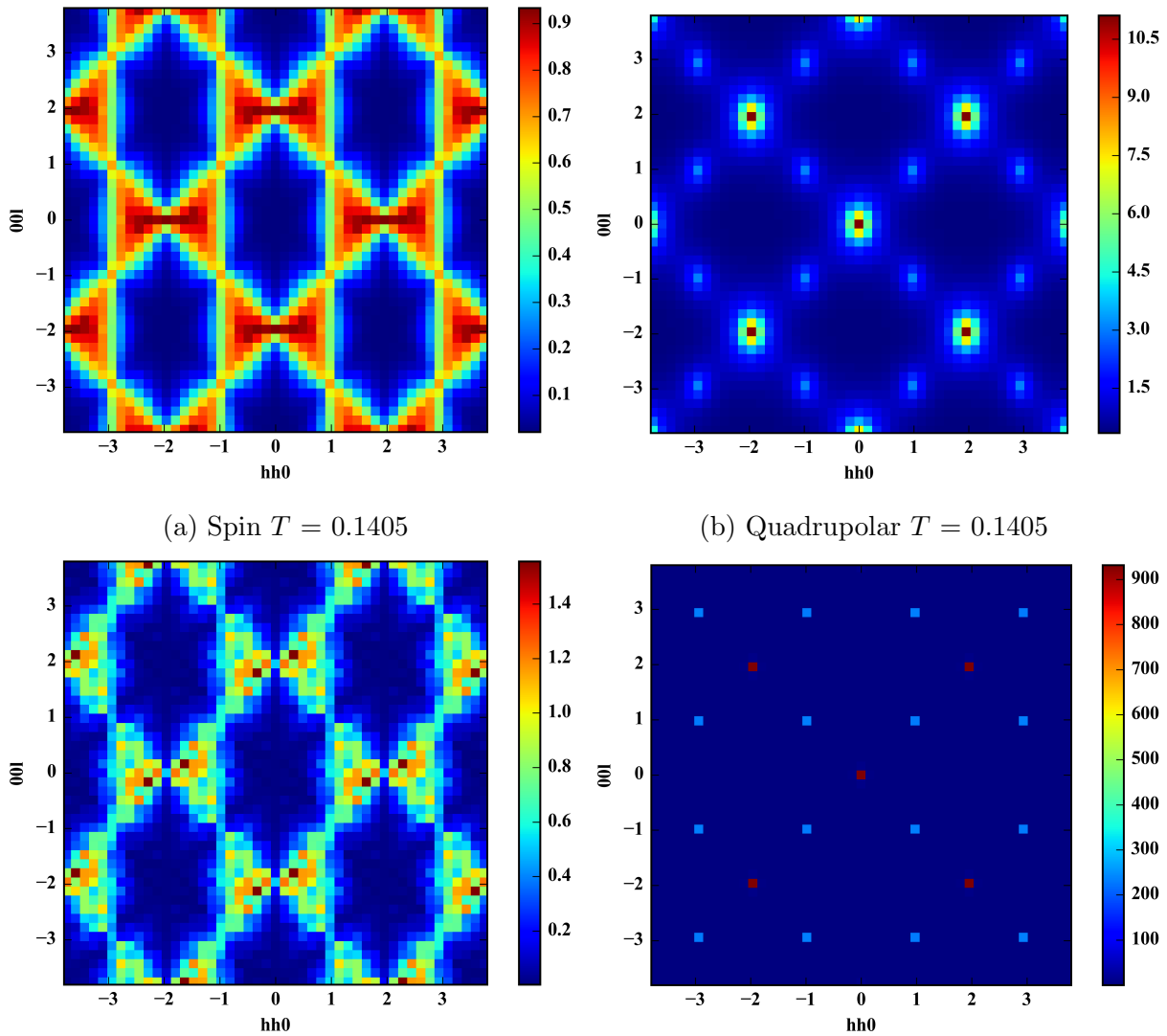

(a) Spin $T = 0.1405$

(b) Quadrupolar $T = 0.1405$

(c) Spin $T = 0.113$

(d) Quadrupolar $T = 0.113$

Figure 3.4: The spin-spin and quadrupolar structure factors just above (panes a and b) and below (panes c and d) the transition temperature of $T \sim 0.13$ for a system size of L=6. Above the transition, we note diffuse $\vec{q} = 0$ peaks indicating the onset of quadrupolar ordering which sharpen as the system undergoes the transition into the nematic state. In the spin-spin structure factor we observe the characteristic pinch points which slowly become quenched in the ordered phase.

We remark again that the quadrupolar tensor order parameter measures effectively two types of spin orientation – oriented parallel or antiparallel to the nematic axis – and must weight each as equivalent. As such it is not a good indicator of the type of quadrupolar order present. This is because a spin oriented parallel or antiparallel to the nematic axis will be seen as identical by the quadrupolar order parameter and so $\vec{q} = 0$ ordering is always observed. Potential long range ordered states must instead be noted through other potential features in the structure factor.

Finally, it must be said that although one might be tempted to see "lines" connecting the $\vec{q}$ =0 and Bragg peaks in Figure 3.4b, there are none present – this is a visual artifact due to the diffuse scattering of the nearby peaks.

This paramagnetic to quadrupolar transition is observed by the jump in the quadrupolar order parameter and the sharpening of the peaks in the quadrupolar structure factor as the system enters a nematically ordered phase. Looking forward, we would expect similar behaviour in the octupolar order parameter and its associated structure factor as an indication of octupolar ordering for $b > 0$ biquadratic interactions. Potential differences between the quadrupolar ordering shown in this chapter and the octupolar ordered state discussed in Chapter 4 may be indicative of more complex ordering, indicating that the ground state of the $b > 0$ system could potentially possess some form of long-range order.

3.3 Summary

With $b < 0$, the bilinear-biquadratic Heisenberg pyrochlore undergoes a first-order transtion at $T \sim$ b into a nematic ordered state [18]. We note that a Monte Carlo simulation with $b < 0$ with single spin flips and simulated annealing is capable of producing good quality results – although nonlocal algorithms involving loops have been previously presented [60], we have had no difficulty reproducing the work of Shannon, Penc and Motome[18] who themselves utilize single spin-flips. Although we have not presented new work in this chapter, we have briefly described the properties of the $b < 0$ model as a comparison to our work with $b > 0$ in Chapter 4. As shall be seen in the following chapter, probing the biquadratic interaction with $b > 0$ presents a series of new computational challenges.

Chapter 4

The $b > 0$ Bilinear-Biquadratic Heisenberg Pyrochlore

In this chapter, we utilize the Monte Carlo methods and associated techniques presented in Chapter 2 to investigate the ordering of the classical $b > 0$ bilinear-biquadratic Heisenberg pyrochlore into a putative octupolar state. We will discuss the order parameters associated with octupolar ordering and show that this octupolar ordered state possesses no long-range order. Numerous difficulties encountered in the simulation of this system such as severe ergodicity issues with a single spin-flip algorithm due to the glassiness of the low temperature states will be discussed. We will also remark on some of the pecularities that we have encountered such as the sharpness of the first-order transtion and potential metastable weathervane states that bear relation to the work done by Wan and Gingras [31]. The potential adoption of the pyrochlore loop move to a four colour system will be presented and discussed.

4.1 Pertinent Order Parameters

As discussed in Chapter 1, multipolar ordering is often subtle and difficult to characterize; to properly characterize octupolar ordering on the pyrochlore lattice, we must employ a variety of order parameters. The quadrupolar and octupolar tensor order parameters presented in the previous chapter are computed for all simulations – the jump in the octupolar tensor order parameter T marks the onset of octupolar ordering. However the

octupolar order parameter gives less information about the type of octupolar ordering[1] and, like quantities such as the magnetization, cannot convey positional information[2]. Therefore, additional secondary order parameters that allow one to distinguish between generic octupolar states and long range ordered states are necessary.

One useful secondary order parameter is the staggered magnetization, a quantity which represents the magnetization of the four pyrochlore FCC sublattices. The staggered magnetization ranges from 0 in a paramagnetic state or in a random colour ice state, to 1 in a state where each FCC sublattice contains spins of one and only one colour i.e. the spins on each sublattice are ferromagnetically aligned. The staggered magnetization is given in Equation 4.1 where m_α, which ranges from 0 to $\frac{N}{4}$, is the magnetization of each FCC sublattice.

$$M_s = \frac{1}{N}\sum_{\alpha=1}^{4} m_\alpha \ . \tag{4.1}$$

It is also useful to introduce a parameter describing the angle between nearest-neighbours. In a perfectly tetraheral state we would expect spins to orient at a relative angle of $\cos^{-1}(-\frac{1}{3}) \sim 109.5°$. By measuring the angle between nearest-neighbour spins, the tetrahedral order parameter gives a good measure of ordering on each tetrahedron. The tetraheral order parameter has been used elsewhere [66][67][68] and is given for a single tetrahedron by Equation 4.2, where θ_{ij} is the angle between two spins in tetrahedron k.

$$S_k = 1 - \frac{3}{8}\sum_{i<j,(i,j,\in k)}^{4} \left[\cos\theta_{ij} + \frac{1}{3}\right]^2 \ , \tag{4.2}$$

We then sum this quantity over all tetrahedra in the lattice, $S \equiv \frac{1}{N}\sum_k S_k$. In a perfectly tetrahedral state, the tetahedral order parameter S attains a maximum value of 1.

Calculated over each tetrahedron the tetrahedral order parameter best describes local tetrahedral or octupolar order – in simulations a small but discrete jump is observed at the transition temperature. Despite this, the tetrahedral order parameter is important because it gives a measure of the angles between neighbouring spins and thus of the energy

[1]The octupolar order parameter only gives a measure of the degree to which octupolar order is present in the system. It does not tell us what type of ordering may be present – it is not possible to encode this kind of information with a single scalar quantity.

[2]The magnetization (for something like the 2D Ising model) tells us the ratio of *up* to *down* spins. It tells us nothing about **which** spins are up or down; multiple states will possess the same magnetization.

of the system. We clarify here that the octupolar tensor order parameter (Equation 3.7) is a measure of global ordering throughout the lattice i.e. that the four groupings of mutually tetrahedral spins that describe octupolar ordering extend over the entire lattice. It is also possible for local octupolar order to be present – spins in a given tetrahedron order pointing in particular directions at angles of 109.5° with respect to one another, but these directions are local to each tetrahedron (or a small region of the lattice). The local tetrahedral order parameter is therefore not sensitive to global order and serves to measure local octupolar ordering independent of the presence of weathervane rotations (which we will describe later in this chapter).

4.2 Thermodynamic Quantities

Our Monte Carlo simulations show that the $b > 0$ bilinear-biquadratic Heisenberg pyrochlore undergoes a first-order transition at very low temperatures from a disordered state into an octupolar ground state with no long range order[3]. This phase transition appears to be very strongly first-order for weak biquadratic interactions but weakens as the biquadratic interaction increases in strength. The results of single spin-flip Monte Carlo simulations making use of simulated annealing for $\theta_b = 0.12$ are shown in the following figures for system sizes of $L = 4$ and $L = 5$. In contrast to the negative biquadratic interaction discussed in the previous chapter, the simulation must proceed much, much longer in order to obtain good statistics of physical quantities to clearly show the transition into the octupolar ordered state. Four million Monte Carlo steps were run for each temperature in the following results with sampling occuring every 8 steps. In contrast, a mere 80,000 steps and 20,000 samples can be used to obtain reasonably good quality statistics for $\theta_b < 0$.

[3]Disregarding simulation freezing and lack of ergodicity

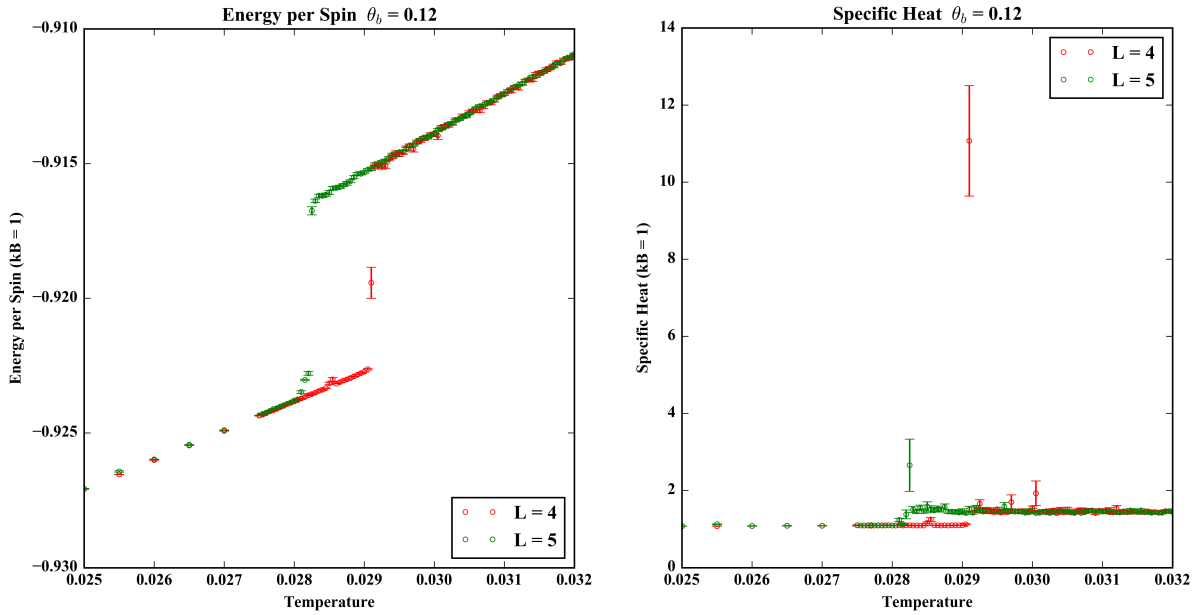

(a) Energy per Spin

(b) Specific Heat

Figure 4.1: The energy per spin and specific heat for L=4 and L=5 with $\theta_b = 0.12$. Note the sharp first order transition. Due to the freeezing of the simulation and therefore the sharpness of the transition, there is difficulty capturing the peak in the specific heat.

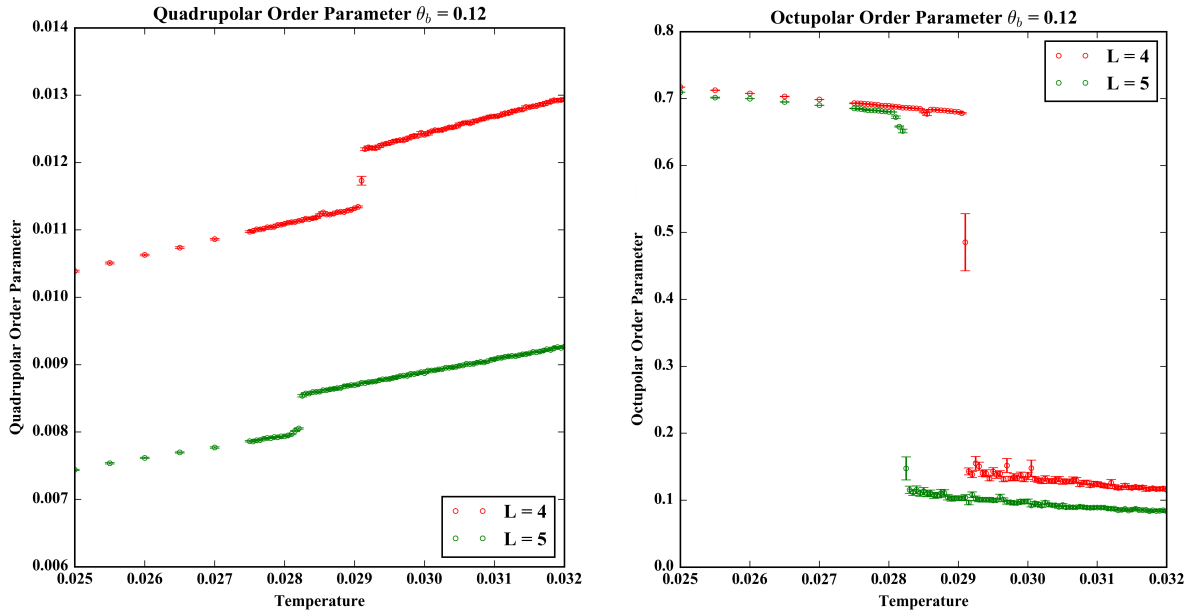

(a) Quadrupolar Order Parameter

(b) Octupolar Order Parameter

Figure 4.2: The quadrupolar and octupolar order parameters for L=4 and L=5 with θ_b = 0.12.

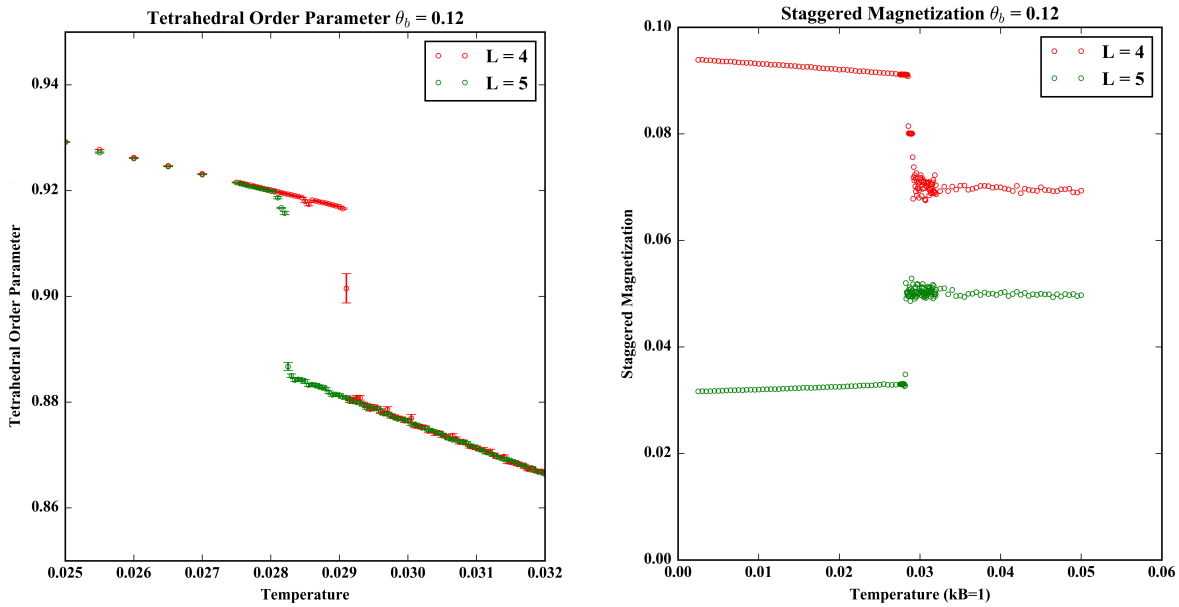

(a) Tetrahedral Order Parameter

(b) Staggered Magnetization

Figure 4.3: The tetrahedral order parameter and the staggered magnetization for L=4 and L=5 with $\theta_b = 0.12$.

Considering Figure 4.1, we note a sharp discontinuity in the energy that is difficult to capture in the simulation (we elaborate below) leading to the poor behaviour of peak in the specific heat as we calculate the heat capacity of the simulation as $C = \frac{\langle E^2\rangle - \langle E\rangle^2}{T^2}$. In general, we find that the specific heat is not well-behaved at the transition for all values of θ_b, as shall be found throughout this chapter. Thus standard methods that involve an analysis of the specific heat peak cannot be employed – at a first-order transition the height of the peak of the specific heat should be proportional to the size of the system ($C_v \propto L^d$ where d is the dimension of the system); as we cannot capture the peak we cannot comment on finite-size effects in this manner. We will comment on finite-size effects later in this chapter, but we note that for a weak biquadratic interaction it would seem that the supposed critical temperature T_c can be obtained to what appears to be a high degree of precision due to the observed sharpness of the first order transition. This is merely an illusion – due to the freezing of the simulation the transition temperature is in principle very ill-defined.

As the strength of the biquadratic interaction is increased, the jump in the order pa-

rameter becomes less pronounced and the system appears to become more weakly first order (and/or the simulation experiences significantly more issues). For example, for $\theta_b = 1.2$ (Figure 4.4) the drop in the energy occurs over a much larger temperature range. The peak of the specific heat remains poorly defined. It thus appears that the simulation proceeds very slowly through the transition and that the region near the transition may not be as depicted in Figures 4.4 to 4.6 due to freezing. Typically, thermodynamic values computed by a Monte Carlo simulation at a first order transition will possess large errors as the simulation transitions between the ordered and disordered states. This can be noted by the relatively large error bars as seen in Figure 4.1. The small error bars in the simulations with $\theta_b = 1.2$ would therefore imply that something is amiss. Unlike simulations with small θ_b, the simulation takes longer to order from the paramagnet to octupolar state with the simulation appearing to be briefly stuck in local metastable states (Figure 4.10c).

Observing the essentially flat staggered magnetization below the transition, we note extreme ergodicity and freezing issues. This freezing of the staggered magnetization implies that the ratio of spins of a given colour on each sublattice remains the same without fluctuations. While the spins in the lattice are free to rotate around (O(3) symmetery) their orientations relative to one another do not change; the lattice has frozen into a particular octupolar configuration or colour ice state. We elaborate on this later in the chapter.

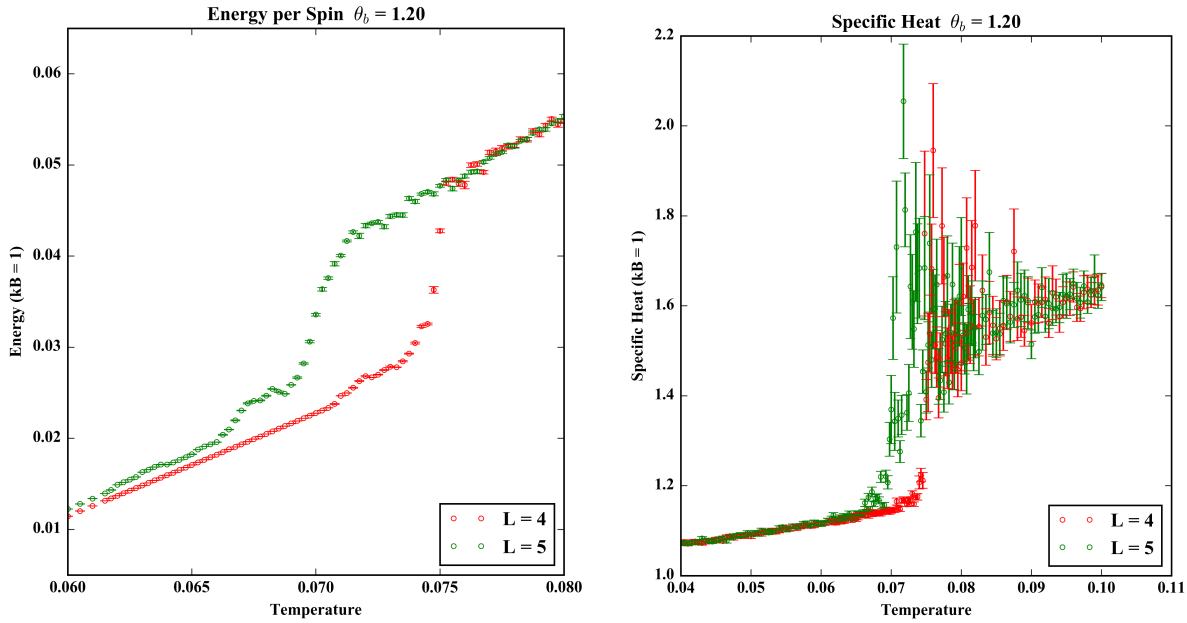

(a) Energy per Spin

(b) Specific Heat

Figure 4.4: The energy per spin and specific heat for L=4 and L=5 with $\theta_b = 1.20$.

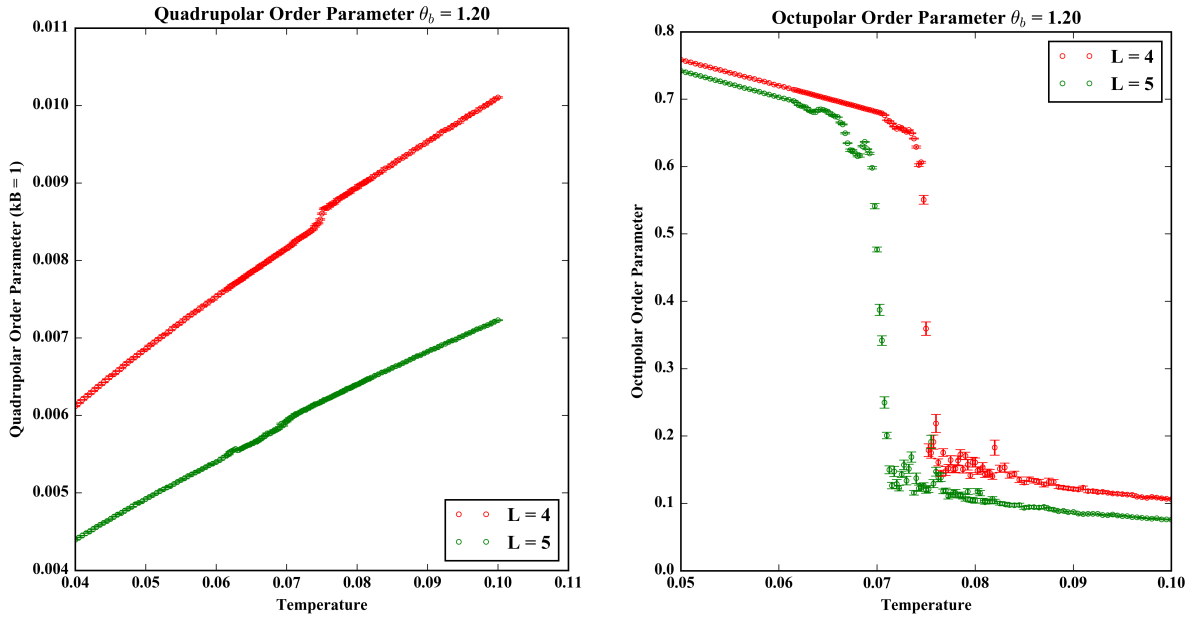

(a) Quadrupolar Order Parameter

(b) Octupolar Order Parameter

Figure 4.5: The quadrupolar and octupolar order parameters for L=4 and L=5 with θ_b = 1.20.

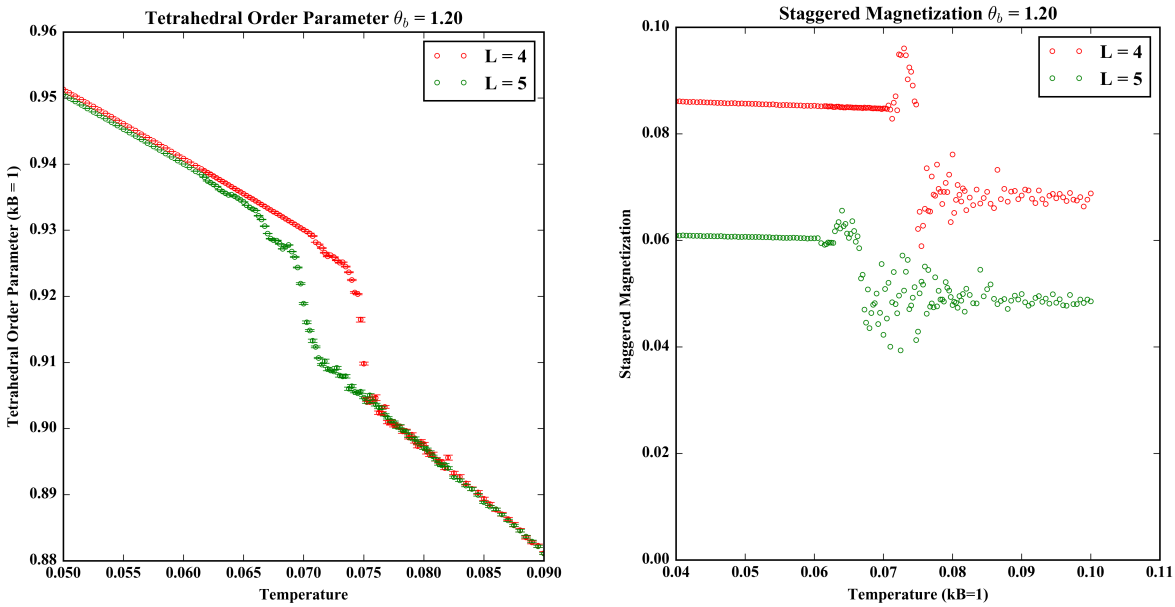

(a) Tetrahedral Order Parameter

(b) Staggered Magnetization

Figure 4.6: The tetrahedral order parameter and the staggered magnetization for L=4 and L=5 with $\theta_b = 1.20$.

Figures 4.1 to 4.6 for $\theta_b = 0.12$ and $\theta_b = 1.20$ strongly suggest the formation of a low temperature octupolar ordered phase, despite the ergodicity and freezing issues. We observe a clear drop in the energy along with a sharp rise in the octupolar order parameter giving all indications of a first order transition. Secondary order parameters such as the tetrahedral order parameter and staggered magnetization also signal this transition. The quadrupolar order parameter is included for completeness. As the system enters an octupolar phase with spins in a tetrahedral arrangement the quadrupolar order parameter, a measure of mutual collinearity, abruptly drops.

Figure 4.7 illustrates the orientation of spins in a conventional 16 spin cubic unit cell in the paramagnetic and octupolar regime. Simulations show that upon cooling, the octupolar colour ice state that is reached possess no long-range order and freezes completely into a random colour ice state. Evidence for this freezing is illustrated in Figure 4.8 and discussed in the accompanying caption. It is quite apparent that due to the freezing of the Monte Carlo simulation it is difficult to describe this system below the critical temperature; it is possible that the lack of long-range order that we observe is a consequence of freezing.

Later in this chapter we will present a brief exploration of the low temperature regime by investigating warming starting from various candidate ground states.

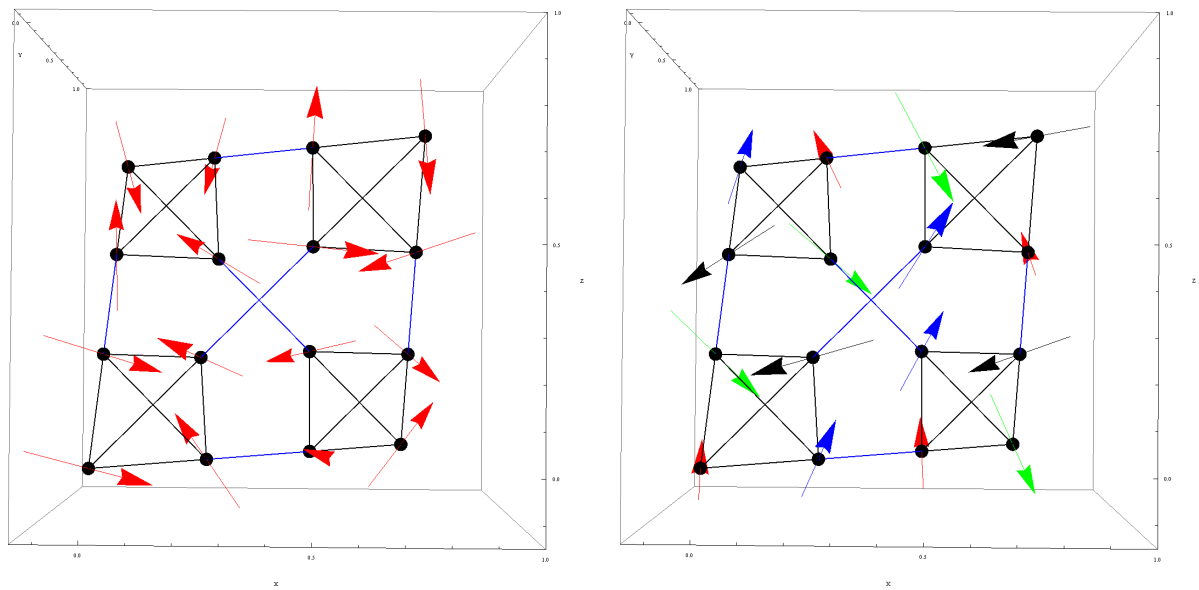

(a) Paramagnetic State

(b) Octupolar Colour Ice State

Figure 4.7: The orientation of the spins in a single conventional cell for the paramagnetic state and a random octupolar colour ice state are shown. The a sublattice tetrahedra are shown in black with blue lines corresponding to the sides of the b sublattice tetrahedra. Above the critical temperature in the paramagnetic state, we see that the spins (shown in red) on each tetrahedron are organized such that the vectors describing their orientation sum to 0 with no obvious similarities between the spins on different tetrahedra. In the octupolar state, each tetrahedron possesses four spins angled at $\sim 109.5°$ with respect to one another. Unlike in the paramagnetic state, these spins can be organized into four groups across the entire lattice with each tetrahedron possessing one spin of each colour– a global octupolar ordered phase. The spins belonging to each of these four groups have been painted different colours; black, red, blue, and green.

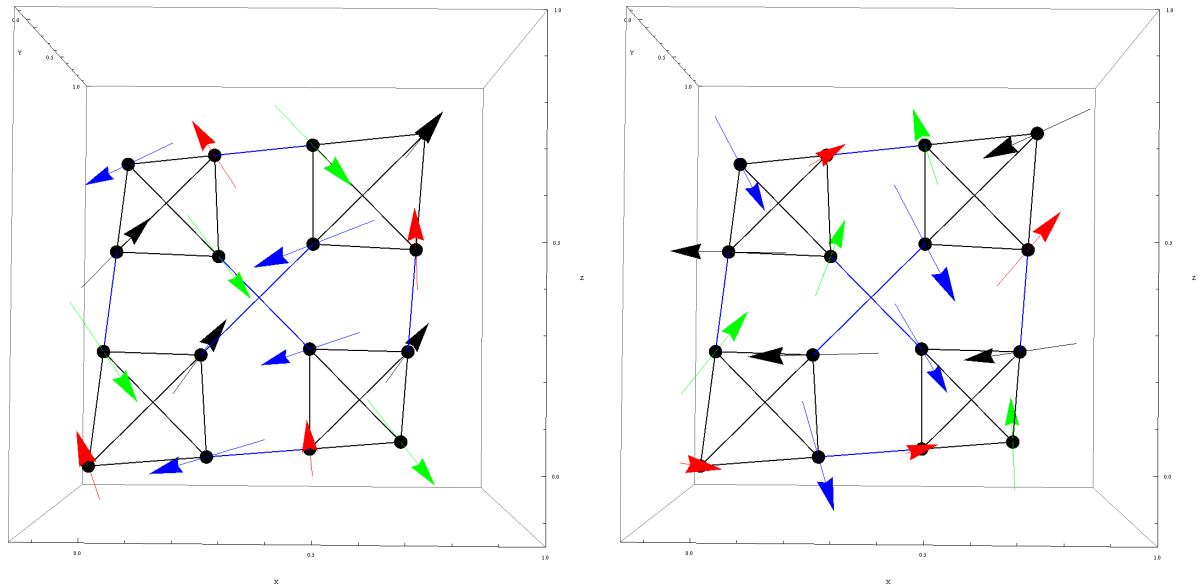

(a) $T = 0.005$ (b) $T = 0.025$

Figure 4.8: The orientation of the spins in a single conventional cell for the **same simulation** at temperatures of $T = 0.005$ (right) and $T = 0.025$ (left) with $\theta_b = 0.12$, L =4. The spins in the left and right panes have rotated due to the O(3) nature of the Hamiltonian but the colours of the spins have not changed – the simulation has *frozen out* below the critical temperature $T_c \sim 0.0291$ indicated in Figure 4.1. This same section of the lattice for this simulation at $T = 0.010$ can be seen in Figure 4.7b. Note that as the temperature is increased, spins of a given colour show greater deviations from their expected colour orientation. Four million Monte Carlo steps are completed for each temperature with temperature points spaced $\Delta T = 0.005$ apart and so 1.6×10^8 Monte Carlo steps seperate the left and right panels. This shows quite concretely that these Monte Carlo simulations are completely nonergodic.

In an attempt to characterize this first-order transition we ran simulations with sizes ranging from $L = 3$ to $L = 7$. As previously noted, the specific heat is, and remains not well-behaved and cannot be captured accurately. However, the first order transition is found to be exceptionally sharp (see Figure 4.9) at small θ_b and we can observe the critical temperature. This of course assumes that the Monte Carlo simulation, with its extreme freezing and lack of ergodicity, can be assumed to be somewhat accurate. However we note some pecularities. In Monte Carlo simulations of finite sized systems at a first order phase

transition in the metastable window between the critical temperatures upon cooling T_{cool} and warming T_{warm}, one expects to see the ordered and paramagnetic phases separated by an energy barrier. The simulation will exist in either the ordered or disordered phase, occasionally traversing the energy barrier and entering the other phase. In general this is not what we observe here as our simulation appears to exist in the paramagnetic state for an extremely long period of time before entering the octupolar state. The simulation never re-enters the paramagnetic state.

The time series of the simulation shown in Figures 4.10a and 4.10b at a temperature of 0.029074 (the histogram in Figure 4.9b) is instead characterized by the slow and gradual transition from the paramagnetic to octupolar state over a significant fraction of the 4 million Monte Carlo steps that comprise that data point. This agrees with simulations where it was observed that failure to spend sufficient time at the transition temperature resulted in the simulation failing to enter an octupolar state and having defects[4] *freeze in* as the temperature dropped rapidly. It appears that the dynamics of the bilinear biquadratic Heisenberg pyrochlore with $b > 0$ is **exceptionally slow**[5]. Furthermore, we must note the extremely small temperature ranges presented here. Note that the simulation in question has dozens of data points, each consisting of 4 million Monte Carlo steps in a temperature range of $\Delta\, T = 0.0001$. It is thus difficult to comment on the nature of this transition due to the freezing and extremely long equilibration times but these slow dynamics provide an explanation for the behaviour of the specific heat as fluctuations in energy are slow compared to the time spent to simulate "running" at each temperature.

[4]Tetrahedra which do not obey the colour ice rule.

[5] At least with a single spin flip algorithm.

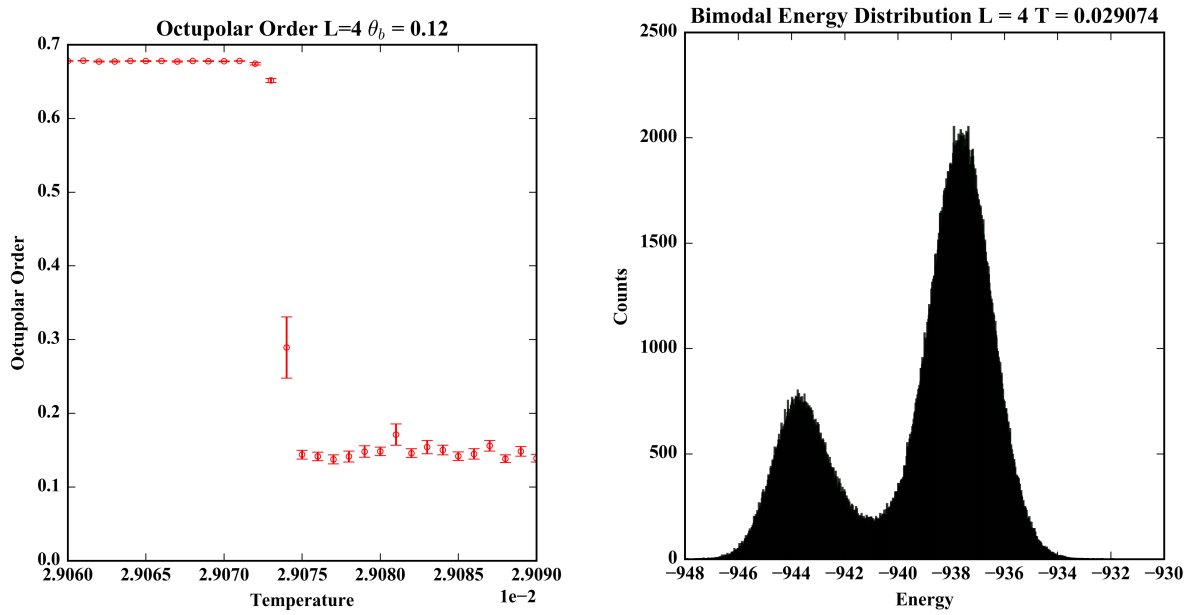

(a) Ordering occurs over an extremely small temperature range. $T_c \sim 0.029074$.

(b) Bimodal energy histogram at the transition

Figure 4.9: Monte Carlo simulation with $\theta_b = 0.12$, L=4. a) A critical temperature of approximately 0.029074 is observed. The spacing between temperature points is extremely small (10^{-6}). Yet the transition from the paramagnetic to octupolar state occurs over 1-2 data points or a temperature range of ΔT = 1-2 $\times 10^{-6}$. We thus observe what appears as a very, very strong first order transition (assuming ergodicity issues do not render our discussion of the transition irrelevant). Repeating the simulation confirms that exceptionally sharp ordering is not an abberation, although the critical temperature may vary sligthly from run to run. b) A bimodal energy distribution at the critical temperature.

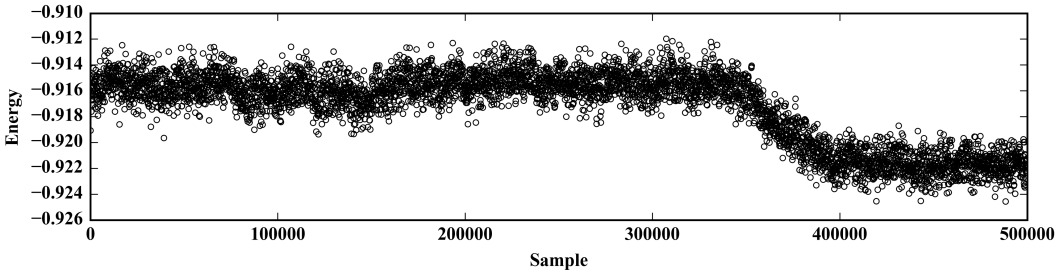

(a) Energy $\theta_b = 0.12$, $T = 0.029074$

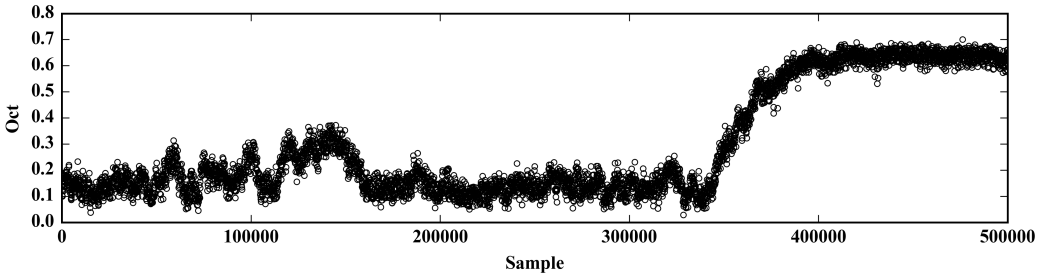

(b) Octupolar order $\theta_b = 0.12$, $T = 0.029074$

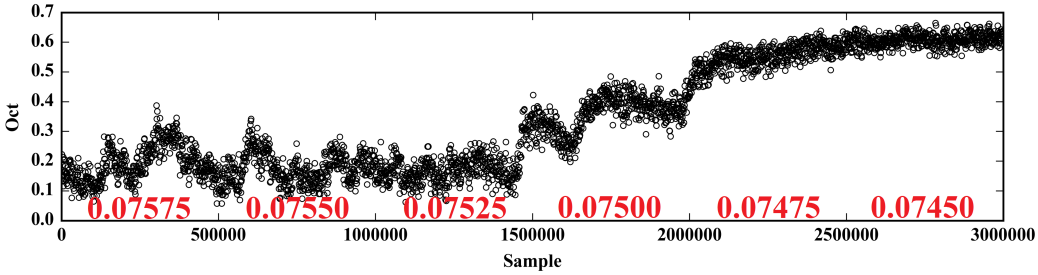

(c) Octupolar order $\theta_b = 1.20$, $T = 0.07450$ - 0.07575

Figure 4.10: Monte Carlo time series data of the energy per spin (top) and octupolar tensor order parameter (middle) at $T = 0.029074$ with $\theta_b = 0.12$, L=4 as shown for Figure 4.9. The bottom panel shows the time series of the octupolar order parameter for a simulation with $\theta_b = 1.20$ and L=4 for six temperatures as the simulation enters the ordered state. Four million Monte Carlo steps are run with sampling every 8 steps. We see one transition from the paramagnetic ground state to the ordered octupolar state. In the entire simulation, this transition is only made once – the simulation never re-enters the paramagnetic state. In the above figures only every 100th (top, middle) or 1000th (bottom) sample is shown for clarity.

For a first order transition, the transition temperature should scale as $T_c \sim \frac{1}{L^d}$ [40] where $d = 3$ is the dimension of the system as plotted in Figure 4.11. Unfortunately, due to the slow simulation dynamics and freezing, the transition temperature is not well defined, even if the transition appears sharp in the simulation results. Thus it is quite difficult to accurately identify the transition temperatures of simulations upon cooling, which appear to possess a somewhat random component to the temperature at which they order. While the transition temperature between the paramagnetic and octupolar phases appears to be sharp it is not necessarily accurate. Nevertheless, Figure 4.11 shows an attempt at describing finite-size effects in the system. We note the absence of error bars; due to the lack of ergodicity and other simulation issues it is not possible to place accurate error bars (which are only meaningful if the simulation is ergodic) in Figure 4.11. The attempted linear fit in Figure 4.11 is visually equivalent for various values of d ranging from 1 to 5 ($R^2 > 0.95$); nothing meaningful can be inferred from the figure and we include it for completeness.

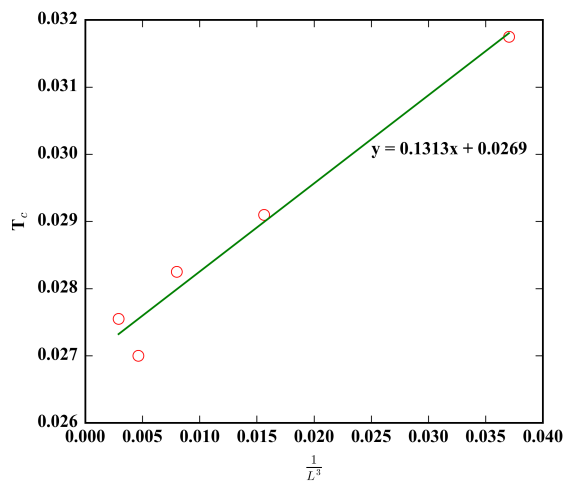

Figure 4.11: Finite size scaling of $T_c \sim \frac{1}{L^d}$ with $d = 3$ and $\theta_b = 0.12$. Systems of size $L =$ 3, 4, 5, 6, and 7 are used.

4.2.1 Parallel Tempering

As described in the preceeding chapters, methods such as parallel tempering have been employed to significant success in systems that encounter difficulty equilibrating near the transition temperature. We must first caution that parallel tempering is not *magic* and may

not necessarily return better results than a generic single spin flip algorithm. Named after the fact that algorithmically, multiple simulations are performed simultaneously, parallel tempering often involves running simulations in parallel computationally as well, due to a significant increase in the total required computational time. Unfortunately, efficient multithreading[6] is often nontrivial.

As described in Chapter 2, simulations of the same system are run at different temperatures with the lowest temperature being the target temperature. Periodically, the orientation of the spins are swapped between simulations with similar temperatures according to the Boltzman distribution. While the simulations themselves can be multithreaded and run independently of one another, they must be re-synchronized every time swaps take place[7].

Results for the $b > 0$ bilinear-biquadratic model with both parallel tempering and simulated annealing (cooling) are shown in Figure 4.12. Due to the computational overhead, the spacing between temperatures was increased for simulations involving parallel tempering. It was expected that this would not have a significant effect on the results due to the larger number of temperatures that would be accessed (for each target temperature there were 15 more higher temperature simulations – a "chain" of 16 simulations) and the swapping that would occur between simulations. Unfortunately, due to the extremely slow dynamics exhibited by the system, there was difficultly equilibrating near the transition and the simulations often froze with significant defects (tetrahedra which do not obey the colour ice rule), especially for the simulations with higher temperatures in the chain. This became pronounced as θ_b was increased.

[6]Multithreading or running a single piece of code across multiple CPU cores, is often difficult due to the way in which algorithms must be structured (both with respect to computing resources and the algorithm itself) in order to properly utilize parallel resources.

[7]This resynchronization is not permitted under the OpenMP (the multithreading library used here) standard. The threads must be re-created constantly with simulation data statically saved and reassigned to the appropriate thread.

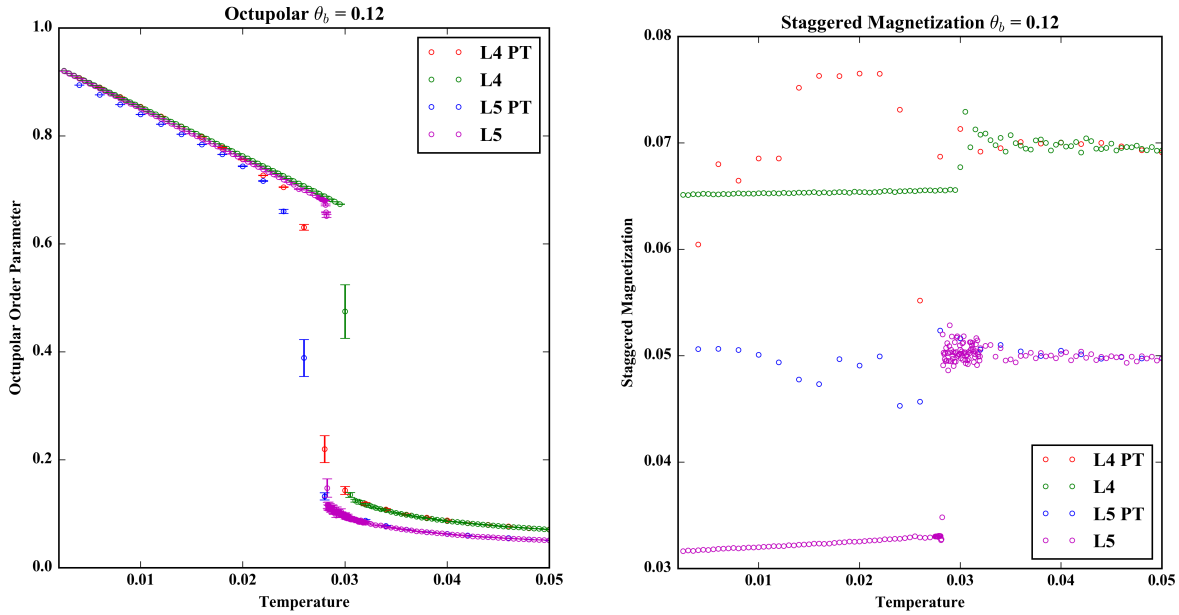

(a) Octupolar order parameter

(b) Staggered magnetization

Figure 4.12: Comparison of parallel tempering + simulated annealing with simulated annealing alone for $\theta_b = 0.12$ for system sizes of $L = 4$ and $L = 5$. The inclusion of parallel tempering appears to drive the critical temperature down. In the left pane, the slightly lower octupolar order for the $L = 5$ simulation with parallel tempering is suggestive of frozen-in defects or tetrahedra violating the colour ice rule. With parallel tempering, the magnetization does not appear to be frozen anymore below the transition. This is not precisely true – while the 16 simulations are frozen the parallel tempering algorithm only swaps spin configurations between simulations. Therefore the staggered magnetization with parallel tempering turned on is just a randomly weighted average of the frozen magnetizations of the 16 simulations.

As we have seen, the first-order transition that we have observed utilizing only single spin flips and simulated annealing is to a large degree questionable due to extreme lack of ergodicity in Monte Carlo simulations. With the addition of parallel tempering, it is tempting to believe that this has been fixed – the transition is much less 'sharp' and we see a more gradual entry into the ordered phase. However, it is important to note that parallel tempering does not add new spin configurations but only moves spin configurations between simulations according to their Boltzmann weighted energies. Thus, the issue of

exceptionally slow dynamics remains as the system must first order into the ordered state before the swapping of spin configurations becomes beneficial. The apparent advantage of parallel tempering, better ergodicity, may not count for much if transitions between states are extremely slow with respect to simulation and swapping times.

The inclusion of parallel tempering reduces the apparent critical temperature. This may be attributed to two things. First, the temperature spacings are tighter for the runs without parallel tempering. As the dynamics of the system appear to be exceptionally slow in comparison to the time the simulation spends at each temperature, we would expect simulations sampling closely spaced temperatures to enter the octupolar phase first[8]. Second, the swapping frequency of every 80 Monte Carlo steps is very quick compared to the time the simulation takes to transition between states – on the order of 400,000 - 800,000 Monte Carlo steps as shown in Figure 4.10 (samples are 8 Monte Carlo steps apart). Thus swapping configurations quickly between systems may have the effect of introducing high frequency noise and inhibiting ordering as systems so to speak will *live* at multiple temperatures and thus may encounter difficulty equilibrating. A system attempting to enter the ordered state at the lowest temperature T_0, where ordering may be energetically favourable, will have to contend with frequently being swapped to temperature T_1 where ordering may be less favourable – inhibiting ordering as a whole. The solution of course would be to swap less often. However, the dynamics of the single spin-slip simulation are so slow that swapping would occur so infrequently as to render parallel tempering mostly pointless. There is no way to fix this other than to run the simulation for significantly longer at each temperature, dramatically increasing computation times.

[8] A useful though not strictly correct way to picture this is to imagine a mean time τ that a simulation in the disordered state will exist in the disordered state before transitioning to the ordered state. If a system is started in the disordered state and the dynamics of the system is very very slow relative to the simulation time, then one would expect a simulation which runs longer in a given temperature range to enter the ordered phase at a lower temperature than a simulation that quickly traverses that temperature range.

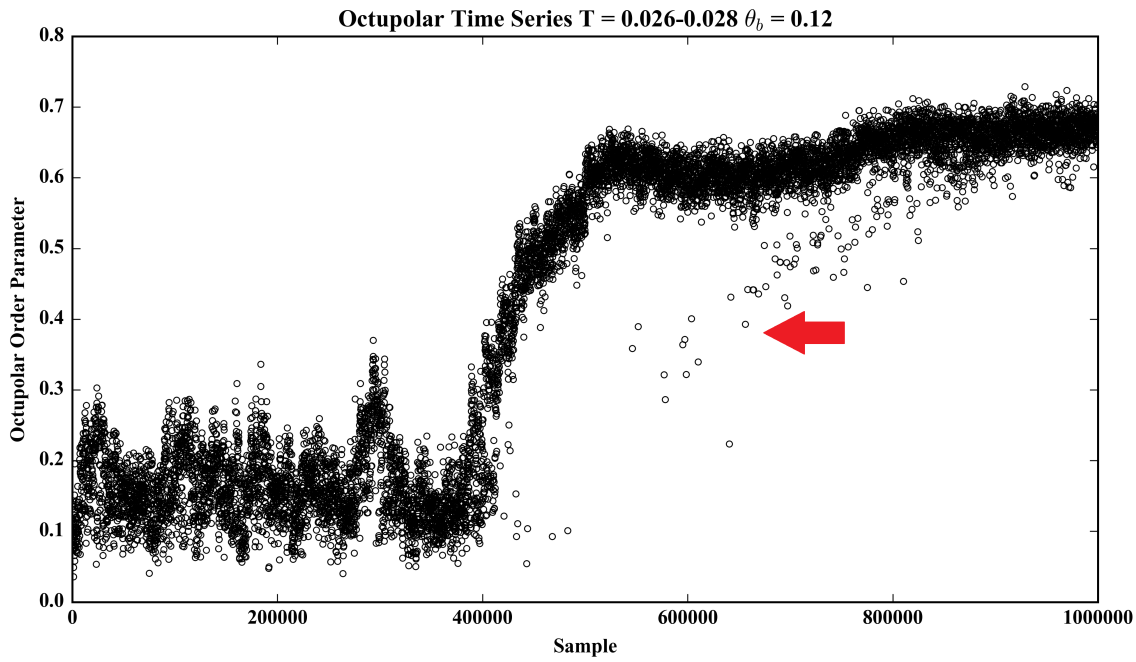

Figure 4.13: Time series of the octupolar order for the simulation with $\theta_b = 0.12$, L = 4 with parallel tempering and simulated annealing for the temperatures of $T = 0.028$ to $T = 0.026$ (first and second 500,000 samples respectively) shown in Figure 4.12a. The collection of points below the main band at the latter half of the time series shown by the red arrow indicates swapping with the simulation at the next higher temperature (i.e. temperature T_1 in the "chain" of temperatures $T_0, T_1, T_2, ...T_{15}$) in the paramagnetic phase. Gradually the simulation at temperature T_1 in the chain enters the ordered phase at around sample 900,000. For clarity, only every 100th sample is shown. There is a short equilibration period between the two temperatures which shows as a subtle discontinuity at sample 500,000.

The end result is that it is difficult to say whether the addition of parallel tempering improves our Monte Carlo simulation. We can say with certainty that significantly longer simulations that ergodically sample configuration space would be required to obtain truly trustworthy results.

4.3 Speculative Paramagnetic-Octupolar Phase Diagram

Another indicator of a first order transition is a *hysteresis* where the transition lags behind its driving forces. In principle, the transition temperature obtained by simulation should be lower for simulations undergoing cooling from the paramagnetic (T_{cool}) phase than for simulations being warmed from the octupolar phase (T_{warm}) as simulations are finite in time and first order transitions proceed through nucleation (with a corresponding energy barrier).

Upon warming the simulations starting in a low temperature random state, we observe that the simulation remains in the disordered state until the general vicinity of T_{cool} at which point it gradually enters a random colour ice state. Upon further warming the simulation then rapidly collapses back to the paramagnetic state at T_{warm} (a jump followed by a drop is observed in the octupolar order parameter). A plot of this is shown later in this chapter (e.g. Figure 4.21b).

The transition temperature is the midpoint of the jump in the octupolar order parameter between the octupolar and paramagnetic phases. The error in temperature is calculated as half the temperature range between the temperatures at which the simulations enters/leaves the pure octupolar and paramagnetic states (i.e. the transition region). We note that the boundary of the paramagnetic-octupolar transition resembles the speculated semiclassical phase diagram proposed by Wan and Gingras [31]. The existence of a potential long range ordered state in relation to the classical order-by-disorder calculations of Wan and Gingras are presented later in the chapter.

We show the hysteresis gap, or the difference between T_{warm} and T_{cool}, for a variety of biquadratic strengths $0.05 \leq \theta_b \leq 1.30$ in Figure 4.14 and confirm that the entire paramagnetic-octupolar phase boundary appears to be first order (simulation issues aside) due to its presence. There is a small irregularity at $\theta_b \sim 0.42$ which we cannot comment on and persists through repeated simulations.

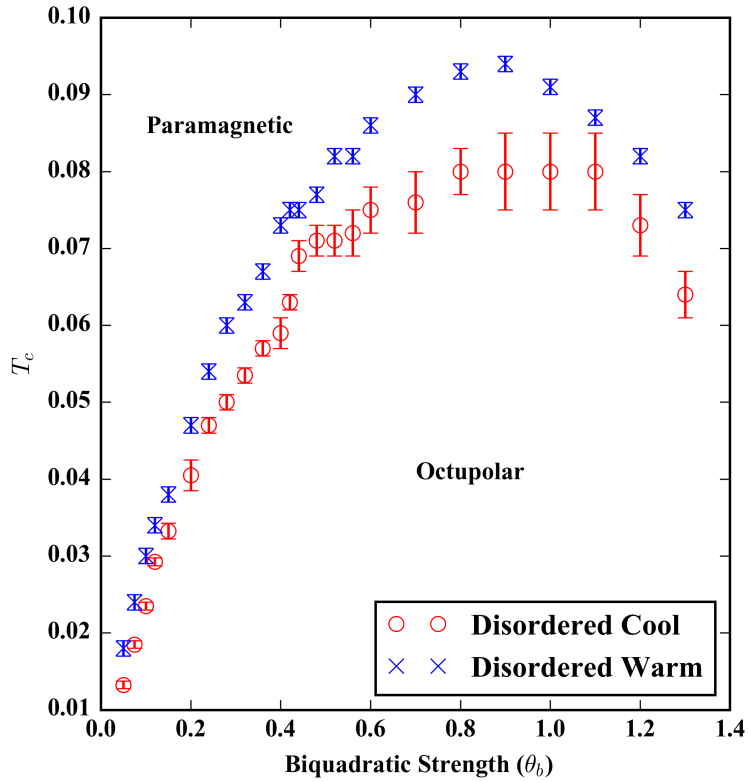

Figure 4.14: Paramagnetic-octupolar transition showing the hysteresis gap upon warming and cooling from disordered states for $0.05 \leq \theta_b \leq 1.30$ for simulations with $L = 4$. Upon warming, the simulation rapidly collapses from the octupolar to the paramagnetic state hence the small error bars. A small jump in T_c at $\theta_b = 0.40$ to $\theta_b = 0.44$ is observed and confirmed from many simulations.

4.4 Correlations

We plot the spin and octupolar structure factor just above and just below the paramagnetic to octupolar transition. In a random colour ice state, we would expect the number of spins of a given colour to be found in roughly equal quantities on each FCC sublattice and the spin-spin structure factor to cancel to zero. However, in the all-in/all-out (AIAO) ordered phase in which each FCC sublattice contains spins of one and only one colour (i.e. ferromagnetic ordering on each FCC sublattice), we would expect to observe peaks in both the spin and octupolar structure factor due to the regular ordering of spins on the

sublattices. Here, we would expect to see peaks at $\vec{q} = [111]$ (and all symmetry related $\vec{q}$'s) corresponding to correlations between spins along the direction of the stacked triangular and kagome planes and at $\vec{q} = [220]$ and $[002]$ corresponding to correlations between spins on their FCC sublattice. In contrast, in the paramagnetic phase, we would expect to see the characteristic pinch point scattering cited in the literature [63][64][65]. The spin-spin and octupolar structure factor are presented below for simulations well above the transition, just above the transition, and below the transition. Structure factors are calculated over 1000 samples with interpolation[9] between points due to the small system sizes to increase resolution.

$$S_T(\vec{q}) = \sum_{i,j,\alpha,\beta} \left[e^{i(r_{\vec{i}\alpha} - r_{\vec{j}\beta}) \cdot \vec{Q}} \right] \langle T_{i\alpha} \cdot T_{j\beta} \rangle \tag{4.3}$$

The octupolar structure factor is calculated as defined in Equation 4.3. We again stress that the presence of a $\vec{q} = 0$ peak does not imply the existence of $\vec{q} = 0$ ordering but instead means that the entire system is in *some* octupolar state. Therefore the octupolar structure factor of any octupolar ordered phase will contain a $\vec{q} = [000]$ peak.

[9] This can create visual artifacts.

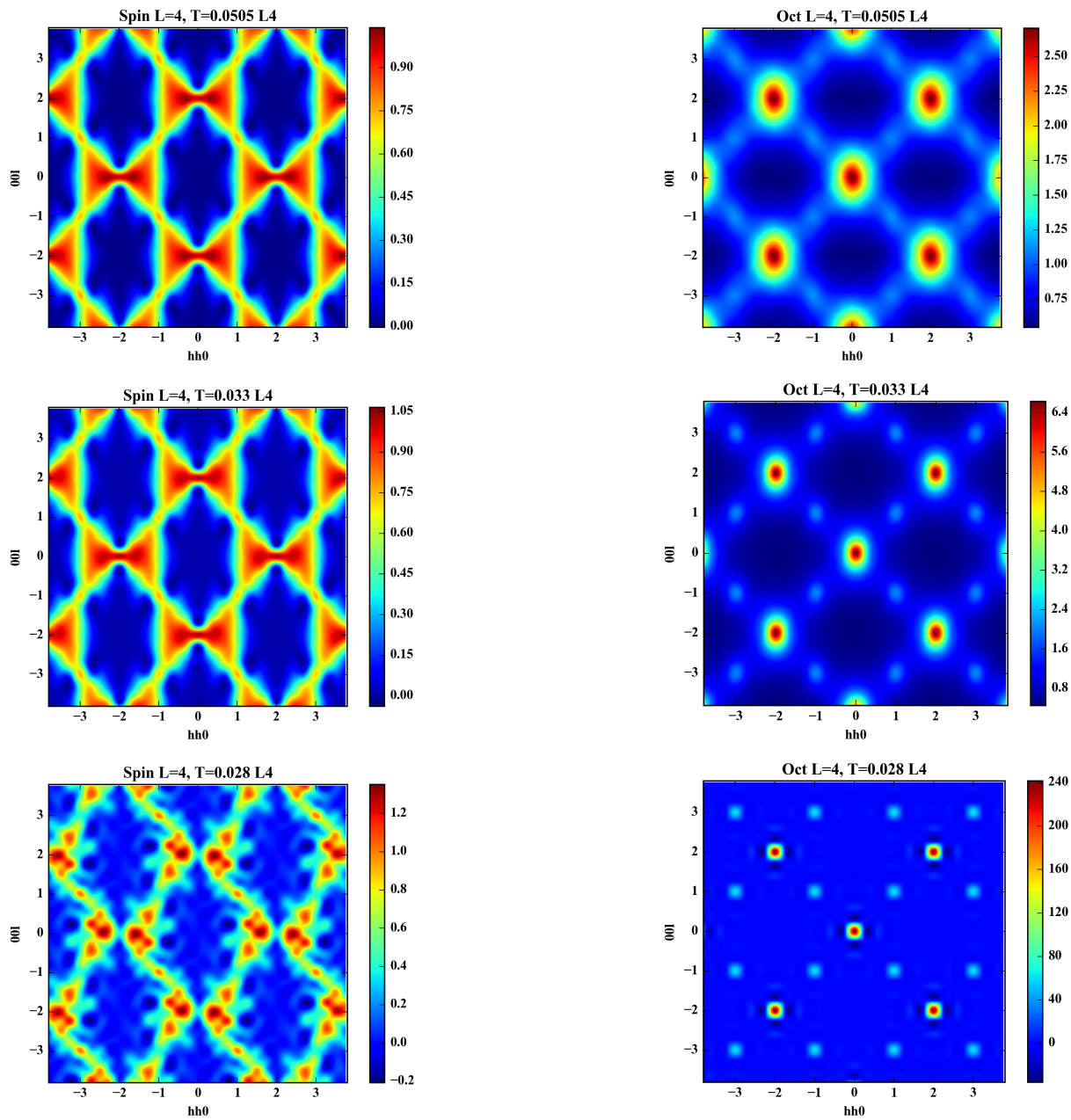

Figure 4.15: The spin and octupolar structure factors well above ($T = 0.0505$), just above (T =0.033), and just below ($T = 0.028$) the transition temperature ($T_c \sim 0.2907$) for system size $L = 4$, $\theta_b = 0.12$. Above the transition we observe the onset of local octupolar order as diffuse $\vec{q} = 0$ peaks in the octupolar structure factor. As the system cools into the octupolar state the $\vec{q} = 0$ peaks in the octupolar structure factor "sharpens" and grows in intensity. Due to the freezing of the system, the spin-spin structure factor is not flat below T_c with correlations persisting to lower temperatures.

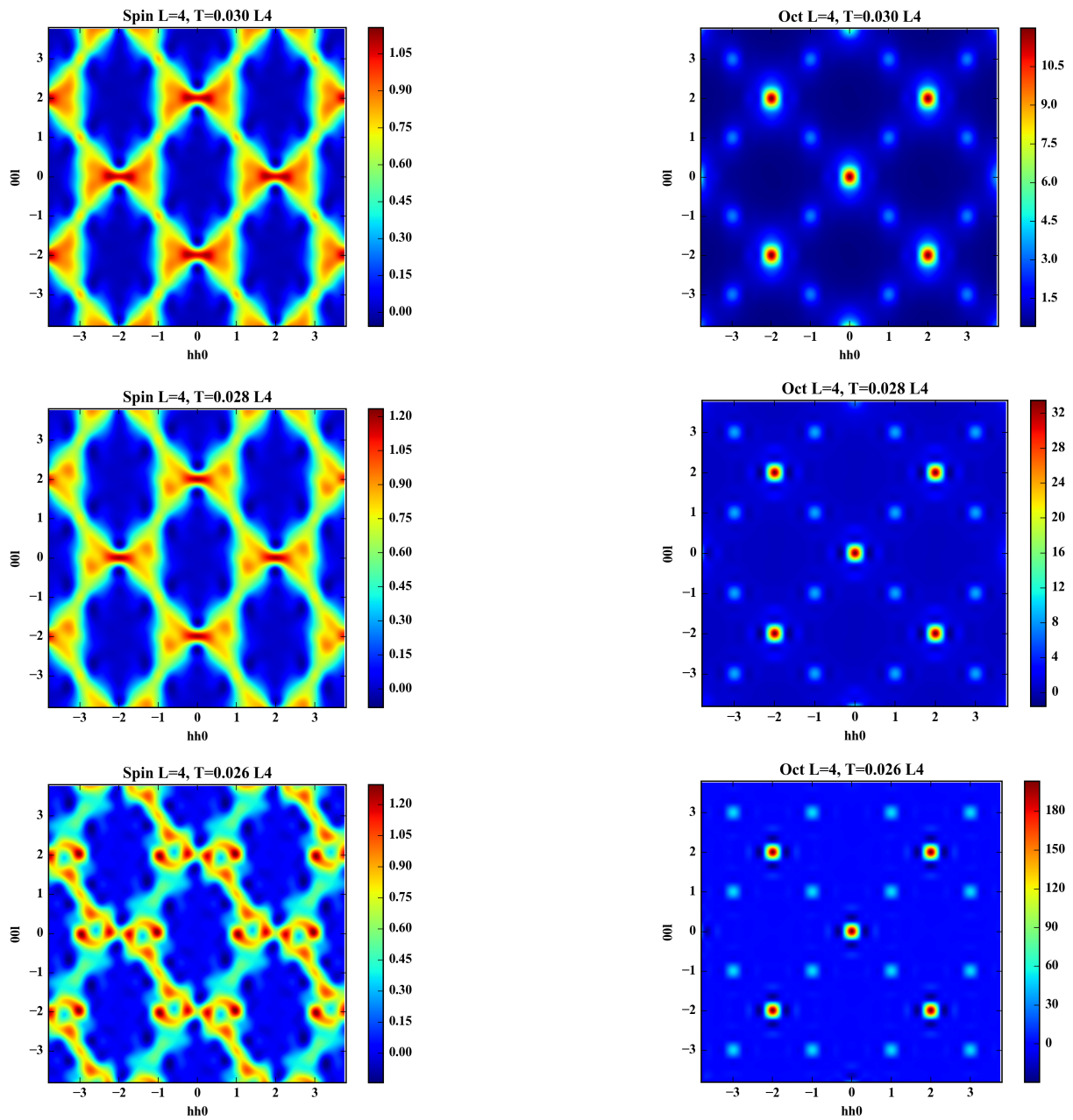

Figure 4.16: The spin-spin and octupolar structure factors near the transition at temperatures of $T = 0.26$, 0.28, and 0.30 with the inclusion of parallel tempering for $L = 4$, $\theta_b = 0.12$ for the simulation shown in Figure 4.12. The top panes show the paramagnetic state, the middle panes the system just above the transition and the lower panes show the system just below the transition. The *swirls* seen in the spin structure factor below the transition (bottom left) are random artifacts that are not seen in subsequent simulations. Despite the addition of parallel tempering, no significant changes are observed in the spin-spin and octupolar structure factors.

Calculations of the structure factor further confirm our expectation of an octupolar state. Above the transition, we see the indications of developing local octupolar order as diffuse $\vec{q} = 0$ peaks. As the system is cooled, it enters a globally octupolar state without any long range dipolar order as evidenced by the increasing height of the $\vec{q} = 0$ peaks. Due to the simulation *freezing-out*, the spin-spin structure factor is not flat below the transition; the "bow-ties" begin to disappear but the spins freeze and leave a random "signature" at the location of the bow ties. The potentially intriguing circular structures in pane e) of Figure 4.16 are random – repeated simulations and simulations at nearby temperatures show no evidence of this specific structure. The structure factors at other values of θ_b are not significantly different.

4.5 Histogram Reweighting

The success of the single and multiple histogram reweighting methods depends on the acquisition of good quality simulation data. Therefore, the slow dynamics and freezing of the simulation below the critical temperature suggests that any attempt at histogram reweighing is doomed to fail. This can be quite clearly understood as only one temperature point (in a simulation with or without parallel tempering) actually contains thermodynamic information sampling both the octupolar and paramagnetic phases. Other temperature points contain only "knowledge" of one of the phases and so there is no *region of coexistence* to reweight. Worse still, is that due to the slow simulation dynamics and lack of ergodicity, we cannot know if that temperature point accurately describes the physics of the $b > 0$ bilinear-biquadratic model or the quantities calculated at that temperature are an artifact of the simulation failing. Attempts to apply histogram reweighting to the $b > 0$ bilinear-biquadratic Heisenberg pyrochlore simulation data using the methodology described in Chapters 2 and 3 were thus met with failure.

4.6 A Potential Loop Move

To aid in our attempt to probe the paramagnetic-octupolar transition and fix ergodicity and freezing issues, we explored potential *loop* moves as utilized previously in the literature for different pyrochlore systems and described in Chapter 2. Such loop moves are expected to aid in equilibration by allowing the system to access states with similar energies that may be separated by large energy barriers not readily traversable via single spin flips. Unfortunately, the tetrahedral ground state ordering of the $b > 0$ bilinear-biquadratic

model presents a number of difficulties in implementing such moves. First, like with $b < 0$, there is no global ordering axis with a fixed direction as present in Ising models; this model possesses an O(3) symmetry and thus local axes must be determined throughout the lattice for **each** attempted loop move. Unlike in the nematically ordered phase for $b < 0$, there are four distinct local axes as spins are assigned 4 mutually different colours. Thus the potential moves as presented by Shinaoka et al.[60] as *flip xyz* and *flip parallel* are invalid as the colour axes for the positivie biquadratic model are positive definite and spins *flipped* with respect to their colour axis break the colour ice rules and are not colour spins.

The *rotate* move, involving the rotation of spins from one position in the loop to the next does remain potentially valid. This move is illustrated in Figure 4.17 and involves the construction of an alternating two color loop. The spins are then rotated or *permuted* through the loop (in a red-green loop the red spin in the first position is moved to the second position while the green spin in the second position is moved to the third position and so on). Loops involving more than two colours are not permitted as a rotation of a three colour loop would break the ice rule (Figure 4.17). However, the construction of such a two colour loop is hampered by the fact that such a two colour loop must live in a four colour environment and there are numerous means in which its construction could be blocked. By sheer probability alone, one should expect that in a random colour ice state, there to exist far fewer two colour loops in a four colour environment than two colour loops in a two colour environment as half the spins, not being the correct colour, cannot be added to the loop.

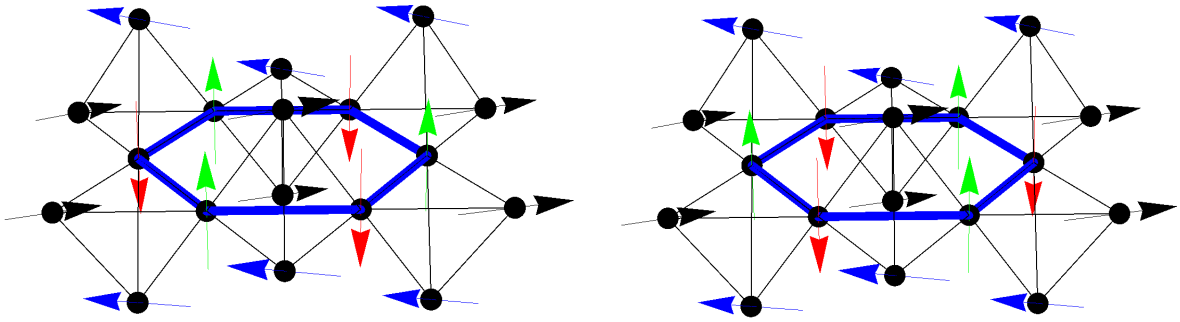

(a) A two colour red-green loop.

(b) Rotation of the two colour loop shown in a)

Figure 4.17: a) A two colour loop composed of alternating red and green spins marked by the thick blue line. Note the boundary of blue and black spins surrounding green and red spins. b) The same loop after rotation. Note that for a given tetrahedron the rotation of spins means that one green (red) spin enters the tetrahedron and one green (red) spin leaves the tetrahedron thus preserving the colour ice state. If one attempted to rotate a three (or more) colour loop, one would break the colour ice rules.

This two colour rotational loop move in a four colour environment has previously been presented and utilized in the literature [31][69][70][71][72] although for Ising-like spins. In contrast to such two colour loops in two colour environments, the loop presented here does not exist without a number of caveats. Random colour ice states are not only significantly less likely to support two colour loops, but there is a significant degree of "colour isolation". In Figure 4.17, we notice that the red and green loop is seperated from the rest of the lattice by a boundary of blue and black spins. This does not mean that the spins of the loop are fixed (a connecting loop of blue and green spins could rotate a single green spin out of the loop.) However, two colour loops in a four colour environment do not posses the richly connected and branching nature that two colour loops in a two colour environment do. Unlike the two-up/two-down ice state where a loop entering a tetrahedron on a black spin may exit the tetrahedron on one of two white spins, two colour loops in colour ice state may only exit a tetrahedron through the one appropriately coloured spin. Two colour loops in a four colour system are therefore highly restricted and lack the interconnected and branching nature of two colour loops in two colour spin ice.

The additional constraint of significantly lower loop *connectivity* is expected to greatly limit the efficacy of two colour loops in a four colour environment. Furthermore, as shown

in Figure 4.17, if loops do not interconnect, loop rotations will not accomplish anything i.e. if there is no interconnecting blue/black-green/red loop in Figure 4.17, the red and green spins in will simply be rotated around in circles. Finally, the "connectivity" of these two colour loops must be sufficiently ergodic as to allow the simulation to organize into potential long-range ordered states.

Complicating these issues, is that loops in potential long-range ordered states are generally on the order of the linear size L of the lattice and will possess "ends" that will only close through the periodic boundaries. This is generally not an issue for Ising-like spins as all spins of the same colour point in the exact same direction and are otherwise identical. However, Heisenberg spins are different and will deviate slightly with respect to the colour axes. As the temperature is increased, this deviation increases. Thus, in a four colour system with Ising spins, the interchange of any two spins of the same colour has an energy cost of 0 (barring the presence of any further interactions); not so for Heisenberg spins. Ising-like loops will have a zero energy cost to rotate independent of the temperature while the energy cost to rotate Heisenberg-like loops grows as the temperature and size of the loop is increased. As long-range ordered states will only possess loops of length L we would expect the loop acceptance ratio in these order states to drop to 0 as the size of the Heisenberg system grows and the energy cost of a rotation increases.

Preliminary work on the implementation of the two colour loop was attempted but not finished due to time constraints. Due to the ergodicity and freezing issues that we have encountered and the potential benefits that nonlocal moves could bring, fully investigating the effect that two colour loops have on the $b > 0$ model is of great importance. Should the loops address these issues, stronger statements could be made regarding the ordered octupolar phase and its low temperature properties.

4.7 Absence of Long-Range Dipolar Order

The investigation of the ground state of the $b > 0$ bilinear-biquadratic model has been extensively hindered by issues of ergodicity and freezing as we approach the transition from above. We then turn our investigation into starting from low temperature ordered states and approaching the transition from *below*. Approaching the transition from below not only allows us to expose the hysteresis of the first order transition compared with simulations cooling from the disordered paramagnetic state, but allows us a window into the behaviour of the "weathervane modes" as described by Wan and Gingras [31].

4.7.1 Metastable Weathervane States

A weathervane mode can be described as a portion or *membrane* of the lattice that collectively rotates at no energy cost. On a single tetrahedron, one observes that if a given spin is "pinned" in place (we dub this spin the *weathervane pole*) one may rotate the remaining three spins around the axis defined by that spin (tracing out the surface of a downwards facing cone) at no energy cost – the angles ϕ between the spins remain constant and so the total energy of the tetrahedron remains constant. Generalizing this to the pyrochlore lattice shows that these rotational membranes should exist for any segment of the lattice that is completely bounded by spins of one colour (i.e. the *pole* spins). This is easily proven as the weathervane membrane is only connected to the lattice through the pole spins and that under the zero energy cost global rotation along the axis of the pole spins, the angles between three colours of spins that make up the membrane do not change (see Figures 1.4 and 1.5. Thus for a system with Hiesenberg spins, there are an infinite number of angles along which a weathervane membrane may be rotated at zero energy cost with angles of $\phi = 0, \pm\frac{2\pi}{3}$ which correspond to permutations of colours within the weathervane membrane. The number of weathervane modes that a system may support ranges from 0 (i.e. a global rotation of spins in the system) to $O(L)$ in the AIAO state [31].

The concept of weathervane modes is not altogether new – regions of a lattice that may rotate at zero energy cost have been previously noted in the kagome lattice [35][32][33][34][36][37]. Here we investigate the weathervane modes present in systems started at low temperatures in the long-range ordered AIAO and $\{001\}$[10] states described by Wan and Gingras [31] and shown in Figure 4.18. The AIAO state consists of spins of one colour on each FCC sublattice while the $\{001\}$ state alternates layers of AIAO tetrahedrons with 'swapped' AIAO tetrahedrons (the pairs of spins in each tetrahedron with the same z value swap colours) along the z axis. The $\sqrt{3} \times \sqrt{3}$ state was not investigated in this work as it requires a different hexagonal unit cell to satisfy periodic boundary conditions and due to time constraints.

Previously, Wan and Gingras [31] investigated order-by-disorder on the weathervane modes in the AIAO, $\{001\}$ and $\sqrt{3}\times\sqrt{3}$ states (shown in Figure 4.18; the $\sqrt{3}\times\sqrt{3}$ state is an ordered state in the kagome lattice. See Ref. [61] for a description.). However, their search only considered stacked weathervane membranes with the spins on the even numbered membranes "pinned" in place; only spins on odd-labeled weathervane membranes were free to rotate. Nevertheless, they found that spins on alternating weathervane membranes possess maximal entropy or minimal zero point energy at weathervane angles of $\phi = \pi$,

[10] We will consider one of these states with modulation $\vec{q} = (001)$ i.e. stacking weathervane membranes along the z direction.

degenerate with $\phi = 0$. Angles of $\pm\frac{2\pi}{3}$ did not correspond to local energy minima or local entropy maxima.

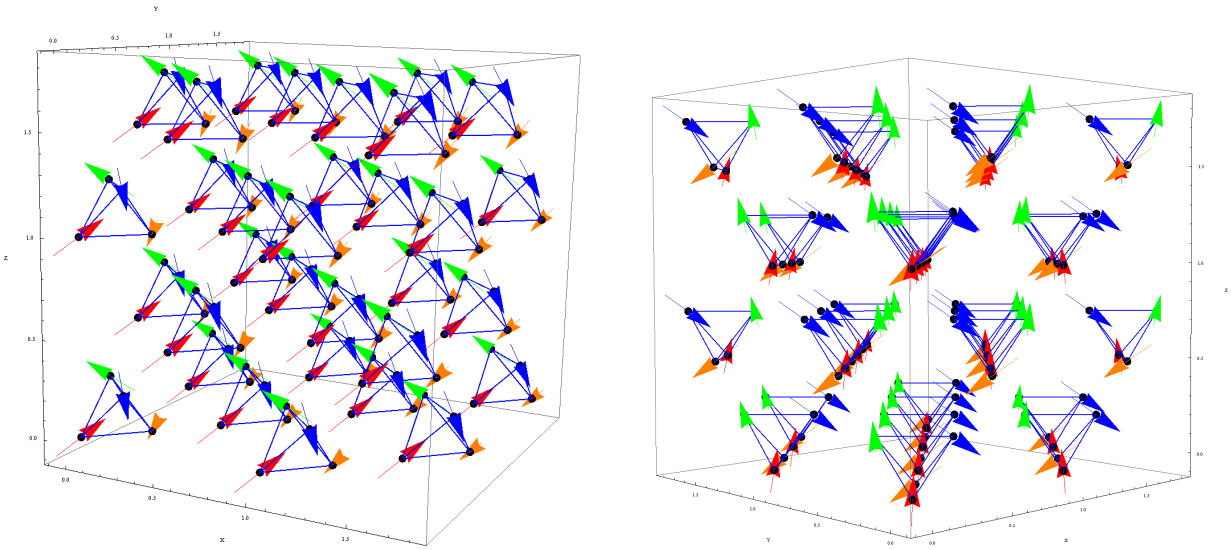

(a) AIAO (b) {001}

Figure 4.18: The AIAO (left) and {001} (right) ordered states. A 2×2×2 section of the lattice is shown. In the AIAO state, every FCC sublattice possesses the same colour spin – all tetrahedra are identical. In pane a), weathervane modes are seen running along the [111] direction bounded by the red spins. In pane (b), the {001} state consists here of stacked layers of tetrahedra along the vertical z axis, one layer consisting of AIAO tetrahedra and the other composed of "inverted" (time-reversed) tetrahedra (the spins in each pair of spins with the same z coordinates exchange colours) possesses weathervane modes along the [001] direction seen by the blue and green spins. For clarity, only the sublattice of a tetrahedra are shown.

The AIAO and {001} states stack weathervane membranes along different directions and thus define different spatial correlations. The spin and octupolar structure factors of these states are illustrated in Figure 4.19 for a system of size $L = 6$. Looking first at the AIAO spin structure factor, we observe two groups of Bragg peaks corresponding to correlations between spins on FCC sublattices ($\vec{q} = (0, 0, \pm 2), (\pm 2, \pm 2, 0)$) and between spins on stacked kagome and triangular planes ($\vec{q} = (1, 1, \pm 1), (-1, -1, \pm 1)$)[11]. The height

[11]Not all these points are seen in the hhl plane.

of these peaks were measured as $\frac{N}{6}$ and $\frac{N}{8}$, respectively, corresponding to cubic symmetry and stacked kagome and triangular planes along the [1,1,1], [-1,-1,1], [-1,1,-1], [1,-1,-1] directions therefore giving aggregate peak intensities on the order of the number of spins N (3456 for a L = 4 system).

In the $\{100\}$ state, the $\vec{q} = (0, 0, \pm 2), (\pm 2, \pm 2, 0)$ correlations are maintained while the $\vec{q} = (1, 1, \pm 1), (-1, -1, \pm 1)$ correlations are broken to include further $\vec{q} = (\pm 1, \pm 1, 0)$ correlations which are indicative of the stacked weathervane membranes along the z axis. The intensity of these peaks were calculated to be $\frac{N}{24}$ and $\frac{N}{12}$ respectively.

Peaks in the octupolar structure factor possess intensities scaled by the octupolar tensor parameter and its scalar products relative to the intensity of peaks in the spin structure factor. We note that the value of the octupolar order parameter in a fully ferromagnetic and tetrahedral states is $\frac{2}{5}\sqrt{10}$ and $\frac{2}{3}\sqrt{2}$ respectively (in a ferromagnetic state the magnetization would be 1 for instance) and that these values scale the heights of the observed peaks in the octupolar structure factor relative to the peak height in the spin structure factor. For instance, the $\vec{q} = (1, 1, \pm 1), (-1, -1, \pm 1)$ octupolar peaks are 1.6× or $(\frac{2}{5}\sqrt{10})^2 = \frac{8}{5}$ ($T_i \cdot T_j$ = 1.6) the intensity of the equivalent peaks in the spin structure factor ($S_i \cdot S_j = 1$). Likewise the $\vec{q} = 0$ peak has an intensity of $N[1 - (\frac{\frac{2}{3}\sqrt{2}}{\frac{2}{5}\sqrt{10}})^2] = N[1 - \frac{5}{9}] = 3456 * \frac{4}{9} = 1535$.

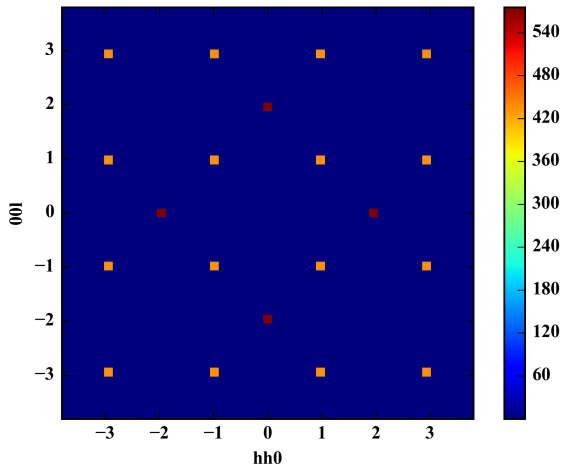

(a) AIAO spin structure factor

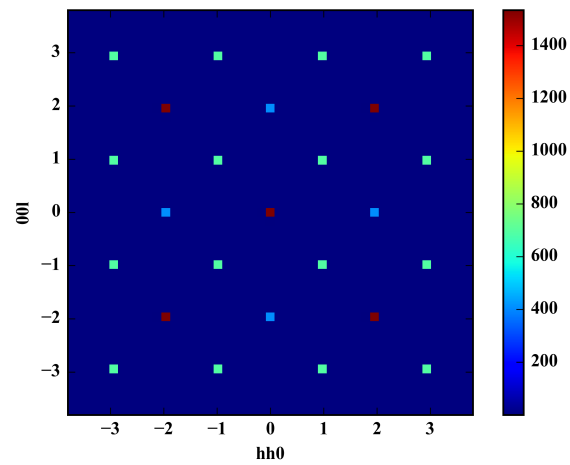

(b) AIAO octupolar structure factor

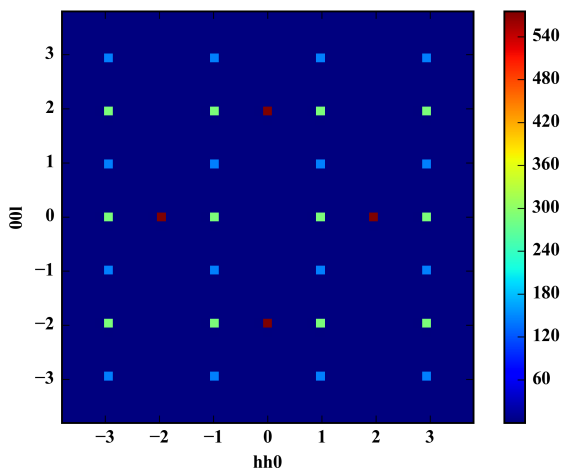

(c) {001} spin structure factor

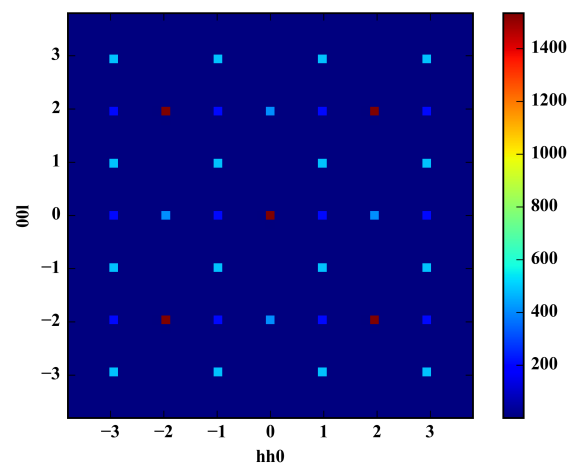

(d) {001} octupolar structure factor

Figure 4.19: Calculated spin and octupolar structure factors for the AIAO and {001} states.

Comparing the octupolar structure factor analytically determined in Figure 4.19 to the results of the Monte Carlo simulation (Figures 4.15 and 4.16) shows that the $\vec{q} = (0, 0, \pm 2)$ and $\vec{q} = (\pm 2, \pm 2, 0)$ peaks are missing in the results of the Monte Carlo simulations. The random octupolar states obtained by Monte Carlo simulation do not contain any sort of ordering – spins on each tetrahedron may be randomly coloured as long as the entire

lattice obeys the colour ice rules. However, the calculated AIAO and {001} states do possess periodic ordering (the AIAO and {001} lattice can be created by the translation of the 16 spin base unit cell). Therefore peaks corresponding to this cubic symmetry are observed in the AIAO and {001} ordered states but not for random octupolar states.

On the following pages we present results for warming from three initial low temperture starting conditions – the AIAO state, the {001} state (Figure 4.18) and a completely random non-colour ice state. Unlike Wan and Gingras [31], we fix no spins in our lattice and thus the rotation of weathervane modes is completely unhindered. The action of all weathervane membranes are thus taken into account. Though the single spin flip move is extremely slow, the simulation will run for a relatively long time in the octupolar phase and single spin flips should not encounter any undue difficulty sampling zero energy rotations which do not require spins to change colour and thus overcome energy barriers. Spins will be free to rotate in the manifold of energetically degenerate weathervane modes and the presence of potential long-range order for that particular state may be uncovered. The caveat, however, is that as the single spin-flip algorithm appears to be unable to break the ice rules and change the colour of a spin, it is unlikely that a simulation started in one particular long-range ordered state will transition into a different long-range ordered state.

4.7.2 Low Temperature Ordered Phases

We observe numerous and intriguing results in these warming simulations which we will briefly summarize here. Warming from a low temperature AIAO state shows the development of distinct metastable states manifested as plateaus in the octupolar order parameter. These states are distinct and clearly defined, as can be seen in Figure 4.20. Repeating the simulation under the same parameters shows that the entry and exit of the simulation into these states is completely random. In contrast, warming the {001} state reveals a system sampling a *metastable manifold* – spins cleanly rotate through the multitude of weathervane modes present in the lattice and quantities such as the octupolar order parameter take on a wide range of values[12]. Warming from a random configuration of spins gives a frozen system that slowly orders into a random octupolar state at a temperature slightly lower than the temperature that a simulation being cooled transitions from the

[12]The octupolar order parameter captures the lattice ordering into a "global colour state" – all spins in the lattice pointing in the same colour directions in a colour ice state. A lattice with weathervane modes will possess spins that do not orient along the four colour groupings (these spins have been rotated by the weathervane angle ϕ) while also being a colour ice state. As the octupolar order parameter sums the global orientations of spins across the entire lattice, octupolar states containing weathervane modes are expected to possess a lower octupolar order than states without weathervane modes.

paramagnetic to octupolar phase. The following section analyses results that do not make use of parallel tempering. This is because the swapping of simulations between different temperatures makes it difficult to observe the plateaus that mark these metastable states. Nevertheless we do note the *fingerprints* of these metastable modes in computations with parallel tempering.

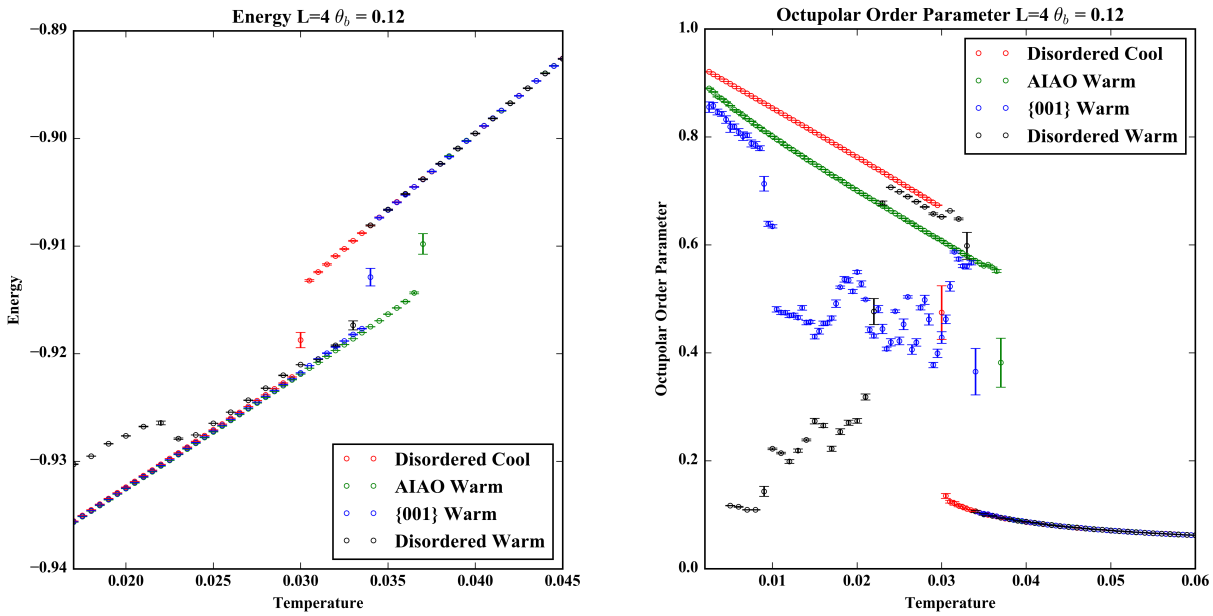

(a) Energy per spin $\theta_b = 0.12$

(b) Octupolar order parameter $\theta_b = 0.12$

Figure 4.20: Energy and octupolar order for systems under various starting conditions with $\theta_b = 0.12$. The simulation started in the disordered state and warmed struggles to equilibrate into the octupolar phase, only fully ordering into an octupolar state at $T \sim 0.022$.

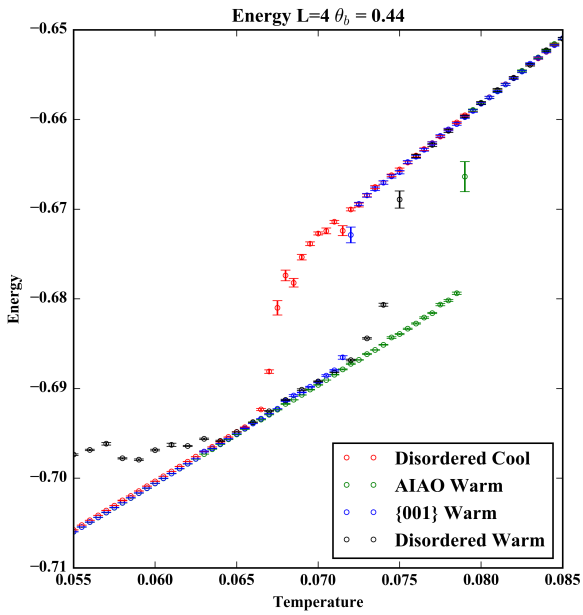

(a) Energy per spin $\theta_b = 0.44$

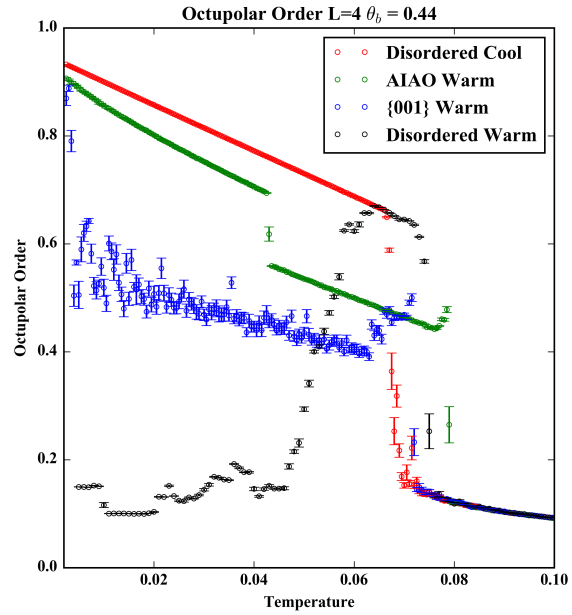

(b) Octupolar order parameter $\theta_b = 0.44$

Figure 4.21: Energy and octupolar order for systems under various starting conditions with $\theta_b = 0.44$.

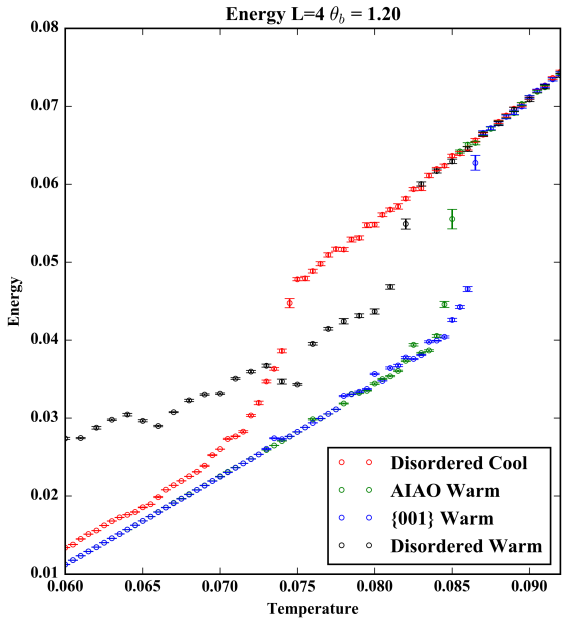

(a) Energy per spin $\theta_b = 1.20$

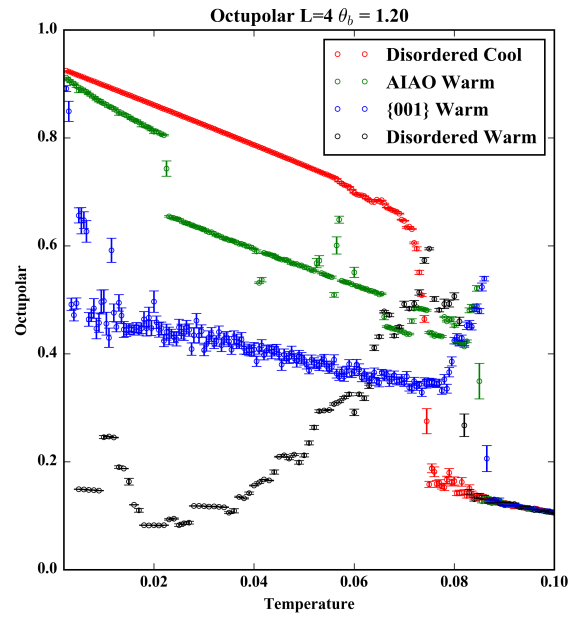

(b) Octupolar order parameter $\theta_b = 1.20$

Figure 4.22: Energy and octupolar order for systems under various starting conditions with $\theta_b = 1.20$.

A number of pecularities are shown in Figures 4.20 - 4.22. The hysteresis gap is observed to increase as θ_b increases to some degree. Interestingly, we note that simulations started in the AIAO phase generally transition upon warming at a *higher temperature* than simulations started in the {001} phase which generally enter the paramagnetic phase at similar temperatures as simulations started in a completely disordered state. All simulations undergoing warming exhibit a transition temperature higher than simulation undergoing cooling for a given biquadratic strength. The octupolar-paramagnetic phase diagram from Figure 4.14 is reproduced in Figure 4.23 showing the transition temperatures of systems started in the AIAO and {001} states.

The energy and the octupolar order parameter as well as other thermodynamic quantities are the same in the paramagnetic phase for all simulations (Figures 4.20 - 4.22). However, in the octupolar phase the energy per spin of the disordered system upon cooling is very slightly higher than the energies of the ordered AIAO and {001} systems (visible in Figure 4.22 and also true for Figures 4.20 and 4.21 but not visible in the plots). This is true for all values of θ_b. Furthermore, a small but consistent difference in the energies

of the ordered AIAO and {001} states is found for weak biquadratic interactions with the AIAO state being of very slightly lower energy. This energy difference is nearly imperceivable (on the order of 10^{-5}) but is observed for all small values of θ_b and is smaller than the error in the energy ($\sim 10^{-6}$ - 10^{-7}). As the biquadratic interaction strength is increased this difference in energy becomes unresolved.

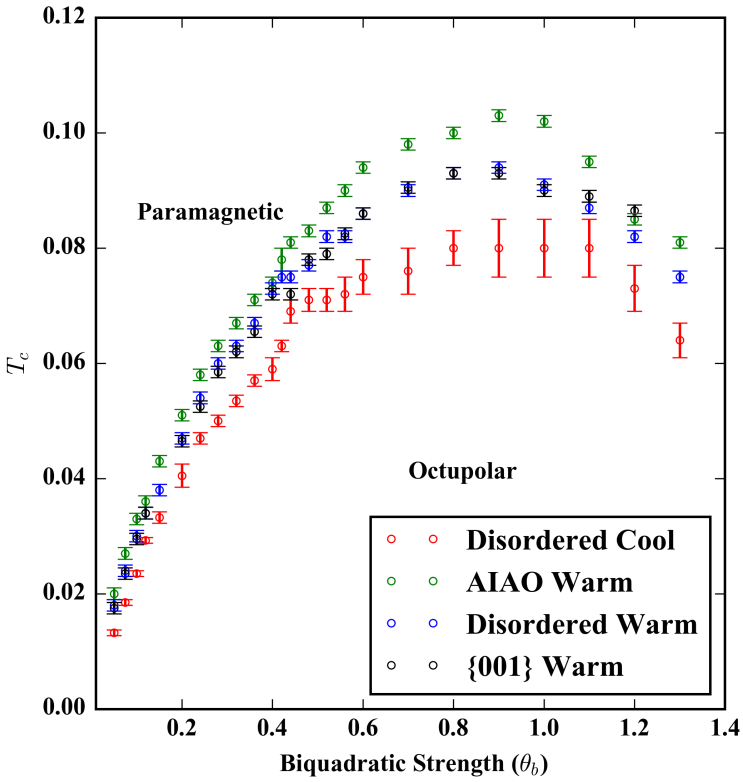

Figure 4.23: Paramagnetic-octupolar transition showing the hysteresis gap upon cooling and upon warming from disordered, AIAO, and {001} states for $0.05 \leq \theta_b \leq 1.30$. The irrelegularity at T $\sim$ 0.40 - 0.44 remains.

A look at octupolar ordering however, reveals a much more complex picture. As might have been expected, the disordered systems undergoing either warming or cooling and which order into a random colour ice state possess the same level of octupolar ordering i.e. they fall on the same *curve* in the ordered phase as shown in Figure 4.21b. However, at very low temperatures, the long-range ordered AIAO and {001} states appear to possess a *lower* level of octupolar ordering than random colour ice states. As noted previously, the

octupolar tensor order parameter does not depend on the position of spins in the lattice - it **cannot** distinguish between random colour ice states and ordered octupolar states such as the AIAO and {001} states. As such the difference in the order parameter must depend entirely on the fluctuations of the spins in each state from their ideal colour positions.

We also note the presence of metastable modes in systems started in the AIAO ordered state seen as plateaus[13] in the octupolar order and label them N1, N2, and N3 (Figure 4.24b). These states are designated as metastable as they are energetically degenerate – no change in the energy is observed as the simulation enters and leaves them[14]. Repeated simulations show that the simulation enters and leaves these metastable states randomly. For small θ_b, the simulation only infrequently enters the first of these metastable modes (Figure 4.21). As θ_b is increased, simulations begin to enter the N2 and N3 metastable states (Figure 4.24b). The small but consistent uptick in octupolar order as the system exits the octupolar phase is intriguing as it suggests that the transition from the metastable weathervane state into the paramagnetic regime is unfavoured.

[13]The *plateaus* in the plots are flat in the expected sense, rather we use plateau to refer to linearly decreasing segments in the octupolar order parameter separated by jumps or discontinuities.

[14]Weathervane modes are *zero* energy excitations and so there should be no difference in energy between otherwise identical classical systems with and without weathervane modes.

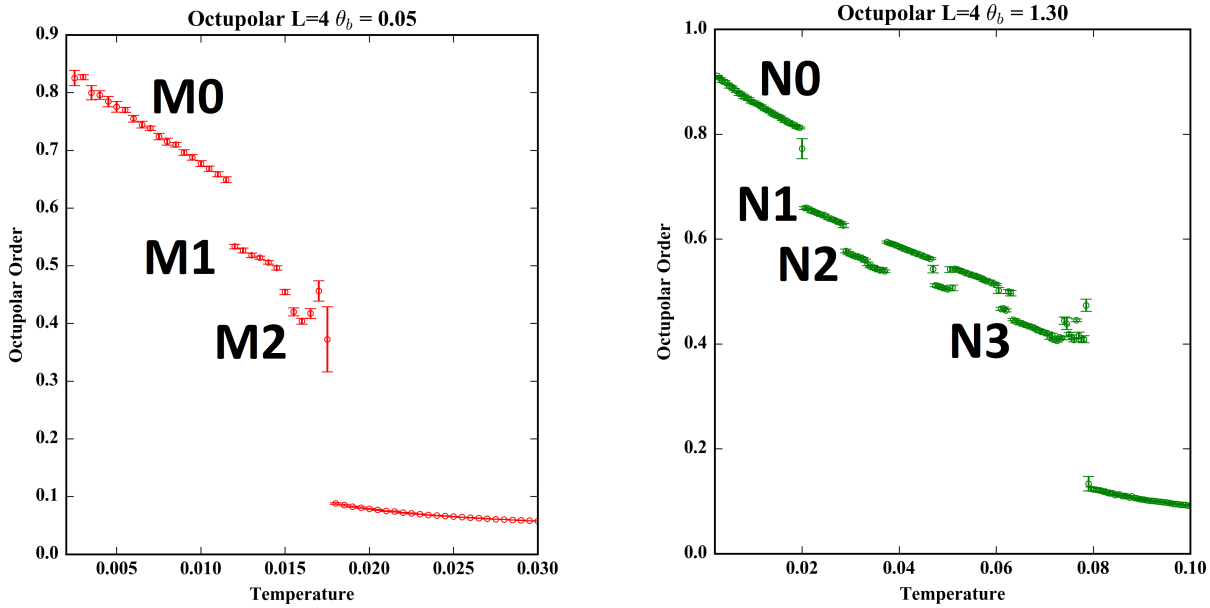

(a) {001} start, $\theta_b = 0.05$

(b) AIAO start, $\theta_b = 1.30$

Figure 4.24: Octupolar order for a) {001} starting state, $\theta_b = 0.05$ and b) AIAO starting state, $\theta_b = 1.30$. Metastable states are shown. "M" labels refer to {001} metastable states while "N" labels refer to AIAO metastable states. M0 and N0 are the {001} and AIAO long range ordered states respectively. M1 and M2 label metastable {001} states. N1, N2, and N3 label three metastable AIAO states. N2 and N3 possess very similar levels of octupolar ordering and are difficult to distinguish.

Metastable weathervane states are also subtly present in systems initialized in the {001} state as can be carefully observed in Figure 4.24a (labeled M1) although only for weak biquadratic interactions. It appears that these {001} weathervane modes are similar to the AIAO weathervane modes albeit occuring at significantly weaker biquadratic strengths. For very weak biquadratic interactions, the {001} system tends to exist for a long period of time in the {001} state before dropping into less ordered weathervane states. As θ_b is increased, the simulation rapidly exits the {001} state, entering less ordered weathervane states. We note a difference between the M2 metastable state and the N1, N2, N3, and M1 states as it possesses a relatively chaotic nature; here the simulation rapidly varies in its energy and octupolar order over very short timeframes. Finally, we note the same upwards "tick" in the octupolar order for {001} simulations as we do for AIAO simulations just

before the system transitions into the paramagnetic state.

The octupolar tensor order parameter we utilize is susceptible to changes in the global ordering and rotations of weathervane modes as it measures the orientation of spins relative to one another across the lattice. Thus, states without weathervane modes ($\phi \neq 0$) will possess a lower degree of octupolar ordering. The different levels of octupolar ordering in the ground states of the AIAO and $\{001\}$ systems compared with the more ordered random colour ice states are due to larger possible global fluctations allowed by the weathervane modes – the presence of weathervane modes allows for greater fluctuations in the orientations of spins in a weathervane membrane and consequently a lower degree of octupolar ordering.

4.7.3 AIAO Metastable States

Investigating the orientation of spins in the AIAO metastable states reveals that the N1, N2 and N3 states are AIAO states with varying numbers of rotated weathervane membranes. In these states the three coloured groups of spins composing the kagome weathervane membrane have been rotated by $\phi = \pi$ degrees (into what we term a colour conjugate (CC) layer). This is the same angle as noted by Yuan and Gingras in their classical order-by-disorder calculations where the weathervane rotation angle $\phi = 0$ was found to be degenerate with $\phi = \pi$. We find that the N1 state corresponds to a 3:1 ratio of AIAO/CC layers (along the [111] direction) with the N2 state corresponding to a 2:2 AIAO/CC layering. It is not until the M3 state with the lowest octupolar order is reached that a 1:1 alternating stack of AIAO and CC layers are encountered.

We note the restricted stacking ratios of the weathervane layers as they do not appear to be free to rotate independently on their own with weathervane angles of $\phi = 0, \pi$, but rather stack in a periodic arrangement that respects the periodic boundary conditions. Due to this system size dependence, it is not possible to comment precisely on the properties of weathervane modes in the thermodynamic limit. However, we expect that as the simulation size is increased more and more weathervane stacked modes should become accessible.

We remark that it is quite likely that these AIAO weathervane mode states are not "distinct" from one another at all – it may only be due to the slow simulation dynamics and confinement by periodic boundary conditions that these different states are individually stabilized and observed. Instead a weathervane manifold state (a state that moves rapidly between multiple weathervane modes) might be observed in the absence of periodic boundary conditions. It is not our intention to fully characterize the general properties of these zero energy excitiations. Nevertheless, a description of the weathervane modes

present in a system with $L = 4$ is presented. The orientations of spins in the lattice in the N2 and N3 weathervane mode states are shown in Figures 4.25 and 4.26 respectively.

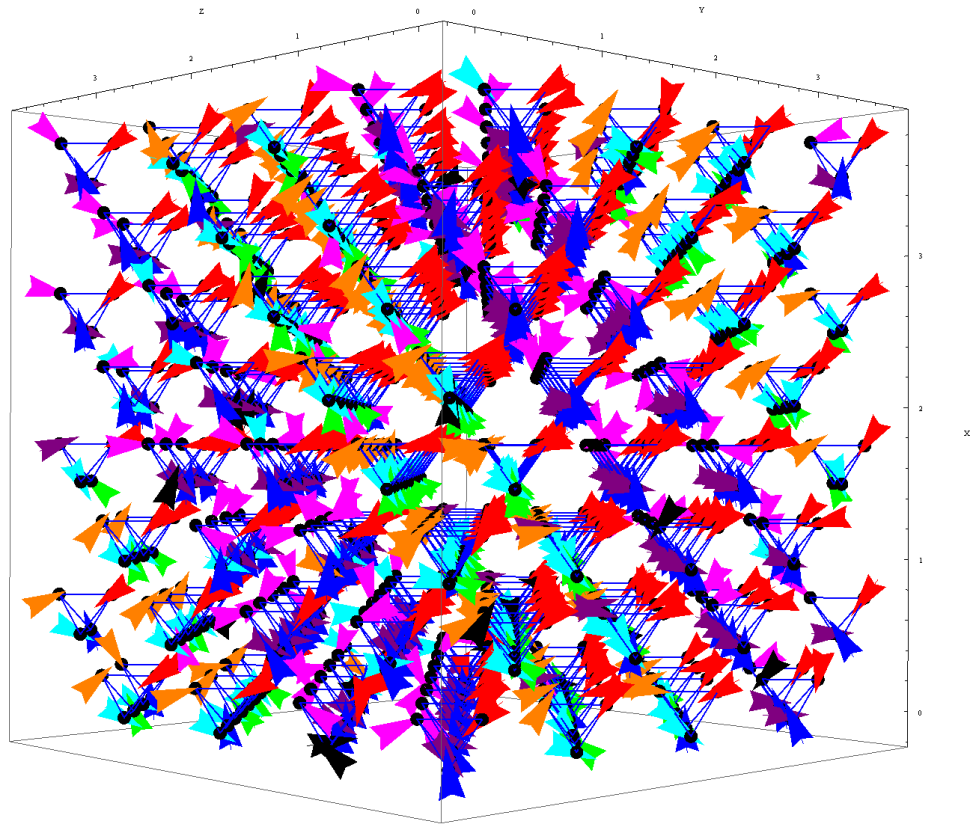

Figure 4.25: The N2 (2:2 AIAO/CC) state for a $L = 4$ simulation at a temperature of $T = 0.05$, $\theta_b = 0.60$. The entire 1024 spin system is shown. The weathervane pole spins are coloured red while other AIAO colour spins are painted green, orange and magenta with the colour conjugates (CC) pained blue, purple, and magenta. AIAO layers therefore consist of orange, green, and orange spins while CC layers are made of purple, blue, and magenta spins. A 2:2 stacking arrangement along the [111] direction consisting of two layers of AIAO spins with $\phi = 0$ followed by two layers of colour conjugate spins with $\phi = \pi$ is observed. Colours are painted on the spins via projection along the colour axis; higher temperatures and greater fluctuations may lead to misassigned or unassigned (black) spins.

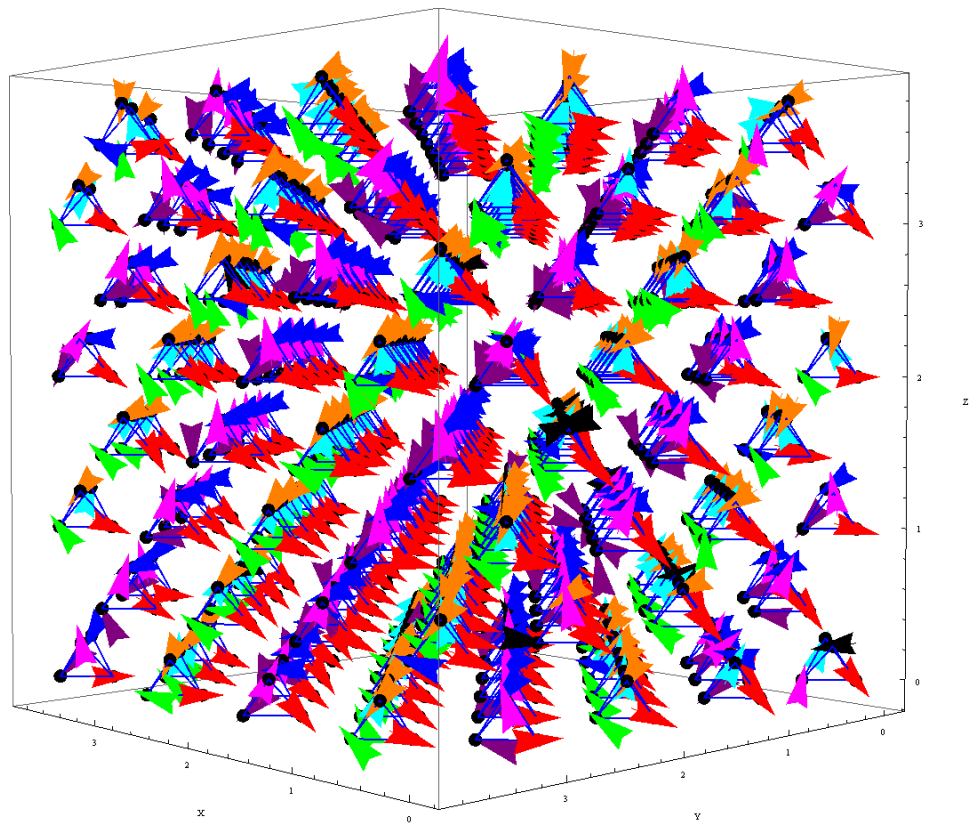

Figure 4.26: The N3 (1:1 AIAO/CC) state for a $L = 4$ simulation at temperature of $T = 0.065$, $\theta_b = 0.80$. The entire 1024 spin system is shown. The weathervane spins are coloured red; other colour spins and their colour conjugates are respectively green-purple, orange-magenta, and cyan-blue. AIAO layers are shown as planes of green, cyan, and orange spins while the CC layers are blue, purple, and magenta. A 1:1 stacking arrangement of AIAO and CC layers along the (111) direction is observed.

Looking at the structure factors of these weathervane states we observe that the spin and octupolar structure factors are flat (0 intensity) with the exception of the previously described expected Bragg peaks and the $\vec{q} = 0$ peak in the octupolar structure factor. The structure factor of the AIAO state under Monte Carlo simulation (not shown) is identical to the calculated results shown in Figure 4.19.

In the N1, N2, and N3 states we observe additional correlations in the spin structure factor (Figure 4.27) along the line described by $\vec{q} = (\delta, \delta, \pm 2 \pm \delta)$[15] in the *hhl* plane. This

[15] A line in 3D space can be written in vector parametric form (defining the x, y, and z components of the

corresponds to the correlations between layers of spins. We note that the effect that the different stacking ratios have on points in along this line. For 1:1 AIAO/CC stacking, this manifests as a peak at every other point along the $\vec{q} = (\delta,\ \delta,\ \pm 2 \pm \delta)$ line. The effect of this stacking is also seen in the octupolar order parameter along the $\vec{q} = 0$ lines.

line in terms of a parameter t) i.e. $\vec{r} = \vec{r_0} + t \cdot \vec{m}$ where $\vec{r_0}$ is the *intercept* of the line and $\vec{m} = (m_x, m_y, m_z)$ is the directional vector. To describe a line parallel to the [111] direction we set $m_x = m_y = m_z = \delta$.

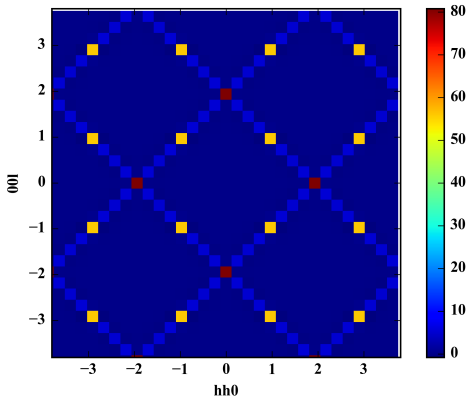

(a) N1 Spin

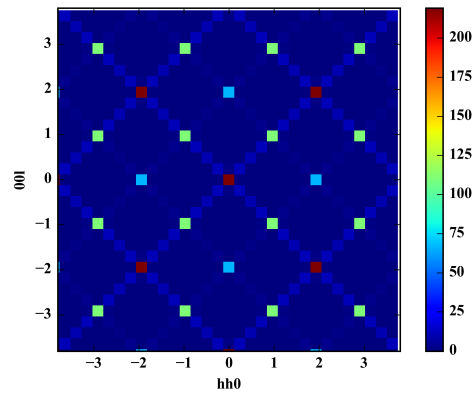

(b) N1 Octupole

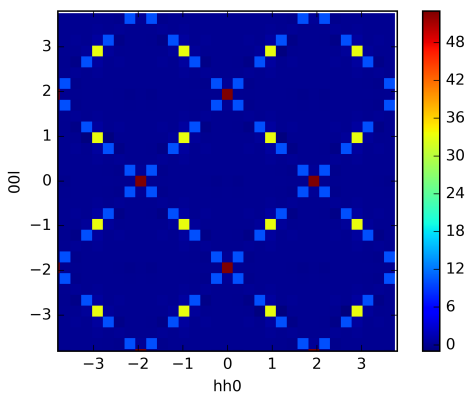

(c) N2 Spin

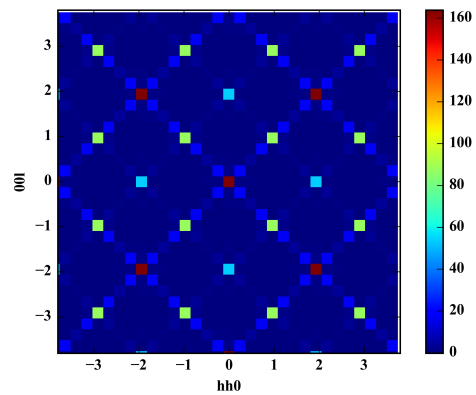

(d) N2 Octupole

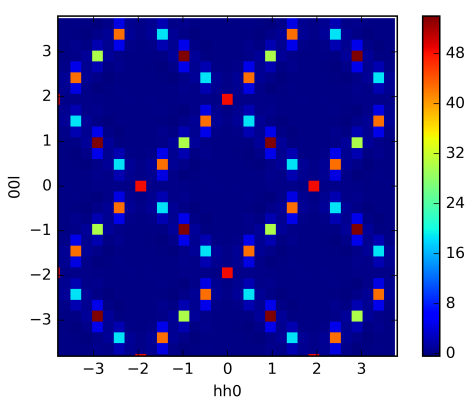

(e) N3 Spin

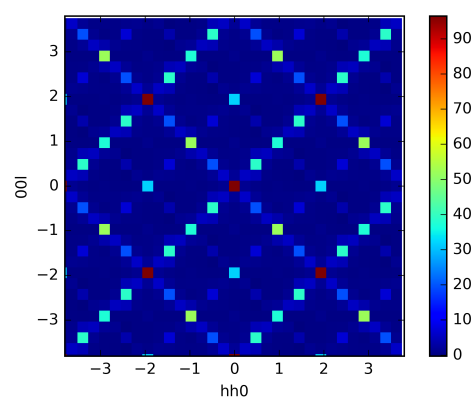

(f) N3 Octupole

Figure 4.27: Spin and octupolar structure factors for the N1, N2, and N3 weathervane states with $\theta_b = 1.30$, L=4 for the simulation shown in Figure 4.24b.

4.7.4 {001} Metastable States

Simulations started in the M0 or {001} ground state rapidly order into the M1 and M2 states, spending the vast majority of their time for most biquadratic strengths in the M2 state (Figure 4.24a). Unlike the AIAO ordered phase where weathervane stacking occurs along the [111] direction, the {001} state as considered here stacks weathervane modes along the $\vec{z}$ direction (Figure 4.18b). The z-stacked weathervane modes in the {001} state are parallel to the z axis, and are thus constrained by the periodic boundary conditions in only two dimensions. The plateau labeled M1 represents a system with a significant degree of order where 3:1 colour/conjugate colour stacking is observed. The M2 *manifold* state, however, consists of parallel weathervane membranes whose boundaries may be delineated by spin of any colour – weathervane membranes may be *interleaved* with one another. We observe the system in a variety of states with greatly variable degrees of octupolar ordering (Figures 4.20 - 4.22). Furthermore, the colours of spins on each FCC sublattice may change as the simulation rotates weathervane membranes relative to one another.

We first note that the M1 state bears many similarities to the AIAO N1 metastable state with 3:1 stacking layers. Only spins of one colour form the weathervane poles as shown in red in Figure 4.28. The simulation is only found in this arrangement for weak biquadratic interactions and for short periods of time. It is quite possible that this state simply represents the first transition step into the M2 weathervane manifold phase. The other stacking arrangements of 2:2 and 1:1 are likely possible, but are not observed.

The colours of the lattice as shown in Figure 4.30a depict what appears to be a perfect arrangement of weathervane modes. Careful eyes will notice however that the groups of orange spins in the two orange membranes along the center portion of the lattice appear to point in subtly different directions in the figure. Interestingly, the orange spins on the non-weathervane alternating orange-blue line of spins appear to have orientations exactly between the directions that the weathervane membrane spins point (3 way colour splitting). This does not appear to be a coincidence or a visual projection artifact. We note that the green weathervane membrane spins are slightly tilted with respect to all the non-weathervane membrane green spins. This may be related to the predicted weathervane angle of $\phi = \pi$ [31]; spins in the lattice could be rotated by a similar angle[16]. However, this would violate the colour ice rules as a colour and its colour conjugate are not permitted in the same tetrahedron. This colour spin would have to compose the weathervane pole spins while the colour conjugate would take the place of this colour at all other positions in this

[16]The system may lack a global weathervane "pole", with interleavened weathervane membranes spins may be rotated with respect to more than one set of *pole spins* and so this angle may not be precisely 180°.

lattice. This explanation is unsatisfactory as there appears to be more than a two-fold colour splitting as shown in Figure 4.30a. However, one must note that the M1 3:1 stacked state (Figure 4.28) does possess a weathervane angle of $\phi = \pi$ and so has conjugate colours.

Finally, is very difficult to visually assign colours due to the interleaved spin colour groups and so they are not assigned in the following figures. A small section of the lattice showing this in more detail is seen in Figure 4.30 along with a Mercator projection[17] showing one of many general arrangements that spins take in the M2 manifold.

[17] A projection of a sphere onto a 2D surface. Most commonly used for maps, a Mercator projection is a cylindrical projection of the surface of a sphere onto a 2D plane. Lines of both latitude and longititude are drawn as parallel vertical and horizontal lines leading to significant differences in the distances between equally spaced points at the equator and at the poles. The advantage is that shapes and bearings are preserved.

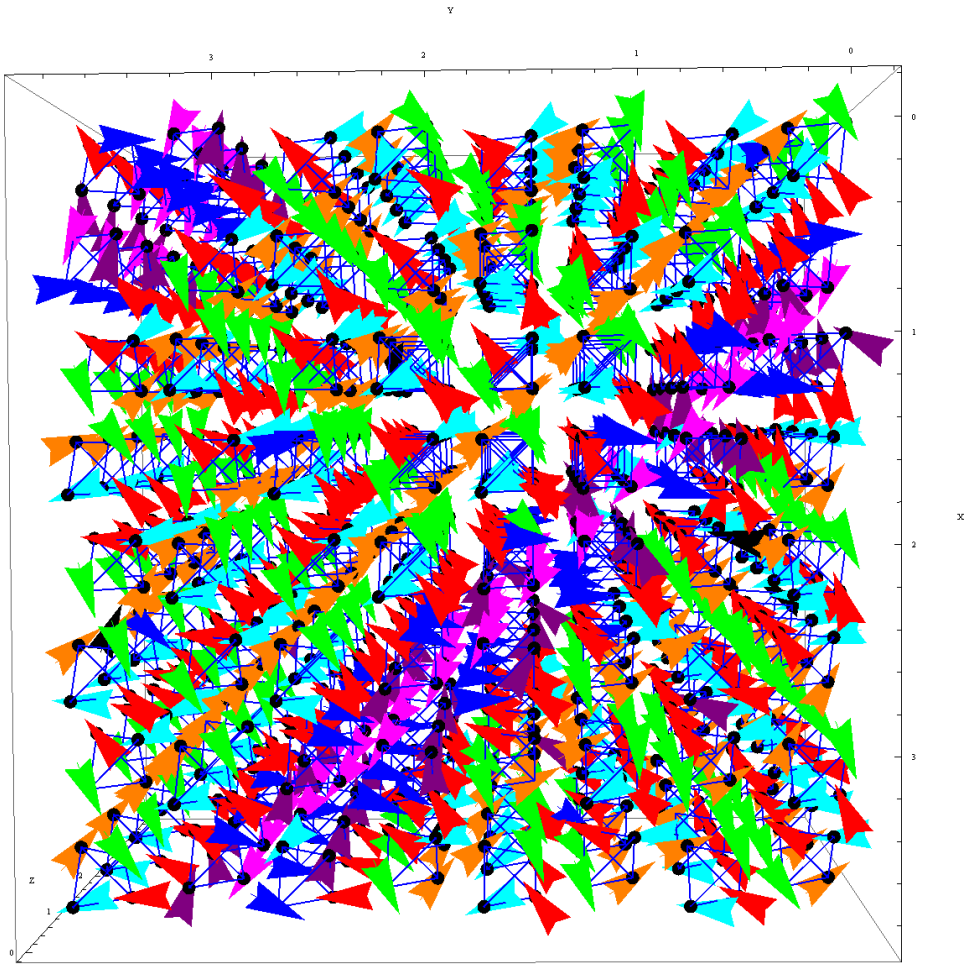

Figure 4.28: The {001} M1 3:1 stacked weathervane state showing the stacking of AIAO and CC layers along the z axis. Colours and their colour companions are assigned with the weathervane "poles" coloured red. The xy plane of the lattice is shown with the z axis extending into the page.

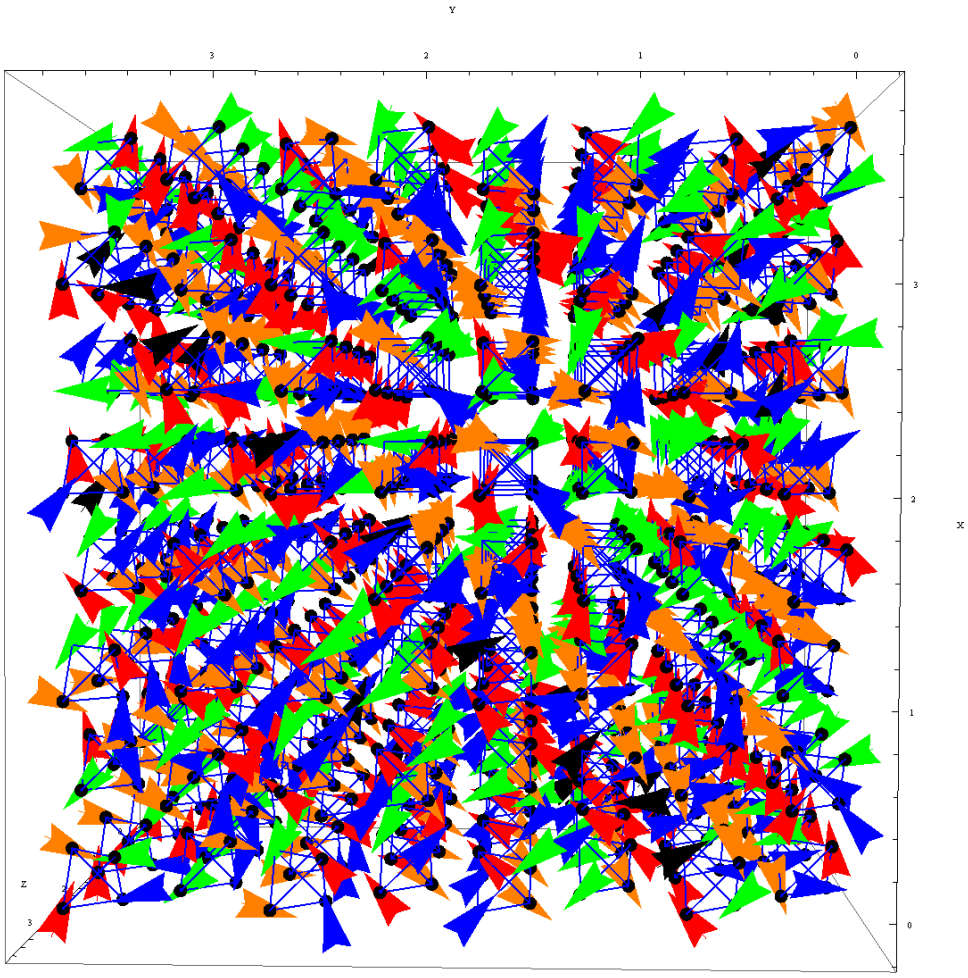

Figure 4.29: The {001} M2 *manifold* state. We observe the random stacking of weathervane membranes along the z direction. In the image shown all colours of spins (red, blue, green, and orange) are seen to delineate a weathervane boundary at least once. While colour conjugates are almost certaintly present, it is difficult to assign colours accurately.

The M2 weathervane manifold state shows rapid fluctuations between various weathervane states on significantly faster timescales than observed for the AIAO weathervane states and for the paramagnetic to octupolar transition observed in the systems undergoing cooling (Figure 4.30c). Observing "snapshots" of the spins in the system on the unit sphere (not shown), we note the presence of many temporary arrangements of spins including, but not limited to, the standard 4 colour cluster, the four colour cluster with each cluster elongated into ovals, the four colour cluster with a varying number of "strings"

– spins connecting one cluster to another in "chains" that include varying number of clusters (these "strings" may be sufficiently thick that clusters "merge" with one another), and 7+ cluster configurations (i.e. 3 of the four colours possess a colour companion, one colour forms the "pole"). Occasionally, 10+ groupings of spins are seen. A time series of octupolar order is shown in Figure 4.30c showing short lived spikes and drops representing the simulation exploring various weathervane states (i.e. a very high measure of octupolar order implies the absence of weathervane modes). As a zero energy excitation with no substantial energy barriers between states, the rotation of weathervane membranes does not appear to be hindered by any significant extent by the single spin flip algorithm and the dynamics of the system are fast. Only a brief investigation of the M2 manifold state has been completed; it is quite likely that the complete description of the state is quite a bit more complex than presented here.

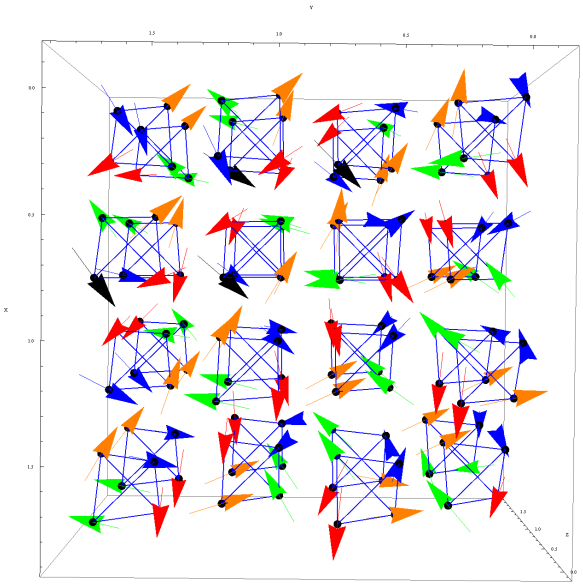

(a) 2×2×2 section of the lattice showing small spin deviations within spins of the same colours

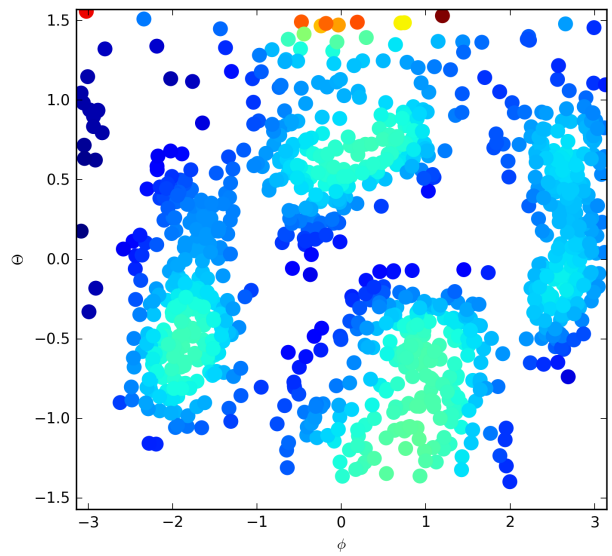

(b) Mercator projection of spins on the unit sphere

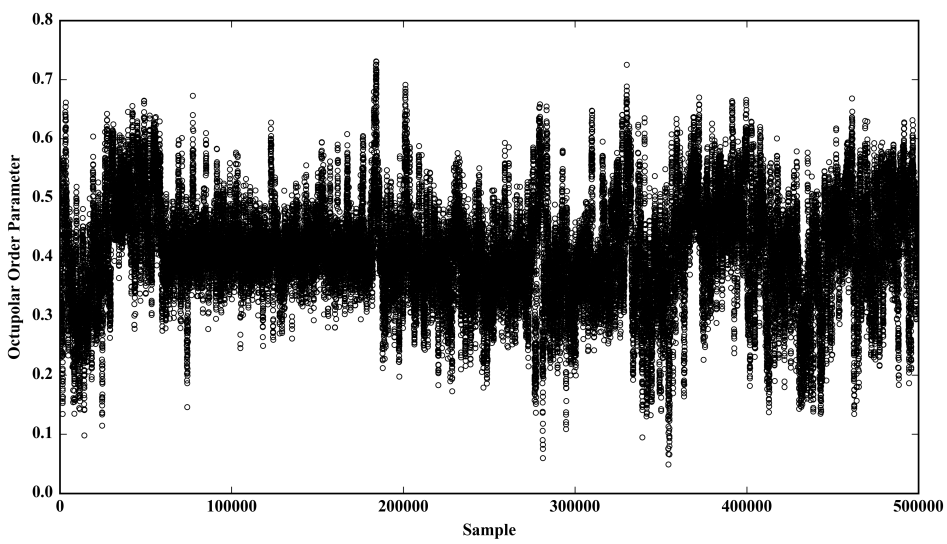

(c) Time series

Figure 4.30: A snapshot of the $L = 4$ lattice a) A section of the lattice in the M2 state showing colour fluctuations. Companion colours are difficult to assign but we notice groupings within each colour indicative of a weathervane angle of 180°. b) Mercator projection of a snapshot of spins in the lattice on the unit sphere. We notice that the four tetrahedral groupings appear bimodal. The tightness of the grouping of the spins is indicated by colour. c) Time series of octupolar order parameter. The dynamics of simulations in the {001} state are significantly faster than for simulations of random colour states due to the presence of the zero energy rotational modes.

Finally, we characterize the starting $\{001\}$ state with stacking along the z axis using the structure factor to describe general (i.e. the sum of the contributions of all weathervane modes) spin correlations. The spin and octupolar structure factor are shown in Figure 4.31. We note that the fully ordered $\{001\}$ structure factor differs greatly from the fully ordered AIAO structure factor as it possesses weathervane modes parallel to the z axis and thus we observe peaks at $\vec{q} = (\pm 1,\ \pm 1,\ 0)$. As weathervane rotations are introduced, we note correlations "splitting" with $q_z = 0$ (i.e. spins in the plane extending in the z direction are the same colour if they are part of a weathervane membrane). As weathervanes stack in the xy plane with random periodicity these correlations smear out and form *bars* with $\vec{q_z} = 0$. These correlations between planes along the z axis are also observed in the octupolar structure factor with its $\vec{q} = 0$ ordering.

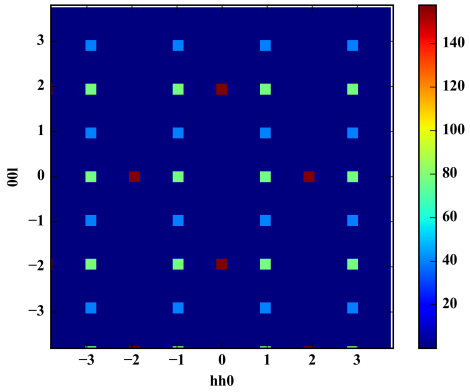

(a) M0 Spin

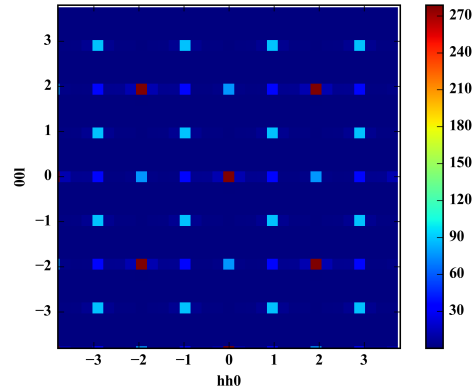

(b) M0 Octupole

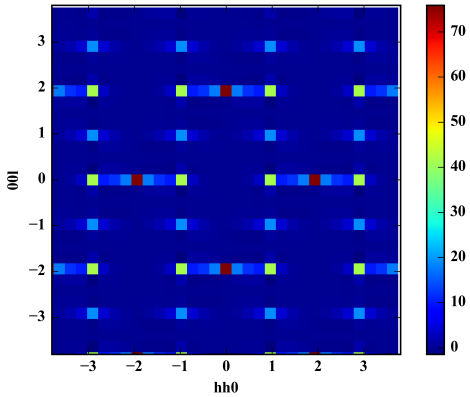

(c) M1 Spin

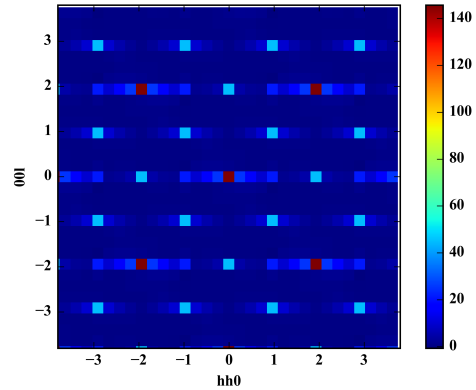

(d) M1 Octupole

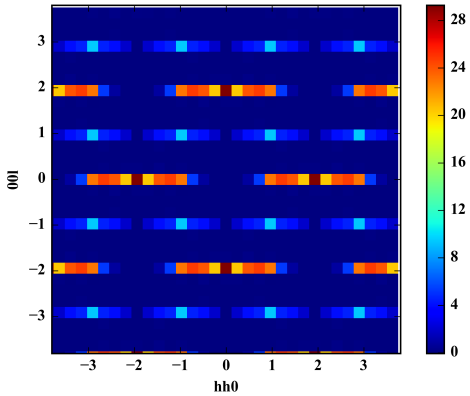

(e) M2 Spin

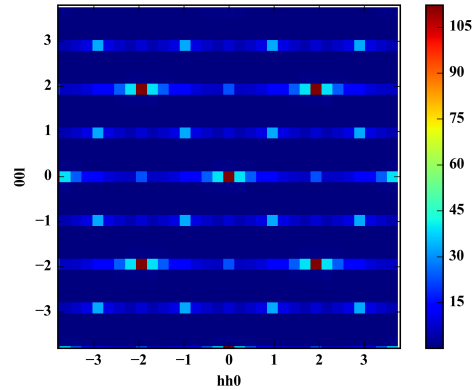

(f) M2 Octupole

Figure 4.31: Spin and octupolar structure factors for the M0 ($\theta_b = 0.05$, T = 0.007), M1 ($\theta_b = 0.05$, T = 0.012), M2 states ($\theta_b = 0.48$, T = 0.037).

4.7.5 Potential Dipolar Long-Range Order

This preliminary investigation into the low temperature ordered phases of the $b > 0$ bilinear biquadratic Heisenberg pyrochlore has revealed several important new things. First, it appears that the single spin-flip algorithm is sufficient (although perhaps still not fast) at sampling weathervane states, especially states started in a $\{001\}$ arrangement. The imposition of periodic boundary conditions forces specific weathervane mode arrangements in the AIAO state (and to some degree in the $\{001\}$ state). Finally, it must be noted that this investigation is far from complete as numerous other potential ground states exist such as the $\sqrt{3} \times \sqrt{3}$ state [31] which we have obmitted from this search.

We note a potential point of major significance in the spin structure factors of the AIAO and $\{001\}$ states which are distinct from one another due to the different stacking of weathervane membranes and possess the *fingerprints* of different rotational weathervane states. First, the $\{001\}$ structure factor, even in its ground state, is distinct from the AIAO structure factor due to the stacking of weathervane layers parallel to the z axis. Second, as the system is cooled towards the transition temperature, it begins to display short-range correlations indicative of its lower temperature behaviour – *fingerprints* of the lower temperature ordered phase. These fluctuations should be observable in the structure factor *just above* the critical temperature. It is tempting to attribute the similarity in the octupolar structure factor of the system undergoing cooling as shown in Figures 4.15 and 4.16 just above the critical temperature and which appears to possess the same diagonal $\vec{q} = (\delta, \delta, \pm 2 \pm \delta)$ correlations as the simulations started in the AIAO phase as significant. However, calculations with larger system sizes indicate that this potential fingerprint of long range octupolar order is just a visual artifact of the constructive interference of the diffuse scattering on the nearby peaks – no intensity is observed along the $\vec{q} = (\delta, \delta, \pm 2 \pm \delta)$ lines. We therefore observe that the correlations in the spin and octupolar structure factors indicating the presence of weathervane modes in the AIAO and $\{001\}$ states do not appear to be present, leading us to believe that simulations are unlikely to order into the long-range dipolar AIAO and $\{001\}$ states at low temperatures. Such a conclusion is not without caveats. As discussd eariler, the single spin flip algorithm cannot be shown to be reliable and it is possible that the addition of a loop move would aid in equilibration potentially revealing interesting physics in the octupolar ordered phase.

4.8 Summary

We have shown that the bilinear-biquadratic Heisenberg pyrochlore with positive biquadratic interactions appears to undergo a first-order transition at low temperatures into an octupolar ordered state with no long-range spin dipolar order. This has been confirmed with classical Monte Carlo simulation using single spin-flips. The dynamics of the single spin flip algorithm remains exceedingly slow for simulations cooling below the transition and the implementation of non-local loop moves that are capable of flipping multiple spins at once could possibly dramatically improve simulation ergodicity. Although it appears that the octupolar ordered state of the $b > 0$ biquadratic pyrochlore possesses no long-range dipolar order, the freezing of the simulation below the transition temperature makes this statement somewhat tenuous.

An investigation into the dynamics of the low temperature AIAO and $\{001\}$ long-range ordered states confirms the presence of weathervane modes with angles of $\phi = 0$ and π as initially predicted by Wan and Gingras [31]. Low temperature simulations starting in the AIAO state reveal the periodic 3:1, 2:2, and 1:1 stacking of kagome layers along the [111] direction with weathervane angles of $\phi = 0$ or $\phi = \pi$ and which are stabalized by the periodic boundary conditions of the lattice. Weathervane modes are less constrained in the $\{001\}$ state, and simulations started in this state rapidly enter a weathervane manifold state characterized by rapid dynamics as the simulation samples the various allowed weathervane rotational states.

Chapter 5

Conclusion

We have shown that the bilinear-biquadratic Heisenberg pyrochlore with $b > 0$ undergoes a first-order transition from the paramagnetic to an octupolar or tetrahedral state and is unlikely to possess long-range dipolar order. The spin and octupolar structure factors have been calculated and serve as an indicator for this transition with sharp $\vec{q} = 0$ peaks forming in the octupolar structure factor as the system is cooled below the transition temperature. We note that octupolar ordering can be subtle to observe and that care must be taken when interpreting multipolar order parameters which can have difficulty distinguishing random octupolar states from those of long-range ordered spin states.

An investigation into the low temperature physics of the potential AIAO and $\{100\}$ long range ordered states has helped to reveal potential intricacies of the weathervane mode rotations. We confirm that the rotational modes predicted by Wan and Gingras [31] exist for weathervane rotational angles of $\phi = 0$ and π. For the AIAO low temperature state, we find that the stacking of the AIAO ($\phi = 0$) and colour-conjugate ($\phi = \pi$) rotated weathervane membranes along the [111] direction are constrained by the periodic boundary conditions. For a small $L = 4$ simulation, we find stacking of AIAO and colour conjugate (CC) layers with 3:1, 2:2 and 1:1 periodicities.

The $\{100\}$ state with weathervane membranes stacked along a cubic axis is less constrained by the periodic boundary conditions and system size. We find that while the simulation does potentially possess stacked states (only a 3:1 stacked state was observed for small θ_b), the simulation rapidly evolves into a weathervane manifold state in which a large variety of distinct weathervane states are sampled in the course of the simulation. These states involve interleaved weathervane membranes of all colours stacked in the z (or symmetrically equivalent) direction; however the simulation appears to also sample a

vast variety of other weathervane states such as fully tetrahedral ordered states and states whose octupolar order is indistinguishable from that of the paramagnetic state.

We note the *fingerprints* of the weathervane modes in these states in the spin and octupolar structure factors as additional correlations in the spin and octupolar structure factors. The low-temperature AIAO states show correlations along this reciprocal space direction = (δ, δ, $\pm 2 \pm \delta$) with periodicity given by the stacking ratio. The {100} state shows weathervane membranes stacking along the direction of the alternating layers of tetrahedra (z axis) and correlations of various length scales in the perpendicular xy plane i.e. $\vec{q_z} = 0$.

Just above the transition temperature, and before the Monte Carlo simulation freezes, the onset of potential dipolar order may be visible if the low temperature ordered state of the system would possess dipolar long range order. However, the spin structure factor of the simulation upon cooling just above the critical temperature did not display the characteristic scattering of weathervane rotations in the AIAO or {100} states, or in the case of the {100} state, the additional (± 1, ± 1, 0) peaks representative of the $\vec{q_z} = 0$ stacked weathervane membranes. We therefore see no indication of a potential long-range ordered state developing upon cooling although this cannot be confirmed due to the freezing of the simulation at, and below, the transition temperature.

The simulation dynamics of the $b > 0$ bilinear-biquadratic Heisenberg pyrochlore using single spin-flips is found to be extremely slow with simulations freezing upon cooling below the transition temperature. Simulation timescales are extremely long (the transition from the paramagnetic to octupolar state takes hundreds of thousands of Monte Carlo sweeps) and therefore statistics cannot be significantly improved by the use of parallel tempering. However, the weathervane dynamics of the low temperature ordered states was found to be approachable with single spin flips owing to the zero energy nature of the rotations of weathervane modes.

Looking forward, the addition of two colour loop moves should aid in the equilibration and help address the ergodicity issues that were encountered in this thesis project. It is hoped that the addition of zero energy moves that do not violate the colour ice rules might help prevent freezing at the transition. Furthermore, two colour loop moves may shed more light on the dynamics of the low temperature ordered states. As an example, rotating the colours in the inverted tetrahedra in the {100} state will allow the transformation into the AIAO state. At the moment, the ergodicity issues due to the extremely slow single spin-flip dynamics make it difficult to assign certainty to the specifics of the paramagnetic to octupolar transition such as the exact location of the transition or the behaviour of the specific heat. It may also be worthwhile to investigate other potential long-range ordered

states such as the $\sqrt{3} \times \sqrt{3}$ state which would require a modified Monte Carlo code making use of a hexagonal unit cell.

The collapse of the "cooperative paramagnet" ground state of the classical nearest-neighbout Heisenberg pyrochlore into magnetically ordered states in the presence of further interactions such as dipole interactions [8] or further neighbour interactions [73][74] has been well defined, however, little work as been has been done exploring these perturbations in quantum systems [1] . Specifically what is the role that quantum fluctuations play in the low temperature physics of Heisenberg systems and the selection of a ground state? How do quantum fluctuations lift the degeneracy of the classical ground state? While preliminary work investigating quantum fluctutations has been completed [75], the effect of biquadratic coupling is unknown.

Finally, we remark that unique properties can present themselves in models and materials where they would not normally be expected. An example of this are the pyrochlore antiferromagnets $NaSrMn_2F_7$ [76] and $NaCaNi_2F_7$ [76][77][78] which behave like Heisenberg antiferromagnets with additional interactions. These materials have motivated work investigating the role that small perturbations play in the ordering of Heisenberg pyrochlore in the presence of further interactions [75] and possess interesting properties characteristic of quantum spin liquids, nematic order, and glassy systems [77]. Interesting and novel physics often manifests itself in subtle manners.

[1] A *very* recently published paper by Iqbal *et al.* [75] provides some insight towards this question.

Bibliography

[1] Edwards, S. F., and Anderson, P. W. (1975). Theory of spin glasses. Journal of Physics F: Metal Physics, 5(5), 965.

[2] Wannier, G. H. (1950). Antiferromagnetism. The triangular Ising net. Physical Review, 79(2), 357.

[3] Gardner, J. S., Gingras, M. J. P., and Greedan, J. E. (2010). Magnetic pyrochlore oxides. Reviews of Modern Physics, 82(1), 53.

[4] Anderson, P. W. (1956). Ordering and antiferromagnetism in ferrites. Physical Review, 102(4), 1008.

[5] Villain, J. (1979). Insulating spin glasses. Zeitschrift für Physik B Condensed Matter, 33(1), 31-42.

[6] Reimers, J. N. (1992). Absence of long-range order in a three-dimensional geometrically frustrated antiferromagnet. Physical Review B, 45(13), 7287.

[7] Moessner, R., and Chalker, J. T. (1998). Properties of a classical spin liquid: the Heisenberg pyrochlore antiferromagnet. Physical Review Letters, 80(13), 2929.

[8] Palmer, S. E., and Chalker, J. T. (2000). Order induced by dipolar interactions in a geometrically frustrated antiferromagnet. Physical Review B, 62(1), 488.

[9] Tsuneishi, D., Ioki, M., and Kawamura, H. (2007). Novel ordering of the pyrochlore Heisenberg antiferromagnet with the ferromagnetic next-nearest-neighbour interaction. Journal of Physics: Condensed Matter, 19(14), 145273.

[10] Nakamura, T., and Hirashima, D. (2007). Classical antiferromagnet on the pyrochlore lattice. Journal of Magnetism and Magnetic Materials, 310(2), 1297-1299.

[11] Tchernyshyov, O., Moessner, R., and Sondhi, S. L. (2002). Order by distortion and string modes in pyrochlore antiferromagnets. Physical Review Letters, 88(6), 067203.

[12] Tchernyshyov, O. (2004). Structural, orbital, and magnetic order in vanadium spinels. Physical Review Letters, 93(15), 157206.

[13] Bellier-Castella, L., Gingras, M. J. P. , Holdsworth, P. C. W., and Moessner, R. (2001). Frustrated order by disorder: The pyrochlore anti-ferromagnet with bond disorder. Canadian Journal of Physics, 79(11-12), 1365-1371.

[14] Saunders, T. E., and Chalker, J. T. (2007). Spin freezing in geometrically frustrated antiferromagnets with weak disorder. Physical Review Letters, 98(15), 157201.

[15] Blume, M., and Hsieh, Y. Y. (1969). Biquadratic exchange and quadrupolar ordering. Journal of Applied Physics, 40(3), 1249-1249.

[16] Gramsbergen, E. F., Longa, L., and de Jeu, W. H. (1986). Landau theory of the nematic-isotropic phase transition. Physics Reports, 135(4), 195-257.

[17] Takata, E., Momoi, T., and Oshikawa, M. (2015). Nematic ordering in pyrochlore antiferromagnets: high-field phase of chromium spinel oxides. arXiv preprint arXiv:1510.02373.

[18] Shannon, N., Penc, K., and Motome, Y. (2010). Nematic, vector-multipole, and plateau-liquid states in the classical O(3) pyrochlore antiferromagnet with biquadratic interactions in applied magnetic field. Physical Review B, 81(18), 184409.

[19] Santini, P., Carretta, S., Amoretti, G., Caciuffo, R., Magnani, N., and Lander, G. H. (2009). Multipolar interactions in f-electron systems: The paradigm of actinide dioxides. Reviews of Modern Physics, 81(2), 807.

[20] Tokunaga, Y., Walstedt, R. E., Homma, Y., Aoki, D., Kambe, S., Sakai, H., ... and Shiokawa, Y. (2006). ^{237}Np – ^{17}O cross relaxation in NpO_2 driven by indirect spin-spin coupling. Physical Review B, 74(6), 064421.

[21] Uimin, G. (1997). Quadrupolar and magnetic ordering in CeB_6. Physical Review B, 55(13), 8267.

[22] Demishev, S. V., Semeno, A. V., Bogach, A. V., Paderno, Y. B., Shitsevalova, N. Y., and Sluchanko, N. E. (2006). Antiferro-quadrupole resonance in CeB_6 Physica B: Condensed Matter, 378, 602-603.

[23] Demishev, S. V., Krasnorussky, V. N., Bogach, A. V., Voronov, V. V., Shitsevalova, N. Y., Filipov, V. B., ... and Sluchanko, N. E. (2017). Electron nematic effect induced by magnetic field in antiferroquadrupole phase of CeB_6. Scientific Reports, 7(1), 17430.

[24] Matsumura, T., Yonemura, T., Kunimori, K., Sera, M., Iga, F., Nagao, T., and Igarashi, J. I. (2012). Antiferroquadrupole order and magnetic field induced octupole in CeB_6. Physical Review B, 85(17), 174417.

[25] Takatsu, H., Taniguchi, T., Kittaka, S., Sakakibara, T., and Kadowaki, H. (2017). Thermodynamic properties of quadrupolar states in the frustrated pyrochlore magnet $Tb_2Ti_2O_7$. In Journal of Physics: Conference Series (Vol. 828, No. 1, p. 012007). IOP Publishing.

[26] Kadowaki, H., Takatsu, H., Taniguchi, T., Fk, B., and Ollivier, J. (2015). Composite Spin and Quadrupole Wave in the Ordered Phase of Tb_{2+x} $Ti_{2-x}O_{7+y}$. Spin (Vol. 5, No. 02, p. 1540003). World Scientific Publishing Company.

[27] Takatsu, H., Onoda, S., Kittaka, S., Kasahara, A., Kono, Y., Sakakibara, T., ... and Taniguchi, T. (2016). Quadrupole order in the frustrated pyrochlore Tb_{2+x} $Ti_{2-x}O_{7+y}$. Physical Review Letters, 116(21), 217201.

[28] Penc, K., Shannon, N., and Shiba, H. (2004). Half-magnetization plateau stabilized by structural distortion in the antiferromagnetic Heisenberg model on a pyrochlore lattice. Physical Review Letters, 93(19), 197203.

[29] Shannon, N., Ueda, H., Motome, Y., Penc, K., Shiba, H., and Takagi, H. (2006). Half-magnetization plateaux in Cr spinels. In Journal of Physics: Conference Series (Vol. 51, No. 1, p. 31). IOP Publishing.

[30] Henley, C. L. (1989). Ordering due to disorder in a frustrated vector antiferromagnet. Physical Review Letters, 62(17), 2056.

[31] Wan, Y., and Gingras, M. J. P. (2016). Color ice states, weathervane modes, and order by disorder in the bilinear-biquadratic pyrochlore Heisenberg antiferromagnet. Physical Review B, 94(17), 174417.

[32] Harris, A. B., Kallin, C., and Berlinsky, A. J. (1992). Possible Néel orderings of the kagome antiferromagnet. Physical Review B, 45(6), 2899.

[33] Ritchey, I., Chandra, P., and Coleman, P. (1993). Spin folding in the two-dimensional Heisenberg kagome antiferromagnet. Physical Review B, 47(22), 15342.

[34] Chandra, P., Coleman, P., and Ritchey, I. (1991). Magnets without moments: Spin nematics and beyond. Journal of Applied Physics, 69(8), 4974-4978.

[35] Chalker, J. T., Holdsworth, P. C. W., and Shender, E. F. (1992). Hidden order in a frustrated system: Properties of the Heisenberg kagome antiferromagnet. Physical Review Letters, 68(6), 855.

[36] Sachdev, S. (1992). Kagome-and triangular-lattice Heisenberg antiferromagnets: Ordering from quantum fluctuations and quantum-disordered ground states with unconfined bosonic spinons. Physical Review B, 45(21), 12377.

[37] Huse, D. A., and Rutenberg, A. D. (1992). Classical antiferromagnets on the kagome lattice. Physical Review B, 45(13), 7536.

[38] Metropolis, N., Rosenbluth, A. W., Rosenbluth, M. N., Teller, A. H., and Teller, E. (1953). Equation of state calculations by fast computing machines. The Journal of Chemical Physics, 21(6), 1087-1092.

[39] M. E. J. Newman and G. T. Barkema. Monte Carlo Methods in Statistical Physics. 2001 reprint. Oxford University Press: New York, USA, 2001.

[40] Landau, D. P., and Binder, K. (2014). A guide to Monte Carlo simulations in statistical physics. Cambridge University Press.

[41] Swendsen, R. H., and Wang, J. S. (1986). Replica Monte Carlo simulation of spin-glasses. Physical Review Letters, 57(21), 2607.

[42] Swendsen, R. H., and Wang, J. S. (1987). Nonuniversal critical dynamics in Monte Carlo simulations. Physical Review Letters, 58(2), 86.

[43] Adler, S. L. (1981). Over-relaxation method for the Monte Carlo evaluation of the partition function for multiquadratic actions. Physical Review D, 23(12), 2901.

[44] Creutz, M. (1987). Overrelaxation and Monte Carlo simulation. Physical Review D, 36(2), 515.

[45] Wolff, U. (1989). Collective Monte Carlo updating for spin systems. Physical Review Letters, 62(4), 361.

[46] Van Laarhoven, P. J., and Aarts, E. H. (1987). Simulated annealing. In Simulated annealing: Theory and applications (pp. 7-15). Springer, Neatherlands, Dordrecht.

[47] Kirkpatrick, S., Gelatt, C. D., and Vecchi, M. P. (1983). Optimization by simulated annealing. Science, 220(4598), 671-680.

[48] Cerny, V. (1985). Thermodynamical approach to the traveling salesman problem: An efficient simulation algorithm. Journal of optimization theory and applications, 45(1), 41-51.

[49] Marinari, E., and Parisi, G. (1992). Simulated tempering: a new Monte Carlo scheme. EPL (Europhysics Letters), 19(6), 451.

[50] Earl, D. J., and Deem, M. W. (2005). Parallel tempering: Theory, applications, and new perspectives. Physical Chemistry Chemical Physics, 7(23), 3910-3916.

[51] Romá, F., Risau-Gusman, S., Ramirez-Pastor, A. J., Nieto, F., and Vogel, E. E. (2009). The ground state energy of the Edwards–Anderson spin glass model with a parallel tempering Monte Carlo algorithm. Physica A: Statistical Mechanics and its Applications, 388(14), 2821-2838.

[52] Ballesteros, H. G., Cruz, A., Fernandez, L. A., Martin-Mayor, V., Pech, J., Ruiz-Lorenzo, J. J., and Ungil, C. (2000). Critical behavior of the three-dimensional Ising spin glass. Physical Review B, 62(21), 14237.

[53] Wang, W., Machta, J., and Katzgraber, H. G. (2015). Comparing Monte Carlo methods for finding ground states of Ising spin glasses: Population annealing, simulated annealing, and parallel tempering. Physical Review E, 92(1), 013303.

[54] Hukushima, K., and Nemoto, K. (1996). Exchange Monte Carlo method and application to spin glass simulations. Journal of the Physical Society of Japan, 65(6), 1604-1608.

[55] Ferrenberg, A. M., and Swendsen, R. H. (1988). New Monte Carlo technique for studying phase transitions. Physical Review Letters, 61(23), 2635.

[56] Ferrenberg, A. M., and Swendsen, R. H. (1989). Optimized Monte Carlo data analysis. Computers in Physics, 3(5), 101-104..

[57] Melko, R. G., and Gingras, M. J. P. (2004). Monte Carlo studies of the dipolar spin ice model. Journal of Physics: Condensed Matter, 16(43), R1277.

[58] den Hertog, B. C., and Gingras, M. J. P. (2000). Dipolar interactions and origin of spin ice in Ising pyrochlore magnets. Physical Review Letters, 84(15), 3430.

[59] Shinaoka, H., and Motome, Y. (2010). Loop algorithm for classical Heisenberg models with spin-ice type degeneracy. Physical Review B, 82(13), 134420.

[60] Shinaoka, H., Tomita, Y., and Motome, Y. (2011). Loop algorithm for classical antiferromagnetic Heisenberg models with biquadratic interactions. In Journal of Physics: Conference Series (Vol. 320, No. 1, p. 012009). IOP Publishing.

[61] Zhitomirsky, M. E. (2008). Octupolar ordering of classical kagome antiferromagnets in two and three dimensions. Physical Review B, 78(9), 094423.

[62] Lubensky, T. C., and Radzihovsky, L. (2002). Theory of bent-core liquid-crystal phases and phase transitions. Physical Review E, 66(3), 031704.

[63] Moessner, R., and Ramirez, A. P. (2006). Geometrical frustration. Phys. Today, 59(2), 24.

[64] Henley, C. L. (2005). Power-law spin correlations in pyrochlore antiferromagnets. Physical Review B, 71(1), 014424.

[65] Moessner, R., and Sondhi, S. L. (2003). Theory of the [111] magnetization plateau in spin ice. Physical Review B, 68(6), 064411.

[66] Chau, P. L., and Hardwick, A. J. (1998). A new order parameter for tetrahedral configurations. Molecular Physics, 93(3), 511-518.

[67] Errington, J. R., and Debenedetti, P. G. (2001). Relationship between structural order and the anomalies of liquid water. Nature, 409(6818), 318.

[68] Kumar, P., Buldyrev, S. V., and Stanley, H. E. (2009). A tetrahedral entropy for water. Proceedings of the National Academy of Sciences, 106(52), 22130-22134.

[69] Kondev, J., and Henley, C. L. (1995). Four-coloring model on the square lattice: A critical ground state. Physical Review B, 52(9), 6628.

[70] Khemani, V., Moessner, R., Parameswaran, S. A., and Sondhi, S. L. (2012). Bionic Coulomb phase on the pyrochlore lattice. Physical Review B, 86(5), 054411.

[71] Chern, G. W., and Wu, C. (2011). Orbital ice: An exact Coulomb phase on the diamond lattice. Physical Review E, 84(6), 061127.

[72] Chern, G. W., and Wu, C. (2014). Four-coloring model and frustrated superfluidity in the diamond lattice. Physical Review Letters, 112(2), 020601.

[73] Reimers, J. N., Berlinsky, A. J., and Shi, A. C. (1991). Mean-field approach to magnetic ordering in highly frustrated pyrochlores. Physical Review B, 43(1), 865.

[74] Tsuneishi, D., Ioki, M., and Kawamura, H. (2007). Novel ordering of the pyrochlore Heisenberg antiferromagnet with the ferromagnetic next-nearest-neighbour interaction. Journal of Physics: Condensed Matter, 19(14), 145273.

[75] Iqbal, Y., Mller, T., Ghosh, P., Gingras, M. J. P., Jeschke, H. O., Rachel, S., and Thomale, R. (2019). Quantum and classical phases of the pyrochlore Heisenberg model with competing interactions. Physical Review X, 9(1), 011005.

[76] Sanders, M. B., Krizan, J. W., Plumb, K. W., McQueen, T. M., and Cava, R. J. (2016). $NaSrMn_2F_7$, $NaCaFe_2F_7$, and $NaSrFe_2F_7$: novel single crystal pyrochlore antiferromagnets. Journal of Physics: Condensed Matter, 29(4), 045801.

[77] Plumb, K. W., Changlani, H. J., Scheie, A., Zhang, S., Krizan, J. W., Rodriguez-Rivera, J. A., ... and Broholm, C. L. (2018). Continuum of quantum fluctuations in a three-dimensional S= 1 Heisenberg magnet. Nature Physics 15 , 5459.

[78] Zhang, S., Changlani, H. J., Plumb, K. W., Tchernyshyov, O., and Moessner, R. (2018). Dynamical structure factor of the three-dimensional quantum spin liquid candidate $NaCaNi_2F_7$. arXiv preprint arXiv:1810.09481.